

Histone methyltransferase G9a drives  
inflammation-induced neurodegeneration by  
transcriptional control of ferroptosis

**Dissertation**

zur Erlangung der Würde des Doktors der Naturwissenschaften  
des Fachbereichs Biologie, der Fakultät für Mathematik, Informatik  
und Naturwissenschaften der Universität Hamburg

vorgelegt von

Nicola Rothhammer

aus Straubing

Hamburg 2021

Conducted at

Institute of Neuroimmunology and Multiple Sclerosis (INIMS)

Center for Molecular Neurobiology Hamburg (ZMNH)

University Medical Center Hamburg-Eppendorf (UKE)

Chair: Prof. Dr. Thomas Oertner

Supervisor and referee: Prof. Dr. Manuel Alexander Friese

Referee: Prof. Dr. Christian Lohr

Date of defense: May 4, 2022

## Table of contents

I	List of figures .....	6
II	List of tables .....	7
III	Abbreviations .....	8
1	Introduction.....	12
1.1	Multiple sclerosis.....	12
1.1.1	Epidemiology and aetiology.....	12
1.1.2	Immunopathology .....	13
1.1.3	Animal models .....	15
1.2	Neurodegeneration .....	16
1.2.1	Oxidative stress.....	17
1.2.2	Glutamate excitotoxicity.....	18
1.2.3	Iron toxicity in neurodegenerative diseases .....	20
1.2.4	Neuronal cell death mechanisms of neurodegeneration .....	21
1.3	Epigenetic regulation.....	25
1.3.1	Epigenetic modifications.....	25
1.3.2	Epigenetic regulation in multiple sclerosis .....	29
1.3.3	Transcriptional repression by G9a .....	30
1.4	Aim of the study .....	33
2	Material and Methods .....	34
2.1	Material .....	34
2.1.1	Laboratory animals .....	34
2.1.2	Clinical data of brain specimens .....	34
2.1.3	Chemicals and reagents.....	35
2.1.4	Primer, antibodies, and Taqman probes .....	38
2.1.5	Buffers, solutions, and media .....	41
2.1.6	Consumables.....	42
2.1.7	Equipment and devices.....	43
2.1.8	Software.....	44
2.2	Methods .....	45
2.2.1	Genotyping .....	45
2.2.2	Experimental autoimmune encephalomyelitis.....	45
2.2.3	Candidate gene identification.....	46
2.2.4	Isolation of CNS-infiltrating immune cells and flow cytometry .....	46

2.2.5	Mouse Immunohistopathology .....	48
2.2.6	Human Immunohistochemistry .....	48
2.2.7	RNAscope <i>in situ</i> hybridization .....	48
2.2.8	Primary mouse neuronal culture .....	49
2.2.9	Human induced pluripotent stem cell-derived neurons.....	49
2.2.10	Immunocytochemistry.....	50
2.2.11	RealTime-Glo™ MT Cell Viability Assay .....	50
2.2.12	Calcium imaging.....	51
2.2.13	Oxidative stress detection .....	51
2.2.14	Cell death induction.....	52
2.2.15	Glutathione measurement .....	52
2.2.16	Neuronal nuclei isolation and sorting.....	52
2.2.17	Intra-nuclear staining and flow cytometry .....	53
2.2.18	RNA isolation, cDNA synthesis, and quantitative real-time PCR.....	53
2.2.19	Computational and statistical analysis .....	54
<b>3</b>	<b>Results .....</b>	<b>55</b>
3.1	Neuroinflammation promotes G9a-mediated H3K9me2 induction.....	55
3.1.1	H3K9me2 regulation during EAE time course.....	55
3.1.2	Glutamate-induced control of H3K9me2 induction.....	57
3.2	G9a interference regulates neuronal survival during excitotoxicity .....	58
3.2.1	<i>In vitro</i> models of G9a perturbation .....	58
3.2.2	Neuroprotection by G9a interference during glutamate stress .....	59
3.2.3	G9a perturbation protects neurons from glutamate-induced oxidative stress.....	61
3.3	Neuronal cell death <i>in vitro</i> is induced via ferroptosis by G9a.....	62
3.3.1	G9a activity is induced by ferroptosis.....	62
3.3.2	G9a interference diminish glutamate-induced ferroptotic cell death.....	63
3.3.3	Transcriptional regulation of ferroptosis-relevant genes upon G9a inhibition <i>in vitro</i> ....	64
3.4	G9a induces neuronal cell death during inflammation-induced neurodegeneration <i>in vivo</i>	66
3.4.1	Pharmacological G9a inhibition as neuroprotective treatment in CNS inflammation.....	66
3.4.2	Genetic disruption of G9a during CNS inflammation.....	68
3.4.2.1	Validation of G9a deletion in <i>G9a<sup>fl/fl</sup>;Snap25-Cre</i> mice .....	68
3.4.2.2	Neuronal loss in <i>G9a<sup>fl/fl</sup>;Snap25-Cre</i> mice during EAE .....	70
3.5	G9a inhibition enhances expression of ferroptosis-related genes in neurons during CNS inflammation <i>in vivo</i> .....	72
3.6	Mechanism of G9a-dependent neuroprotective effect in CNS inflammation .....	74

---

3.7	Ferroptosis induction in MS brains and human iPSC neurons.....	75
4	Discussion .....	78
4.1	H3K9me2 regulation during neuroinflammation .....	78
4.2	Neuroprotection by G9a perturbation during glutamate excitotoxicity and oxidative stress .. .....	80
4.3	Pharmacological G9a inhibition as neuroprotective treatment during EAE.....	81
4.4	G9a-dependent protection from ferroptosis .....	83
4.5	G9a-mediated transcriptional regulation of ferroptosis-relevant genes .....	85
4.6	Ferroptosis regulation in MS patients and therapeutic potential of UNC0642.....	87
4.7	Conclusion and outlook.....	89
5	Summary.....	91
6	Zusammenfassung .....	92
IV	Bibliography.....	94
V	Publication list .....	117
VI	Acknowledgements.....	118
VII	Affidavit .....	119

## I List of figures

Figure 2.1:	Gating strategy for immune cell subsets. ....	47
Figure 3.1:	Regulation of epigenetic modifiers during neuroinflammation .....	55
Figure 3.2:	Neuronal upregulation of G9a-mediated H3K9me2 during EAE .....	56
Figure 3.3:	H3K9me2 specific regulation in response to glutamate stress <i>in vitro</i> .....	57
Figure 3.4:	Characterization of pharmacological and genetic perturbation of G9a in primary neurons.....	59
Figure 3.5:	G9a perturbation results in neuroprotection during glutamate exposure.....	60
Figure 3.6:	G9a perturbation protects neurons from oxidative stress .....	61
Figure 3.7:	G9a perturbation counteracts ferroptosis.....	62
Figure 3.8:	Prevention of ferroptosis induction by G9a interference.....	64
Figure 3.9:	Ferroptosis-relevant genes during induction of ferroptosis in primary neurons treated with UNC0642.....	65
Figure 3.10:	Pharmacological inhibition of G9a ameliorated EAE symptoms.....	67
Figure 3.11:	Immune cell infiltration is not affected by UNC0642 treatment during EAE.....	68
Figure 3.12:	G9a expression in brain, spinal cord, and lymph nodes of <i>G9a<sup>fl/fl</sup>;Snap25-Cre</i> mice ...	69
Figure 3.13:	H3K9me2 expression in brain, spinal cord, and lymph nodes of <i>G9a<sup>fl/fl</sup>;Snap25-Cre</i> mice .....	70
Figure 3.14:	Impact of genetic disruption of G9a in <i>G9a<sup>fl/fl</sup>;Snap25-Cre</i> mice during CNS inflammation .....	71
Figure 3.15:	Neuronal loss in spinal cords of <i>G9a<sup>fl/fl</sup>;Snap25-Cre</i> mice during inflammation.....	72
Figure 3.16:	G9a-mediated transcriptional regulation of ferroptosis regulated genes during EAE	72
Figure 3.17:	Gene expression analysis of ferroptosis-related genes during EAE upon UNC0642 treatment.....	73
Figure 3.18:	Mechanism of G9a-dependent ferroptosis regulation .....	75
Figure 3.19:	Ferroptosis induction in MS brains and human iPSC neurons.....	76

## II List of tables

Table 2.1:	Mouse strains .....	34
Table 2.2:	Clinical data of brain specimens .....	34
Table 2.3:	Reagents for animal experiments.....	35
Table 2.4:	Reagents for genotyping.....	35
Table 2.5:	Reagents for flow cytometry and fluorescence-activated cell sorting .....	36
Table 2.6:	Reagents for immunocytochemistry, immunohistopathology and RNAscope.....	36
Table 2.7:	Compounds for cell culture experiments .....	37
Table 2.8:	Assays and plasmids for cell culture experiments .....	38
Table 2.9:	Reagents for nuclei extraction.....	38
Table 2.10:	Reagents for RNA isolation and quantitative real-time PCR.....	38
Table 2.11:	Primer for genotyping.....	38
Table 2.12:	Primary antibodies.....	39
Table 2.13:	Secondary antibodies .....	40
Table 2.14:	Taqman assays.....	40
Table 2.15:	Media and supplements for cell culture.....	41
Table 2.16:	Buffers and solutions .....	41
Table 2.17:	Consumables .....	42
Table 2.18:	Equipment and devices.....	43
Table 2.19:	Software .....	44
Table 2.20:	BD FACS LSR II analyzer configuration and staining panel.....	47

### III Abbreviations

4-HNE	4-hydroxynonenal
5hmC	5-hydroxymethylcytosine
5mC	carbon 5 position
AAV	adeno-associated virus
Acsl4	acyl-CoA synthetase long chain family member 4
AD	Alzheimer's disease
ALS	amyotrophic lateral sclerosis
AMPA	2-amino-3-(3-hydroxy-5-methylisoxazol-4-yl) proprionate
ANOVA	analysis of variance
AP5	D-(-)-2-amino-5-phosphonopentanoic acid
APC	antigen presenting cell
ATP	adenosine triphosphate
AUC	area under the curve
bacTRAP	bacterial artificial chromosome translating ribosome affinity purification
BAK	BCL-2 homologous antagonist/killer
BAX	BCL-2-associated X protein
BCL-2	B-cell lymphoma 2
BH3	BCL-2 homology region 3
BSA	Bovine serum albumin
CBS	cystathionine $\beta$ -synthase
CD	cluster of differentiation
Cnp	2',3'-cyclic-nucleotide 3'-phosphodiesterase
CNS	Central nervous system
CoQ10	coenzyme Q10
COX-2	cyclooxygenase-2
CpG	cytosine-phosphate-guanine
CREB	cAMP response element binding protein
Cx3cr1	C-X3-C motif chemokine receptor 1
DAMP	damage-associated molecular pattern
DC	dendritic cell
DFMO	DL- $\alpha$ -Difluoromethylornithine
div	day <i>in vitro</i>
DMSO	Dimethyl sulfoxide
DMT1	divalent metal transporter 1

---

DNA	deoxyribonucleic acid
DNMT	DNA methyl transferase
EAE	experimental autoimmune encephalomyelitis
EDTA	ethylenediaminetetraacetic acid
EEAT	excitatory amino acid transporter
EGTA	ethylene glycol-bis(2-aminoethylether)-N,N,N',N'-tetraacetic acid
EHMT1	euchromatic histone N-methyltransferase 1
EHMT2	euchromatic histone N-methyltransferase 2
FACS	fluorescence-activated cell sorting
FDR	false discovery rate
Fe <sup>2+</sup>	ferrous iron
Fe <sup>3+</sup>	ferric iron
FSP1	ferroptosis suppressor protein 1
GCL	γ-glutamylcysteine synthetase
Gclc	glutamate-cysteine ligase catalytic subunit
Gfap	glial fibrillary acidic protein
GLP	G9a-like protein
GPX4	glutathione peroxidase 4
GSDMD	gasdermin D
GSS	glutathione synthetase
GST	glutathione-S-transferase
GWAS	genome-wide association study
H <sub>2</sub> O <sub>2</sub>	Hydrogen peroxide
HAT	histone acetyl transferase
HD	Huntington's disease
HDAC	histone deacetylase
HDM	histone demethylases
HLA	human leucocyte antigen
HMT	histone methyltransferases
hPTM	histone post-translational modification
ICC	immunocytochemistry
IF	Immunofluorescence
IFN $\gamma$	interferon gamma
iGluR	ionotropic glutamate receptor
IHC	immunohistochemistry

---

IHP	immunohistopathology
IL	interleukin
iPSC	induced pluripotent stem cell
KDM	histone lysine demethylase
KMT	histone lysine methyltransferases
lncRNA	long-noncoding RNA
MFI	mean fluorescence intensity
mGluR	metabotropic glutamate receptor
MHC	major histocompatibility complex
miRNA	micro RNA
MLKL	mixed lineage kinase domain-like
MOG	myelin oligodendrocyte glycoprotein
MRI	magnetic resonance imaging
MS	Multiple sclerosis
NAGM	normal appearing white matter
NAWM	normal appearing white matter
NBQX	2,3-Dioxo-6-nitro-1,2,3,4-tetrahydrobenzo[f]quinoxaline-7-sulfonamide
NDD	no neurological diseases
NDS	normal donkey serum
NK cell	natural killer cell
NMDA	N-methyl-d-aspartate
NPC	neural precursor cell
NRF2, Nfe2l2	nuclear factor erythroid 2-related factor 2
PBS	phosphate buffered saline
PCD	programmed cell death
PCR	polymerase chain reaction
PD	Parkinson's disease
Pecam	platelet and endothelial cell adhesion molecule 1
PFA	paraformaldehyde
PGC-1 $\alpha$	peroxisome proliferator-activated receptor gamma coactivator 1-alpha
PPMS	primary progressive MS
Ptgs2	gene prostaglandin-endoperoxide synthase 2
Ptprc	protein tyrosine phosphatase receptor type C
PTX	pertussis toxin
PUFA	polyunsaturated fatty acid

---

qPCR	quantitative real-time PCR
Ras	rat sarcoma
Rbfox3	RNA binding protein fox-1 homolog 3
RIPK	receptor interacting kinase
RNA	ribonucleic acid
ROS	reactive oxygen species
RRMS	relapsing-remitting MS
RSL3	RAS-selective lethal 3
RTG	RealTime-Glo™
s.e.m	standard error of the mean
SAM	S-adenosylmethionine
SET	Su(var)3-9, Enhancer-of-zeste, Trithorax)
Sirt	Sirtuin
SLC3A2	solute carrier family 3 member 2
SLC7A11	solute carrier family 7 member 11
Snap25	synaptosome associated protein 25
SPMS	secondary progressive MS
STS	staurosporine
T helper	Th
T reg	regulatory T cell
TET	ten-eleven translocation
TfR	transferrin receptor
TNF $\alpha$	tumor necrosis factor alpha
TSZ	TNF $\alpha$ , Smac mimetics, z-VAD-fmk
TTX	Tetrodotoxin
UKE	University Medical Center Hamburg-Eppendorf
Xc <sup>-</sup>	cystine/glutamate antiporter

# 1 Introduction

## 1.1 Multiple sclerosis

Multiple sclerosis (MS) is the most common chronic inflammatory demyelinating and neurodegenerative disease of the central nervous system (CNS), characterized by the formation of focal demyelinated plaques in the CNS white matter<sup>1</sup>. The incidence of MS is increasing worldwide and currently more than 2 million people are affected, with a disease onset starting in young adulthood<sup>2</sup>. MS is a complex, multifactorial, and heterogeneous disorder, however, the underlying genetic and environmental factors that drive the condition are only poorly understood. The hallmark of the disease is the accumulation of CNS lesions composed of inflammatory cells, demyelinated axons, and astrogliosis, which are caused by processes that involve immune cell infiltration and oligodendrocyte death in response to the breakdown of the blood-brain barrier<sup>3</sup>. The clinical manifestations are in most patients episodes of reversible and unpredictable neurological deficits, correlating with the localization of lesions, that include sensory loss, dyscoordination, limb weakness, loss of bladder control, and cognitive dysfunction<sup>4</sup>. In the early course of the disease, neurological dysfunction usually last for days or weeks and characterize the initial phase of MS, the clinically isolated syndrome often followed by a relapsing course for several years, called relapsing-remitting MS (RRMS)<sup>5</sup>. Early inflammation is correlated with the degree of axonal injury in RRMS<sup>6</sup>, but delayed neurodegeneration is causing non-relapsing progression, which is classified into primary progressive MS (PPMS), where the relapsing phase is missing, and secondary progressive MS (SPMS), that develops after a relapse-remitting disease course in the majority of untreated patients<sup>7</sup>.

The diagnosis of MS is based on clinical symptoms and abnormalities on the magnetic resonance imaging (MRI), which is highly sensitive to detect CNS lesions<sup>8</sup>. Currently, only a few molecular biomarkers from the blood and cerebrospinal fluid have routinely been used in the clinics as their validation and translation is challenging<sup>9</sup>. The early and accurate diagnosis of the disease is essential for evaluating treatment options and associated side effects, but at the moment, there is no treatment available that prevents or halt the progression of MS. However, disease-modifying therapies including immunomodulating and anti-inflammatory drugs have been successfully applied in the clinics that diminish the progression of MS and ameliorate pathological symptoms<sup>3</sup>.

### 1.1.1 Epidemiology and aetiology

Multiple risk factors have been described that contribute to the onset of MS. Epidemiological data suggests a role for both genetic and environmental factors in MS that needs to be further investigated. MS has a geographic pattern of prevalence with a global distribution that can be generalized as

increasing with the distance from the equator<sup>2</sup>. In addition, migration studies indicate that migrants from low-risk to high-risk countries are at low risk to develop MS and vice versa, supporting MS to being secondary to an environmental exposure<sup>10</sup>. The risk to develop MS also depends on various lifestyle factors such as smoking<sup>11</sup>, infectious agents like Epstein-Barr virus<sup>12</sup>, early-life obesity<sup>13</sup>, or shift work<sup>14</sup>, and women are also more susceptible to develop MS compared to men<sup>15,16</sup>. Moreover, low sun exposure and resulting vitamin D deficiency, which correlates with the latitudinal gradient in MS prevalence, is associated with increased MS susceptibility<sup>17,18</sup>. Recently, the type and distribution of gut microbiota has also been shown to influence the risk and course of MS<sup>19,20</sup>.

The genetic component of MS predisposition is indicated in studies from monozygotic twins that have estimated a siblings' relative risk for MS to be increased by 7-fold<sup>21</sup>. Genes within the human leucocyte antigen (HLA) complex are the strongest genetic risk factors for MS. Variants of HLA class II genes presents antigens to cluster of differentiation (CD) 4+ T lymphocytes, and class I products present antigens to CD8+ lymphocytes<sup>22</sup>. Carriers of the major histocompatibility complex (MHC) class II allele HLA DRB1\*15:01 are about three times more likely to develop MS rather than non-carriers<sup>23</sup>, whereas the class I variant HLA-A\*02 is associated with protection from the disease<sup>24</sup>. Recent work has uncovered the genetic basis for the risk of the disease by genome-wide association studies (GWAS) that identified genes that act on genetically susceptible hosts, many of which play a role in the immune system. Thereby, more than 150 single nucleotide polymorphisms associated with MS susceptibility, including HLA and non-HLA risk and protective alleles, has been identified<sup>25</sup>. Each genetic variant has a small effect on the probability to develop MS and genetic variants with minor effects in genes like interleukin (IL) 2RA and IL7RA might contribute to genetic susceptibility in different patients<sup>26,27</sup>.

Besides the hereditary factors that modify MS susceptibility, epigenetic regulation of gene expression also leads to differences in the phenotype without changes in the genetic code itself and may also modulate the response to environmental factors. The importance of the epigenome in MS has been derived from genome-wide studies that investigated transcriptional changes in MS patients resulting from alterations in the chromatin status of various cell types that are particularly affected in MS<sup>28</sup>. The epigenome reveals an enormously complex but meaningful insight into the cell-type specific regulation of gene expression during MS and evaluation of data generated by emerging sequencing strategies will provide a comprehensive mechanistic understanding of how environmental risk factors affect disease development<sup>29</sup>.

### 1.1.2 Immunopathology

The pathological hallmark of MS phenotypes is the formation of focal plaques in the white matter of the CNS in response to the migration of autoreactive lymphocytes that causes inflammation. MS plaques, also known as lesions, are areas of demyelination, typically around post-capillary venules

within the brain, optic nerve, and spinal cord, and are characterized by a profound disturbance of the blood-brain barrier<sup>1,30,31</sup>. Active demyelinating lesions dominate in the relapse-remitting stage of the disease that correlate with infiltrating immune cells and contain activated microglia and macrophages, as well as reactive astrocytes<sup>32</sup>. By contrast, active lesions are less frequent in PPMS or SPMS patients that display reduced inflammatory invasion of autoreactive immune cells and inactive lesions are more common in those patients<sup>4,33</sup>. Chronic, inactive lesions have a well-defined core of demyelination and a reduced axonal density surrounded by a narrow rim of activated microglia and macrophages and have a lower density of lymphocytes than active lesions<sup>34</sup>.

The composition of the inflammatory infiltrates in RRMS and progressive MS is similar and contain T-lymphocytes, dominated by MHC class I-restricted cytotoxic CD8+ T cells, and a relatively small amount of helper CD4+ T cells as well as CD20+ B cells. The antigen specificity of the aberrant immune response in MS remains unresolved even some candidates, such as myelin proteins, have been favored for the initiation of the disease process in MS<sup>35,36</sup>. T cell response can be initiated by the presentation of a specific antigen by antigen presenting cells (APCs) that include B cells, dendritic cells (DCs), microglia, and macrophages<sup>1,34</sup>. The resulting inflammatory response induce the differentiation of CD4+ T cells into T helper (Th) 1, Th2, or Th17 phenotypes which have the ability to secrete special cytokines. Th1 cells produce pro-inflammatory cytokines like interferon gamma (IFN $\gamma$ ) or type II interferon and tumor necrosis factor alpha (TNF $\alpha$ )<sup>37</sup>, whereas Th2 cells secrete anti-inflammatory cytokines such as IL-4 and IL-13<sup>38</sup>. Like Th1 cells, Th17 cells promote inflammation in MS and induce a large number of cytokines (IL-17, IL-21, IL-22, and IL-26)<sup>39</sup>. Another type of CD4+ T cells involved in MS pathology are regulatory T cells (T reg). T reg cells have an immunosuppressive function and play a role in regulating the immune system by maintaining self-tolerance and inhibiting autoimmunity<sup>40</sup>. In MS patients the frequency and suppressive function of T reg cells are impaired which might accelerate the development of the disease<sup>41,42</sup>. Besides the involvement of CD4+ T cells in MS pathogenesis, CD8+ T cells are present in MS lesions and mediate the suppression of CD4+ T cell proliferation by the secretion of perforin, which is cytotoxic to CD4+ cells<sup>43</sup>. In addition, cytotoxic CD8+ cells kill glial cells via the fast perforin-mediated lysis<sup>44</sup>, induce the oligodendrocyte cell death<sup>45</sup> leading to exposed axons, or also kill neurons directly by secreting perforin<sup>46</sup>. In addition to T cells, B cells and their cytokines are implicated in the pathophysiology of MS. B cells transform into plasma cells that produce antibodies and the presence of these polyclonal antibodies in the cerebrospinal fluid of MS patients is recognized as oligoclonal bands<sup>47</sup>. Another function of B cells is the production of pro-inflammatory cytokines such as TNF $\alpha$ , but also anti-inflammatory cytokines like IL-10<sup>48</sup>, suggesting a diverse role of B cells on the disease progression of MS patients.

The pathogenesis of MS includes the interaction between several immune cell types in the periphery but also CNS resident cells such as microglia and astrocytes. Together, they secrete a range

of inflammatory mediators that can recruit immune cells into the CNS leading to neuronal damage. During the progressive phase of the disease, the contribution of the peripheral immune system decreases, and pathogenic immune cell responses are mainly initiated within the CNS<sup>49,50</sup>. Despite the notion that CNS intrinsic inflammation contributes to propagating neurodegeneration, it is poorly targeted by available treatments and additional treatment strategies for progressive MS are needed<sup>51</sup>.

### 1.1.3 Animal models

To elucidate MS pathological mechanisms and develop effective pharmacological treatment for the prevention of relapses and progressive MS, animal models have been developed that provide insights into demyelinating processes that contribute to the degeneration of neurons during the disease course. The best studied animal models are the experimental autoimmune encephalomyelitis (EAE)<sup>52</sup>, the virally induced chronic demyelinating disease via Theiler's murine encephalomyelitis virus<sup>53</sup>, and the toxin induced demyelination by cuprizone<sup>54</sup>.

The most applied animal model of MS to study inflammation-induced neurodegeneration is EAE, in which autoimmunity to CNS components is induced by immunization with self-antigens of CNS peptides<sup>52</sup>. For the immunization of animals, CNS peptides together with mycobacterium are emulsified in Freund's adjuvant<sup>55,56</sup>, which mimics the immune activation pathways caused by infectious agents and potentiate the humoral immune response. In addition, pertussis toxin (PTX)<sup>57</sup> is administered to facilitate EAE induction by disrupting the blood–brain barrier integrity<sup>58</sup>. EAE is a CD4+ T cell mediated demyelinating autoimmune disease characterized by the infiltration of mononuclear cells<sup>59</sup>. EAE has been induced in several animal species including monkeys<sup>52</sup> and guinea pigs<sup>60</sup>, however, mice<sup>61</sup> and rats<sup>62</sup> have been mostly used for EAE experiments as they turned out to best model the relapsing-remitting and chronic progressive course of the disease. The induction of EAE in mice can either be done by active immunization with a myelin protein or peptide depending on the genetic background of the susceptible mouse strain, or by passive induction using the adoptive transfer of pre-activated myelin-specific T cells into naive mice<sup>63</sup>. The disease course in response to immunization depends also on the mouse strain and the relevant CNS-derived immunogen. For instance, immunization of SJL/J mice with the immunodominant epitope of proteolipid protein PLP<sub>139-151</sub><sup>64</sup> induces a relapsing-remitting course, while immunodominant myelin oligodendrocyte glycoprotein (MOG) MOG<sub>35-55</sub><sup>65</sup> in C57BL6/J mice reflects the chronic progression of the disease. Active immunization with myelin antigens results in the breakdown of peripheral tolerance, followed by the proliferation of activated myelin-specific T cells that differentiate into effector cells and cross the blood-brain barrier via the expression of integrins<sup>66</sup>. Once within the CNS they are reactivated by CNS-resident APCs presenting myelin antigens<sup>67</sup>, leading to the expression of pro-inflammatory cytokines by the effector T cells, which additionally recruits non-specific effector cells such as monocytes or

macrophages to the CNS<sup>68,69</sup>. These processes are largely responsible for the destruction of myelin sheath, which is reflected by EAE symptoms characterized by an ascending paralysis, beginning at the tail, followed by a hind limb and fore limb paralysis<sup>70</sup>.

EAE represents a useful animal model for MS since several of the CNS pathologies found in EAE mice have strong similarities to the pathologies found in the CNS of MS patients. Both are characterized by demyelinating lesions in the CNS that contain immune cell infiltrate<sup>71,72</sup> and myelin debris<sup>73,74</sup>. Additionally, oligoclonal bands have been found in the cerebrospinal fluid of EAE mice and MS patients<sup>47,75</sup>. Although the EAE model provides a meaningful system to study the inflammatory aspects of MS, it also has its limitations. In particular, the inherent innate and adaptive immune functions of rodents and humans are different, which may influence their response to auto-immune attacks. Moreover, the EAE models favors immune mechanisms driven by CD4+ T cells, whereas immune mechanisms in MS are associated with CD8+ T cells<sup>76</sup>. Also the implication of cortical areas have not been studied well in the EAE model as it mainly affects the spinal cord, whereas MS is primarily a brain disease<sup>77</sup>. Despite the limitations of the EAE model, a wide variety of phenomena relevant to understand pathologies of MS can be extracted from this animal model, which classifies it for pre-clinical testing of relevant therapeutic options.

## 1.2 Neurodegeneration

Besides the inflammation-induced neurodegeneration in MS that dominates in the relapsing-remitting stage, demyelination and neuronal loss slowly propagates during a progressive disease course, when immune cell infiltration is less pronounced<sup>78</sup>. Inflammation dependent lesions have been mainly detected within the white matter of the CNS and recently, several studies have indicated that demyelination is also present to a varying degree in the cerebral cortex and deep grey matter, whereas the extend of axonal damage is variable and might depend on earlier inflammatory processes causing demyelination<sup>79,80</sup>. The presence of extensive grey matter pathology in later stages of MS suggests a substantial role of neurodegenerative processes with increasing disease duration that affect the entire brain<sup>81</sup>. Axonal loss in the white matter tracts of the CNS correlates with clinical disability, however, an increasing degree of cortical lesions have also been suggested to enhance the accumulation of motor, sensory, and cognitive disability in progressive forms of MS<sup>82</sup>. Therefore, it is highly valuable to investigate the underlying neurobiological mechanisms that may be relevant for tissue injury in MS and identify pathways that can be modulated and thereby enhance neuronal resilience to ameliorate neurological symptoms in MS patients.

Due to the limited access to human biopsies to study neuron intrinsic mechanisms during inflammation, most of our current knowledge originates from the EAE model. Cytotoxic T lymphocytes can directly trigger the destruction of myelin sheaths and oligodendrocytes, which is associated with

axonal degeneration in MS plaques<sup>83,84</sup>. Impairment of neuronal transmission and function is also potentiated by microglia activation and macrophage infiltration, as their secretion of pro-inflammatory cytokines and enzymes lead to the formation of oxygen and nitric oxide radicals<sup>85</sup>. In addition, functional disturbance of astrocytes within active lesions<sup>86</sup> may promote the inflammatory reaction and affect their expression of molecules involved in maintaining homeostasis, glutamate buffering, and trophic support that increases the vulnerability of oligodendrocytes or neurons<sup>87,88</sup>. Pathways of cell stress and degeneration may be facilitated by oxidative stress<sup>89</sup>, excitotoxicity<sup>90</sup>, energy deficiency<sup>91</sup>, ion channel disturbance<sup>92</sup>, toxic accumulation of iron<sup>93</sup> and proteins<sup>94</sup>, or the initiation of regulated cell death cascades<sup>95</sup>. How those mechanisms that act primarily at the level of neurons ultimately contribute to MS pathology are important areas for continued investigation. Further insights into the triggers and effectors of neuroinflammation may lead to the discovery of pathways that reduce the production of factors contributing to neurotoxicity.

### 1.2.1 Oxidative stress

In MS lesions, oxidative stress is a major driving force for tissue injury and is particularly pronounced in the progressive stage of the disease. The oxidation of lipids, proteins, and deoxyribonucleic acid (DNA) interfere with the function of those molecules and thereby induce cellular damage and degeneration<sup>96</sup>. In brains of MS patients oxidized lipids and DNA have been detected in active MS plaques, while the extent of oxidation correlated with inflammation. Oxidized DNA was predominantly observed in nuclei of oligodendrocytes that undergo apoptosis and existed to a lesser extent in astrocytes. In addition, lipid peroxidation-derived structures were detected in oligodendrocytes and in some astrocytes. More importantly, oxidative phospholipids have been primarily found in neurons within grey matter lesions that exhibit signs of fragmented neurites<sup>97</sup>. The profound oxidative injury in MS is induced through the generation of reactive oxygen and nitric oxide species predominantly by microglia and macrophages that highly express NADPH oxidase in response to activation, which is necessary to produce these radicals<sup>85</sup>. Moreover, mitochondrial injury leads to radical generation and further propagation of oxidative stress<sup>98</sup>. Reactive oxygen species (ROS) interfere with multiple components of the respiratory chain and results either in the inhibition or increased degradation of the respective proteins<sup>98</sup>. These mechanisms result in the impairment of energy metabolism and reduced adenosine triphosphate (ATP) levels which are particularly important in demyelinating diseases due to the increased energy demand of demyelinated axons<sup>99</sup>. Mitochondria are especially sensitive to free radicals because of their ability to induce DNA mutations and deletions<sup>100</sup>. Another way to amplify oxidative injury is by the liberation of iron from intracellular stores of degenerating cells into the extracellular space where highly reactive hydroxyl radicals emerge<sup>101</sup>. Under physiological conditions, oxidative stress can be counteracted by antioxidant defense mechanism. In active MS

lesions, enzymes and small molecules that limit the abundance of excessive oxidative species and thereby mediate neuroprotective mechanisms have been found to be upregulated including superoxide dismutases<sup>102</sup>, catalases<sup>103</sup>, and glutathione<sup>104</sup> whereas their expression appears to be regulated by the transcription factor nuclear factor erythroid 2–related factor 2 (NRF2)<sup>105</sup> and peroxisome proliferator-activated receptor gamma coactivator 1-alpha (PGC-1 $\alpha$ )<sup>106</sup>. The degree of cellular damage and degeneration as a consequence to oxidative stress differ between cell types. Most vulnerable are neurons and oligodendrocytes while astrocytes and microglia are more resistant. Differences in susceptibility to oxidative stress are likely due to intrinsic factors, such as differential expression of antioxidant defense components, or differences in iron storage and regulation<sup>107</sup>.

### 1.2.2 Glutamate excitotoxicity

Besides the involvement of oxidative stress in neuronal injury, excessive glutamate is hypothesized to trigger abnormal neuronal excitatory processes linked to CNS pathologies. The aberrant excitation of neurons by excitatory amino acids such as glutamate and similar substances results in deleterious signaling cascades within neurons leading to excitotoxicity and cell death<sup>108</sup>. Glutamate is the most abundant excitatory amino acid neurotransmitter in the brain and has been hypothesized to have a pivotal role in the pathogenesis of neuronal death<sup>109</sup>. Besides the function of glutamate as a neurotransmitter to exchange signals between neurons, it can serve as a source of energy in the absence of glucose<sup>110</sup>. Nevertheless, it predominantly exerts its function in response to depolarization that stimulates its release from nerve terminals into the synaptic cleft, where it can act on postsynaptic excitatory receptors or is taken up by astrocytes. The glutamatergic synapse is ensheathed by astrocytic processes that remove glutamate from the synapse using high affinity sodium-dependent glutamate transporters, also known as excitatory amino acid transporters (EAATs)<sup>111</sup>, thereby maintaining a very low extracellular glutamate concentration. Within astrocytes, glutamate is converted to glutamine by the enzyme glutamine synthetase. Glutamine is then released and transported to neurons, where it is converted to glutamate, which is stored in synaptic vesicles and can be used for neurotransmission again<sup>112</sup>.

Several different glutamate receptors have been identified within the postsynaptic membrane, which are functionally divided in ionotropic and metabotropic receptors. Ionotropic glutamate receptors (iGluRs) include the N-methyl-d-aspartate (NMDA), 2-amino-3-(3-hydroxy-5-methylisoxazol-4-yl) proprionate (AMPA), and kainate receptors, which open their associated ion channel upon activation to allow a rapid influx of sodium, potassium, and calcium ions<sup>113</sup>. While AMPA and kainate receptors primarily mediate sodium influx, NMDA receptors have high calcium conductivity. In contrast to other iGluRs, NMDA receptors exhibit a voltage-dependent magnesium-blockade at the regular membrane potential, which is removed from the ion channel pore upon membrane depolarization<sup>114</sup>.

Moreover, NMDA receptors requires a simultaneous binding of glutamate and a co-agonist such as glycine or D-serine for its activation, whereas AMPA and kainate receptors require only glutamate<sup>113</sup>. Metabotropic glutamate receptors (mGluRs) do not form ion channels but rather are coupled to G-proteins that mediate slow synaptic responses via various second messenger systems, predominantly stimulating calcium release from internal stores. Currently, eight different mGluRs (mGluR1–8) are known and have been classified into three groups (groups I, II and III) based on sequence homology and their intracellular effects<sup>115</sup>.

Excessive depolarization of the postsynaptic membrane by an overstimulation of glutamate receptors, especially NMDA receptors, increases the sustained influx of calcium ions into the neurons<sup>113</sup>. Under physiological conditions, calcium ions activate several calcium-dependent enzymes that influence a variety of different cellular components, whereas a dysregulation of the calcium concentration leads to deleterious consequences on neuronal homeostasis. In particular, aberrant cytoplasmic calcium concentration results in the degradation of proteins, phospholipids, and nucleic acids that induce different cell death programs<sup>113</sup>. Calcium overload has been suggested as a key mediator of glutamate excitotoxicity, whereby NMDA receptors are the primary source of calcium entry. Besides the synaptic localization of NMDA receptors, they can also be found at extra synaptic sites<sup>116</sup> where they are activated in response to glutamate spillover. The localization of NMDA receptors determines their function, suggesting that synaptic NMDA receptors act through nuclear calcium signaling that activate cAMP response element binding protein (CREB) and mediate neuroprotection, whereas extra synaptic NMDA receptors suppress CREB activity and promote cell death<sup>116-119</sup>.

Glutamate excitotoxicity has been described in several neurodegenerative diseases including MS<sup>120,121</sup>. It has been observed that demyelination and oligodendrocyte death can occur through glutamate excitotoxicity by an overactivation of iGluRs<sup>122</sup>. In MS, the potential role of excitotoxicity was first investigated in the EAE model, where blockers of NMDA<sup>123</sup> and AMPA/kainate<sup>121,124</sup> receptors reduced neurological symptoms, oligodendrocyte loss, and demyelination without affecting the immune reaction. In addition, the role of mGluRs has been demonstrated in the EAE model where a deletion of mGluR8 had a neuroprotective effect during neuroinflammation, that could be validated by pharmacological activation of the receptor<sup>125</sup>. Moreover, elevated glutamate levels have been detected in the cerebrospinal fluid of MS patients with acute lesions<sup>126</sup>, within MS lesions, and normal appearing white matter (NAGM) of MS patients<sup>127</sup>, as well as in plasma from RRMS patients<sup>128</sup>. In accordance with the increased glutamate levels of MS patients, it has been shown that several glutamate receptor subunits of NMDA, AMPA, and kainate receptors have been upregulated in brains of MS patients<sup>129</sup>. Excessive glutamate levels in MS patients have been suggested to originate from inflammatory cells such as monocytes<sup>128</sup>, DCs<sup>130</sup>, or microglia<sup>131</sup> that are able to release glutamate

through the cystine/glutamate antiporter ( $Xc^-$ ) in response to activation, which have been shown to be upregulated in the CNS and peripheral blood cells of MS patients<sup>132</sup>. In addition, impaired glutamate uptake by glial cells as well as alterations in glutamate metabolism contributes to increased extracellular concentrations of glutamate in brains of MS patients<sup>90,133</sup>. Taken together, excessive extracellular glutamate in the brain leads to toxic alterations on different cell types that might contribute to the pathology of MS.

### 1.2.3 Iron toxicity in neurodegenerative diseases

Iron overload has been associated with a variety of neurodegenerative disorders<sup>134</sup>. In view of these findings, the role of iron in the pathogenesis of neurodegenerative diseases is of special interest and have been intensively investigated during the past years. Iron plays an important role in several physiological processes including oxygen consumption, DNA synthesis, and ATP production that results in energy production through its participation in electron transfer<sup>135</sup>. Moreover, in the CNS iron has an additional function, as it is essential for the synthesis of myelin<sup>136</sup>. In the healthy brain, iron transport is highly regulated across the blood-brain barrier, which depends on feedback signals from neurons based on the iron demands of the CNS<sup>137</sup>. Iron transport is initiated by the import into capillary endothelial cells via the transferrin receptor (TfR), in the form of transferrin- $Fe^{3+}$  (holotransferrin), and then transported to the CNS by ferroportin, which is the only known iron exporter<sup>138,139</sup>. The TfR is not only expressed in blood vessels, but also in neurons and glia to regulate the iron import into CNS cells, which occurs predominantly through transferrin-mediated endocytosis<sup>93</sup>. Within the endosome, ferric iron ( $Fe^{3+}$ ) dissociates from transferrin and is reduced to ferrous iron ( $Fe^{2+}$ ) by a STEAP family reductase followed by the export from endosomes into the cytoplasm via the divalent metal transporter 1 (DMT1)<sup>140</sup>. It is then utilized by mitochondria or is stored in the cytosolic iron-storage protein ferritin. The iron-free transferrin (apotransferrin), bound to the TfR, is then recycled back to the plasma membrane, where it is released for further iron delivery<sup>139</sup>.

Iron toxicity in the context of neurodegeneration is associated with an increased blood-brain barrier permeability and corresponding increase in total iron load that might be triggered by inflammation, redistribution of iron within the brain, and changes in iron homeostasis<sup>139</sup>. In the aging brain, it has been shown that the iron transport decreases exponentially<sup>141</sup> and consequently iron accumulates within several brain regions including the basal ganglia and areas related to motor control such as the motor cortex<sup>142</sup>. As neurodegenerative diseases are initiated with aging, it is plausible that the accumulation of iron might play a role in their pathogenesis. And indeed, several neurodegenerative diseases including Alzheimer's disease (AD)<sup>143</sup>, Parkinson's disease (PD)<sup>144</sup>, amyotrophic lateral sclerosis (ALS)<sup>145</sup>, and Huntington's disease (HD)<sup>146</sup> are characterized by insoluble protein aggregates that colocalize with iron, suggesting iron dyshomeostasis as a critical factor in the initiation of

neurodegeneration. Compared to other neurodegenerative diseases, iron toxicity might be particularly important in MS due to the profound destruction of iron-loaded oligodendrocytes and myelin during chronic inflammation<sup>147</sup>. Elevated iron levels have been detected in both white and grey matter regions in the CNS of MS brains<sup>148</sup> and in spinal cord neurons of EAE mice<sup>149</sup>. Based on the ferritin expression, iron is predominantly stored in oligodendrocytes and myelin, but also microglia and neurons contain moderate levels of ferritin, indicating an iron-storage capacity of several cell types within the brain<sup>139,150</sup>. In active MS lesions, iron-loaded oligodendrocytes are destroyed, leading to the liberation of its iron-storage into the extracellular space, which is mainly taken up by microglia and macrophages located at lesion edges, where it results in massive accumulation of iron<sup>151,152</sup>. Nevertheless, iron levels are decreased in the normal appearing white matter (NAWM) of MS patients that correlates with the disease duration, suggesting a redistribution of iron levels throughout the MS disease course<sup>101</sup>.

The liberated form of iron (ferrous iron) is stored within the cytoplasm in a chelatable and redox-active state, also known as labile iron pool, which is supposed to be the main contributor to oxidative stress during iron toxicity<sup>153</sup>. It is hypothesized that iron overload results in the formation of free radicals according to the Fenton reaction, where ferrous iron reacts with hydrogen peroxide and produce ferric iron together with the hydroxyl radical  $\text{OH}^\cdot$  and  $\text{OH}^-$ . Under normal conditions, radicals are removed by reduced glutathione or enzymes with antioxidant functions such as glutathione peroxidases, but when there is a massive production, they have the potential to damage structural proteins, lipids, and nucleic acids, leading to the induction of cell death signaling<sup>134</sup>.

#### 1.2.4 Neuronal cell death mechanisms of neurodegeneration

Under physiological conditions, cell death is highly regulated and required to maintain proper development and maintenance of tissue function, as well as the elimination of damaged or infected cells in organisms. Neuronal cells however, undergo programmed cell death (PCD) in a spatially and temporally restricted manner only during the developmental period to remove an excess of neurons for the establishment of the CNS, while postmitotic cells are required to be long-lived for maintaining intact circuits. Aberrant death of distinct neuronal populations is one of the principles that contributes to the pathogenesis of neurodegenerative diseases and several different forms of PCD might contribute to the excessive neuronal loss during disease progression. The initiation of neuronal cell death is not exclusively cell autonomous but is often triggered through interactions with neighboring cells. The execution of a specific type of cell death depends on the nature and severity of the stressor and is associated with distinct morphological and biochemical features<sup>154</sup>. However, the molecular causes of PCD and their relations to the inflammatory milieu in the MS brain remains still illusive. Based on pre-clinical data, the implication of a variety of cell death pathways has been described in the context of neurodegeneration in MS.

Apoptosis is the first PCD that has been discovered and was first described based on morphological changes including chromatin condensation, cell shrinkage, and the formation of small vesicular bodies, named apoptotic bodies<sup>155</sup>. The execution of apoptotic cell death can be triggered either extrinsically or intrinsically. The extrinsic pathway is activated by the ligation of TNF receptor family death receptors at the cell surface, leading to the formation of an intracellular death inducing signaling complex, which in turn activates caspase-8 and the downstream effector caspases, caspase-3 and caspase-7. On the other hand, the intrinsic pathway depends on internal stimuli such as DNA damage, growth factor deprivation or endoplasmic reticulum stress, which is regulated by pro- and anti-apoptotic members of the B-cell lymphoma 2 (BCL-2) family<sup>156</sup>. In response to intracellular stress, the initiators of apoptotic cell death, the BCL-2 homology region 3 (BH3)-only proteins, are transcriptionally upregulated<sup>157</sup> and bind to anti-apoptotic BCL-2 proteins, releasing the essential effectors of cell death, BCL-2-associated X protein (BAX) and BCL-2 homologous antagonist/killer (BAK)<sup>158</sup>. Once activated, BAX and BAK form oligomers that lead to mitochondrial outer membrane permeabilization, which in turn cause the release of pro-apoptotic factors from the mitochondria into the cytosol, including cytochrome C and Smac/DIABLO. These apoptotic factors activate caspase-9 to cleave and activate downstream caspases, similar to the extrinsic pathway, resulting in the cleavage of hundreds of proteins leading to demolition of the cell<sup>159</sup>. In MS, several studies have shown that there is an impaired apoptosis induction in autoreactive T cells, which results in an inefficient elimination of immune cells and a prolonged brain inflammation in patients. The induction of apoptosis in T cells have been investigated in the EAE model and revealed anti-inflammatory effects, which provided first evidence that the intervention of apoptosis might serve as a potential immunomodulatory treatment for MS<sup>160,161</sup>. In immune cells, the activation of apoptosis serves as a clean-up role and not as a pathogenic one, which is seen during neurodegeneration. Neuronal apoptosis in EAE have first been described in retinal ganglion cells and linked inflammation-induced neurodegeneration to the induction of PCD<sup>162</sup>. In addition, apoptotic neurons have been found in the demyelinated cortex of MS patients<sup>163</sup> and B cells from MS patients were identified to induce apoptosis in cultured neurons<sup>164</sup>, indicating a substantial role of apoptosis in the neuronal decay during inflammation.

Another way to induce cell death is a lytic form of PCD called necroptosis, the best characterized regulated form of necrosis. Unregulated necrosis involves passive processes such as tissue trauma and cannot be modulated, whereas necroptosis is highly regulated and depend on the activity of several kinases<sup>154</sup>. Necroptosis can be induced by the activation of specific death receptors, such as TNF receptor 1, which in turn leads to the recruitment of receptor interacting kinase 1 (RIPK1), which is activated by autophosphorylation<sup>165</sup>. This enables RIPK1 to activate RIPK3 and form a complex, the necrosome, which indicates the initiation of necroptosis<sup>166</sup>. RIPK3 then phosphorylates and activates the terminal effector of necroptosis, the pseudo-kinase mixed lineage kinase domain-like (MLKL),

resulting in the oligomerization of phosphorylated MLKL at the plasma membrane, causing cell rupture and necrosis. This facilitates the release of damage-associated molecular patterns (DAMPs) that propagates an inflammatory response<sup>167</sup>. The activation of the necroptosis pathway has been demonstrated in cortical neurons of MS patients by the phosphorylation of RIPK3 and MLKL<sup>168</sup>. Moreover, pharmacological inhibition of RIPK1 in EAE attenuates inflammation and oligodendrocyte degeneration<sup>169</sup> and reduced the infiltration of immune cells and proinflammatory cytokines<sup>170,171</sup>.

An alternative form of regulated necrosis is pyroptosis, which has first been described in macrophages infected by intracellular bacteria<sup>172</sup>. Pyroptosis is activated by inflammation that causes the formation of the inflammasome, which initiates the cleavage of pro-caspase-1 to active caspase-1. Once active, caspase-1 proteolytically cleave the inflammatory cytokines pro-IL-1 $\beta$  to IL-1 $\beta$  and pro-IL-18 to IL-18 to induce inflammation. However, gasdermin D (GSDMD) is the critical executioner of pyroptotic cell death that is cleaved by caspase-1 to form pores that directly permeabilize the plasma membrane causing necrosis<sup>173,174</sup>. Evidence for pyroptosis has been reported for neurodegenerative diseases such as AD or PD, and inflammasome activation have also been reported in several cell types in MS<sup>175</sup>. GSDMD-mediated inflammasome activation has been shown in macrophages, microglia, and oligodendrocytes in the CNS of MS patients as well as in the EAE model<sup>176</sup>. Moreover, a loss of GSDMD in peripheral myeloid cells suppressed neuroinflammation and demyelination during EAE<sup>177</sup>, and accordingly, the pharmacological administration of pyroptosis inhibiting compounds alleviated EAE symptoms and neuronal loss<sup>178</sup>.

Recent work has led to the identification of ferroptosis, a form of iron-dependent necrotic PCD<sup>179</sup>. Ferroptosis is morphologically and biochemically distinct from apoptosis and programmed necrosis and was initially identified by a novel group of compounds, which induced cell death selectively towards rat sarcoma (Ras) - transformed cell lines<sup>179,180</sup>. The induction of ferroptosis does not lead to chromatin and nucleus condensation, but is characterized by mitochondrial shrinkage, which distinguishes ferroptosis from other forms of cell death<sup>179</sup>. For the initiation of ferroptosis, the iron-dependent lipid peroxidation of polyunsaturated fatty acids (PUFAs) is required, leading to complete cell failure. Numerous effectors have been identified that generate the membrane lipids susceptible to ferroptosis, including acyl-CoA synthetase long chain family member 4 (ACSL4)<sup>181</sup>, promoting the execution of ferroptosis. Nevertheless, several endogenous mechanisms have been described that are critical to halt ferroptosis, whereas glutathione peroxidase 4 (GPX4) is essential for the prevention of overwhelming lipid peroxidation in a glutathione dependent manner<sup>182</sup>. To sustain the intracellular glutathione levels, the glutamate-cystine antiporter system Xc<sup>-</sup>, consisting of solute carrier family 7 member 11 (SLC7A11) and solute carrier family 3 member 2 (SLC3A2), regulates cystine uptake, which serves as a rate-limiting step in providing the intracellular cysteine required for the synthesis of glutathione. To bypass the requirement of cystine import by system Xc<sup>-</sup>, the transsulfuration pathway,

which synthesize cysteine from methionine by cystathionine  $\beta$ -synthase (CBS), is utilized by some cells to be more resistant to ferroptosis<sup>183</sup>. The generation of glutathione from glutamate, cysteine, and glycine is catalyzed sequentially by two cytosolic enzymes, called  $\gamma$ -glutamylcysteine synthetase (GCL) and glutathione synthetase (GSS). First,  $\gamma$ -glutamylcysteine is synthesized from glutamate and cysteine by GCL, followed by the addition of glycine catalyzed by GSS<sup>184</sup>. Glutathione is then utilized by GPX4 as an electron donor to convert potentially toxic hydroperoxides to non-toxic lipid alcohols in the cell membrane<sup>183,185</sup>. Moreover, the micronutrient selenium is an important regulator of ferroptosis, which is required for the biosynthesis of GPX4, where selenocysteine is co-translationally incorporated<sup>182</sup>. In addition, a number of redox enzymes that utilize glutathione to reduce oxidized substrates, such as glutathione-S-transferases (GSTs), have been shown to limit lipid peroxidation during ferroptosis<sup>186</sup>. Besides the glutathione/GPX4 dependent mechanisms to oppose ferroptosis, other pathways have been discovered that are implicated in ferroptosis surveillance. Most recently, a mechanism that involves the ferroptosis suppressor protein 1 (FSP1; also known as AIFM2) have been identified, which scavenge deleterious lipid hydroperoxides and thereby prevent peroxidation of lipid membranes<sup>187</sup>. Fsp1 acts either by reducing ubiquinone from coenzyme Q10 (CoQ10) to yield ubiquinol, which directly reduce lipid radicals to halt lipid autoxidation, or via recycling of  $\alpha$ -tocopherol (vitamin E), which serves as a natural antioxidant<sup>188</sup>.

Modulation of the expression or activity of ferroptosis-relevant molecules via chemical compounds opens a large array of opportunities for neuroprotective therapies. Initially, ferroptosis inducers have been discovered for anti-cancer-therapies, as cancer cells are more susceptible to undergo ferroptosis due to their higher metabolism and ROS load<sup>189</sup>. Induction of ferroptosis can be achieved with compounds that either block the cystine import via the system Xc<sup>-</sup> (e. g. by erastin), or by the inhibition or even degradation of GPX4 (e. g. by RAS-selective lethal 3 (RSL3))<sup>190</sup>. For the prevention of neuronal cell death in degenerative diseases, small molecule ferroptosis inhibitors have been identified, which have antioxidant properties and exhibit significant potential to directly inhibit lipid peroxidation, including lipophilic radical-trapping antioxidants such as ferrostatin-1 or  $\alpha$ -tocopherol, and iron chelators like deferoxamine<sup>191</sup>. Almost all neurodegenerative diseases appear to have prerequisites for the execution of ferroptotic cell death as displayed by excessive lipid peroxidation, dysregulated iron homeostasis, and intracellular depletion of glutathione<sup>192</sup>. Therefore, the use of ferroptosis inhibitors might be the most reliable evidence for the participation of ferroptosis in those diseases. Ferroptosis inhibitors have been successfully applied in animal models of ischemic stroke<sup>193,194</sup>, AD<sup>195</sup>, HD<sup>196</sup>, and PD<sup>197</sup>, underlining the emergence of ferroptosis during neurodegeneration. Moreover, several ferroptosis inhibitors have already been assessed in the clinic. One example is the iron chelator deferoxamine, that reduced the rate of cognitive decline in patients with AD<sup>198</sup>. Moreover, another iron chelator, deferiprone, have been applied in PD patients, which significantly impacted brain iron

levels and slowed the progression of symptoms<sup>197</sup>. However, only circumstantial evidence is present that ferroptosis might drive neuronal injury in MS associated CNS inflammation, as until now only one study have reported reduced GPX4 levels in brains of MS patients as well as in spinal cord neurons from EAE mice<sup>199</sup>, however a direct assessment of ferroptosis by using ferroptosis inhibitors in MS mouse models is still lacking. A more comprehensive understanding of ferroptosis and its regulation during CNS inflammation is likely to yield translatable interventions that inhibit inflammatory neurodegeneration in MS and related conditions.

### 1.3 Epigenetic regulation

Neurodegenerative phenotypes involve complex molecular processes that integrates a variety of aberrantly dysregulated pathways, offering a broad spectrum of modifiable processes to increase neuronal susceptibility. Recent studies focused on the identification of neuron-specific adaptations during inflammation in MS and its animal model and provided first insights into molecular pathways that are driving neurodegeneration. Affected pathways have been shown to be reflected within the transcriptome of injured neurons of EAE mice and MS patients and showed a strong upregulation of signatures associated with oxidative stress, mitochondrial dysfunction, and cell death pathways<sup>94,200</sup>. Besides the option to target a specific molecule that rebalance the homeostasis of neurons, transcriptional regulators have a broad impact on the transcriptional landscape. Transcriptional regulators can modify gene expression by targeting the intervention of DNA binding by transcription factors, protein-protein interaction, or epigenetic mechanisms<sup>201</sup>. Emerging data suggested that especially epigenetic regulation including DNA methylation, post-translational histone modification, and micro ribonucleic acid (miRNA) associated gene silencing play an important role in the pathogenesis of MS<sup>202</sup>. Therefore, recognizing the epigenetic changes involved in MS pathogenesis might reveal a better understanding of neuronal response networks to inflammatory challenges that drive neurodegeneration and open a new perspective how to modulate affected pathways to halt neuronal demise.

#### 1.3.1 Epigenetic modifications

Mechanisms of epigenetic regulation are involved in multiple aspects of neuronal function and development. Recent discoveries have outlined that the critical functions of chromatin in the maintenance of a healthy brain relies heavily on epigenetic mechanisms, whereas its dysregulation might be a main contributing factor to accelerate the progression of neurodegenerative disease<sup>203</sup>. Epigenetics is referred to as meiotically or mitotically heritable changes in gene expression that are influenced by environmental changes but without affecting the DNA sequence itself. Several

epigenetic regulatory mechanisms have been shown to control the chromatin structure and thereby regulate cellular processes. Among them are DNA methylation, histone post-translational modifications (hPTMs), chromatin remodeling, histone protein variants, and coding as well as non-coding RNAs, which sustain the cell type identity by controlling cell specific gene and protein expression. Epigenetic related studies in neurons are termed as neuroepigenetics. In contrast to classical epigenetics, neuroepigenetic modifications cannot be inherited as neurons are non-dividing cells and therefore play an enormous role in CNS development and function<sup>203</sup>.

DNA methylation is one of the best characterized and widely studied modification that is traditionally associated with gene repression. Methylated DNA is a stable mark that is mainly inherited, but during development, aging, and in response to environmental stimuli and in diseases, DNA methylation is dynamic, and *de novo* methylation can occur. DNA can be methylated on cytosine residues at the carbon 5 position (5mC), which is particularly common at cytosine-phosphate-guanine (CpG) islands but is also seen in non-CpG sites<sup>204</sup>. The enzymes responsible for DNA methylation are DNA methyl transferases (DNMTs), which are divided into two main families according to their function and structure. DNMT1 maintains global DNA methylation and shows a strong preference for hemimethylated DNA<sup>205</sup>, whereas members of the DNMT3 family, including DNMT3a, DNMT3b, and DNMT3L, carry out *de novo* methylation<sup>205,206</sup>. Although 5mC is very stable, demethylation can take place in an active or passive manner. Passive demethylation occurs during the replication of repetitive DNA during mitosis, whereas the active demethylation involves enzymatic process that removes or modifies the methyl group from 5mC by ten-eleven translocation (TET) proteins. Thereby, TET proteins oxidize 5mC to 5-hydroxymethylcytosine (5hmC) and further oxidize 5hmC to generate 5-formylcytosine and 5-carboxylcytosine<sup>207</sup>.

The chromatin structure is further determined by hPTMs at the N-terminal tails of core histone proteins forming the nucleosome where the DNA is wrapped around. The core histone proteins build a polymer consisting of two copies of H2A, H2B, H3, and H4 whereas the linkers H1 and H5 connect inter-nucleosomal DNA to build the DNA structure. hPTMs are the most diverse and dynamic form of chromatin modification and build the histone code that consists of a combination of several different types of modification, among them are acetylation, methylation, phosphorylation, ubiquitylation, sumoylation, ADP ribosylation, and deamination. The tails of nucleosomal histone proteins can be modified in response to extracellular signals, thereby altering gene expression by modifying the interaction of DNA and histone proteins or other regulatory enzymes. The functional consequences of hPTMs on transcription depend on the type of modification and on the position of the targeted amino acid residue within the histone tails<sup>204</sup>. The most prevalent hPTMs are histone acetylation and methylation that occur predominantly on lysine or arginine residues. Histone acetylation is the modification that is best understood and occurs by the addition of an acetyl group to the  $\epsilon$  amino group

of lysine residues by histone acetyl transferases (HATs). Generally, histone acetylation diminishes the electrostatic affinity between the DNA and histone proteins and thereby promotes a chromatin structure that is more permissive to gene transcription. The removal of acetyl groups is coordinated by histone deacetylases (HDACs) that allow a more compact chromatin state, which results in transcriptional repression<sup>208</sup>. The effect of histone methylation on transcription is a complex process with several histone methylated marks promoting gene activation and others repressing gene transcription. The functional output depends on the number of methyl groups added on lysine or arginine residues and on the position of the specific amino acids, e.g., H3K4me3 signifies the lysine (K) trimethylation (me3) at position four (4) of histone 3 (H3). The methyl groups on histone tails regulates transcriptional activity by conferring a unique structural alteration that function as a recognition template to recruit effector proteins to the chromatin. Methylation is similar to other modifications a dynamic and reversible process with histone methyltransferases (HMTs) adding methyl groups and histone demethylases (HDMs) removing them<sup>209</sup>. Lysine residues are more prominently methylated and their role in epigenetic gene control is well characterized. Generally, methylation on H3K4 and H3K36 is linked to actively transcribed genes, whereas methylation on H3K9, H3K27 and H4K20 is involved in transcriptional repression<sup>210</sup>. Moreover, distinct histone marks are distributed in a specific manner over target genes. For example in transcribed genes, H3K4me1/2/3 marks are mostly found at the promoter region or the transcription start site, whereas H3K79me1/2/3 is predominantly downstream of the transcription start site or within the gene body, and methylation of H3K36 is more prominent toward the 3' end of active genes<sup>211</sup>. In contrast, repressed genes have increased H3K27me3 in promoter regions and H3K9me2 marks are predominantly located within CpG islands and other genomic sites<sup>212,213</sup>. These marks are added by specific methyltransferases known as 'writers' and removed by demethylases that function as 'erasers', with most of these chromatin modifying enzymes possessing a strong site- and methyl-level specificity. Another group of effector enzymes recognizes methylated histone proteins, so called 'readers', and recruit other molecules to alter the chromatin accessibility.

Several histone methyltransferases have been characterized, which catalyze the addition of methyl groups from S-adenosylmethionine (SAM) to histones. Of these methyltransferases, the SET (an acronym for Su(var)3-9, Enhancer-of-zeste and Trithorax) domain containing enzymes<sup>214</sup> methylate lysine residues, with the exception of H3K79 that is methylated by DOT1-like proteins<sup>215</sup>, whereas members of the protein arginine N-methyltransferase family methylate arginines<sup>216</sup>. The removal of methyl groups from lysine residues is catalyzed by histone lysine demethylases (KDMs), the majority of which contain either the Jumonji C domain necessary for the binding of the cofactors Fe<sup>2+</sup> and  $\alpha$ -ketoglutarate, or the Jumonji/ARID domain allowing the binding to DNA. Some exceptions including KDM1A/LSD1 and KDM1B/LSD2 do not contain a Jumonji C domain and represents a distinct family of

KDMs that use flavin adenine dinucleotide as a co-factor. The KDMs are similar to histone lysine methyltransferases (KMTs) sensitive to the degree and position of lysine-methylation<sup>216,217</sup>.

Epigenetic variations on the level of histone proteins that alter the chromatin structure also include variants of histone proteins. Thereby, canonical histones can be replaced either during replication or in a replication-independent manner by histone variants that introduce sequence variations. Histone variants can influence nucleosomal dynamics and gene expression by altering the interaction with chromatin-remodeling enzymes and plays a crucial role during mammalian development<sup>218</sup>. Moreover, the interaction of DNA with histones can be modified by chromatin remodeling complexes that use ATP hydrolysis to allow nucleosome sliding and repositioning. The precise positioning of a nucleosome is a highly regulated process that involve the interaction of chaperones and remodeler complexes. Rearrangements of nucleosomes can consequently facilitate the binding of transcription factors and transcriptional complexes to access the DNA and control gene expression. The best characterized complexes involve the DNA-dependent ATPase helicases SMARCA4 and SMARCA2. Nucleosome dynamics are involved in genome regulation and thereby control diverse cellular processes including gene expression and DNA replication<sup>219</sup>.

Another important epigenetic regulator of gene transcription comprises the family of non-protein-coding RNAs. Those regulatory elements have a broad capacity to modulate gene expression, which is exerted in cooperation with chromatin modifying complexes. One of the most studied members of non-coding RNAs are miRNAs, which typically repress gene expression by translational repression through the degradation of complementary mRNA. miRNAs have the potential to target several mRNA transcripts that share sequence similarities and thereby fine-tune gene expression of entire networks that allow cell type identity<sup>220</sup>. Furthermore, long-noncoding RNAs (lncRNAs), have been shown to regulate the epigenetic status of the genome. They possess a great potential as they are heterogenous in their mechanism of action, depending on their localization and interacting molecules. lncRNAs also play important regulatory roles in gene transcription regulation, as they can silence small transcripts or even entire chromosomes, and they have the ability to exert enhancer function<sup>221</sup>. Within the nucleus, lncRNAs interfere with gene expression by guiding epigenetic regulators to specific loci and thereby regulate the status of protein-coding genes<sup>222</sup>.

Epigenetic regulation of genome activity is highly regulated on various levels of the chromatin structure. A growing body of evidence supports a role of epigenetic processes in the pathogenesis of neurodegenerative disorders including MS, where dysfunction in immune responses and nervous system integrity have been linked to epigenetic related mechanisms<sup>222,223</sup>. The translational use of epigenetics might offer new opportunities in epigenetic-based diagnostics and therapy for MS patients that still needs improvement in data interpretation and implementation but have a high potential to render new mechanistic insights into neuron intrinsic adaption during inflammation.

### 1.3.2 Epigenetic regulation in multiple sclerosis

Neurodegenerative diseases like AD, PD, or ALS<sup>224</sup> as well as MS<sup>202</sup> are greatly influenced by environmental factors and therefore, changes in the epigenome are involved in disease manifestation. A large series of studies on the prevalence of MS patients depending on geographic location, month of birth, vitamin D deficiency, and dietary intake in adolescence<sup>225</sup> supports the role of environment on gene regulation in MS. These findings indicate the importance of the epigenetic machinery in gene expression control in the MS brain and provide a mechanism that can be further investigated to identify the contribution of epigenetics to neurological impairment and neuronal cell death in MS patients.

The most studied epigenetic mechanism in MS patients is DNA-methylation. Several studies focused on the differences on DNA-methylation pattern in T cells or peripheral blood mononuclear cells of MS patients, which identifies methylation differences in MS associated regions such as the HLA locus<sup>226-229</sup>, the vitamin D receptor promotor<sup>230</sup>, or the IL2RA gene<sup>231</sup>. In contrast to the numerous studies that focused on epigenetic mechanisms of inflammation in MS on various levels of the chromatin landscape, only a few revealed epigenetic adaptations in neuronal tissue, which might explain neurological symptoms in patients. Alterations in DNA methylation has been observed in demyelinated hippocampi of MS patients leading to changes in transcriptional activity, which may influence synaptic plasticity, memory, and neuronal survival in MS patients<sup>232</sup>. Profiling of DNA methylation in subcortical neuronal nuclei from post-mortem white matter tissue of MS patients revealed differently methylated and hydroxymethylated positions between MS patients and controls with functional dysregulation of genes implicated in axonal guidance, synaptic plasticity, and CREB signaling<sup>233</sup>. Moreover, abnormalities in the expression and function of histone modifying enzymes are involved in cellular pathways that lead to a neurodegenerative phenotype. In MS patients, the acetylation level of H3 has been shown to be increased in oligodendrocytes that correlated with increased HAT levels and was associated with enhanced expression of transcriptional inhibitors of oligodendrocyte differentiation<sup>234</sup>, which might be linked to an impaired remyelination<sup>235</sup>. The implication of histone modifications has also been linked to axonal degeneration and neuronal atrophy in MS brains. Mitochondrial deficits and energy failure that led to neuronal damage was associated with alterations in methionine metabolism caused by decreased levels of H3K4 trimethylation in cortical neuronal nuclei of MS patients<sup>236</sup>. The role of miRNAs has also been investigated in brains of MS patients, where several differentially expressed miRNAs have been found in active or inactive lesions, whereas CD47 as one of the putative downregulated miRNA targets led to the disinhibition of macrophages and thereby promoted myelin phagocytosis<sup>237</sup>.

Nevertheless, several animal model experiments revealed the impact of epigenetic reprogramming for immune cells, neurons, and glia cells in autoimmunity and supports the idea to improve their

performance by epigenetic therapeutic targeting. One example is the Sirtuin (Sirt) family member Sirt1, a HDAC that has been demonstrated to be upregulated in oligodendrocyte progenitor cells within demyelinated brain lesions of EAE mice<sup>238</sup>, while a genetic deletion of Sirt1 in T cells resulted in an ameliorated EAE disease course<sup>239</sup>. In addition, post-translational histone methylation has been proven to play a crucial role in the severity of EAE symptoms. HDM Jmjd3 that mainly mediates the demethylation of H3K27me3 was shown to regulate the differentiation of Th17 cells and thereby suppress EAE<sup>240</sup>.

The recognition of epigenetic changes involved in MS opens a broad range of therapeutic approaches that are particularly attractive due to their reversible characteristics. But nevertheless, medication that targets the epigenetic machinery might have adverse side effects and needs to be carefully balanced against the risks. Broad inhibitors of DNMTs or HDACs showed a low specificity and results in a global manipulation of the epigenome, thereby causing unwanted effects in several cell types<sup>241-243</sup>. The development of a targeted epigenetic therapy may represent an alternative strategy to improve clinical outcome of MS patients. Thereby, epigenetic enzymes that catalyze specific modifications and display cell specific functions and alterations during disease might serve as modifiable therapeutic targets with a beneficial effect in the disease course.

### 1.3.3 Transcriptional repression by G9a

Since there is growing evidence for significant roles of epigenetic enzymes in neurodegenerative diseases, the targeting of deregulated enzymes by small molecule compounds has been implemented into human clinical trials. Enzymes involved in histone methylation or demethylation are of particular interest as validated targets for drug discovery, as they have a higher substrate selectivity compared to the low specificity and global action of HDAC or DNMT inhibitors<sup>244</sup>. A well-known KMT is the euchromatic histone N-methyltransferase 2 (EHMT2) or also known as G9a. This enzyme has been mainly investigated in the context of cancer research since G9a has been found to be overexpressed in several types of cancer and is associated with the occurrence and development of tumors. Therefore, G9a has become a very promising target for anti-cancer therapy and several G9a inhibitors have been discovered as potential therapeutic agents<sup>245</sup>. Quite recently, the implication of G9a in neurodegenerative diseases has been discovered and thus it represents a meaningful candidate to characterize its function in inflammation-induced neurodegeneration<sup>246</sup>.

G9a was initially discovered as a key enzyme in the mono- and dimethylation of lysine 9 of histone H3 (H3K9) in euchromatin. The methylation of H3K9 is associated with transcriptional silencing and therefore, G9a is considered as epigenetic repressor<sup>247,248</sup>. In human cells, G9a exists in two isoforms, a full-length isoform (isoform A) containing 24 exons and a splice variant (isoform B) that arises from the extinction of exon 10. The two isoforms of G9a are conserved in different species and tissues and

display a similar methyltransferase activity, but the ratio between the isoforms varies<sup>249</sup>. The mouse G9a is also subjected to alternative splicing, whereas the long isoform (G9a L) lacks exon 1 and includes all of exon 2, while the short isoform (G9a S) contains exon 1 but splices out parts of exon 2<sup>250</sup>. G9a belongs to the Su(var)3-9 family of methyltransferases, which are characterized by the presence of the highly conserved SET domain, harboring the catalytic activity<sup>214</sup>. The core of the SET domain is flanked by a pre-SET (nSET) domain providing structural stability, and a post-SET (cSET) domain that forms a hydrophobic channel. In the core SET domain, G9a contains an inserted iSET domain that forms a docking platform and a substrate binding groove with the cSET domain. For proper folding and enzymatic activity, the SET domain contains four structural zinc fingers<sup>251</sup>. Moreover, G9a contains a cysteine-rich region, a polyglutamate region, nuclear localization signals, and seven ankyrin repeats that bind mono- and dimethyllysine and serves for protein-protein interactions<sup>250</sup>.

A closely related paralog of G9a has been identified and is called G9a-like protein (GLP) or euchromatin histone N-methyltransferase 1 (EHMT1) that exhibits 45 % sequence identity with human G9a and differs primarily in the N-terminus<sup>214</sup>. The binding affinities of the ankyrin domains between the two proteins differ, as GLP preferentially binds to monomethylated H3K9 and G9a to dimethylated H3K9<sup>252</sup>. G9a and GLP form homo- and heterodimers via their SET domains, but endogenously act only as heterodimers in a variety of cell types<sup>253</sup>. However, *in vitro*, both enzymes can catalyze lysine methylation by forming homodimers<sup>254</sup>. Most studies have focused on G9a, even though both enzymes possess similar catalytic activities. Nevertheless, their individual effects are hard to discriminate as G9a depletion destabilizes GLP and vice versa<sup>253</sup>.

The role of the dimethylation of H3K9 has been linked to the transcriptional repression of gene expression that controls functional aspects of development, differentiation, and DNA repair, but is also implicated in several human diseases<sup>245</sup>. In general, a global deficiency of G9a delayed embryonic development and results in lethality at embryonic day 9.5<sup>247</sup>. Neuron-specific deficiency of G9a did not show any obvious neuronal developmental deficits but results in behavioral abnormalities and difficulties in learning and memory<sup>255</sup>. Moreover, G9a contributes to neuronal subtype specification in the adult CNS and thereby is critical for cell type specific histone methylation patterns that regulates behavioral responses to environmental stimuli<sup>256</sup>. Another process where G9a function is involved includes DNA repair mechanisms. G9a is recruited to DNA damage sites in response to phosphorylation and induce local histone methylation and subsequent local transcriptional silencing that is necessary for homologous repair or non-homologous end-joining repair<sup>257</sup>. The function of G9a in the maintenance of genome integrity already suggests the implication of G9a in cancer biology.

The dysregulation of hPTMs that affect chromatin structure and gene expression have been shown to contribute to cancer initiation and progression<sup>258</sup>. Indeed, G9a has been shown to be overexpressed in various types of cancer including ovarian cancer<sup>259</sup>, multiple myeloma<sup>260</sup>, or bladder cancer<sup>261</sup>

leading to aberrant H3K9 methylation. Pharmacological or genetical inhibition of G9a in mouse models have been shown to cause growth suppression<sup>260</sup> and induce apoptotic<sup>262</sup> or autophagic death<sup>263</sup> in cancer cells that impairs its progression. Due to the oncogenic character of G9a it is an excellent target for epigenetic therapy and several potent G9a inhibitors have been developed in recent years<sup>264</sup>, but so far, there are no G9a inhibitors currently in clinical trials.

Recent findings of G9a dysregulation in neurological disorders suggests G9a inhibitors as appealing candidates for the treatment of CNS diseases. H3K9me2 has been found to be upregulated in the prefrontal cortex of AD patients, which was mechanistically investigated in the animal model of AD using the 5xFAD mice, which displayed memory deficits and impaired glutamate receptor expression as well as reduced synaptic transmission. Inhibition of G9a by a small molecule inhibitor restored the behavioral and synaptic dysfunctions of the AD mice<sup>265</sup>. Similarly, it has been shown that G9a inhibition improved cognition in 5xFAD mice and reduced inflammatory markers and  $\beta$ -amyloid plaques in brains of 5xFAD mice<sup>266</sup>. The importance of G9a and its repressive H3K9me2 mark has also been investigated in paradigms of contextual fear-conditioning. H3K9me2 was found increased within the CA1 region of the hippocampus one hour after conditioning and decreased 24 h after context exposure, suggesting that G9a-mediated gene repression is required for proper long-term consolidation of contextual fear memories<sup>267</sup>. Moreover, G9a has been found to be upregulated in Shank3-deficient mice, a model of autism spectrum disorders, whereas pharmacological G9a inhibition rescued autism-like social deficits, and restored NMDA receptor mediated synaptic function<sup>268</sup>. In models of addiction, G9a transcript and H3K9me2 were decreased in the nucleus accumbens in response to cocaine administration<sup>269</sup> but on the other hand, ethanol exposure in postnatal day 7 pups increases G9a protein and its catalyzed methylation mark on H3K9 in the brain<sup>270</sup>, indicating a stimulus specific role of G9a. Moreover, G9a contributes to transcriptional repression in primary sensory neurons implicated in neuropathic pain. Nerve injury resulted in the enrichment of H3K9me2 in promotor regions of potassium channels that could be prevented by using sensory-neuron specific G9a knockout mice<sup>271</sup>. Recently, G9a has also been reported to be deregulated in plasma of MS patients. In a screening approach of plasma proteins of MS patients, protein levels were correlated with disease progression and MRI abnormalities in a way that lower G9a levels were associated with increased brain atrophy<sup>272</sup>.

Epigenetic alterations mediated by G9a in neurological and neuroinflammatory diseases might contribute to the emergence and progression of the disease. Identifying the underlying mechanisms that leads to the propagation of neuronal decay could render new options for the exploration of therapeutics that halt neuronal loss. The role of G9a in MS and its mouse model has only been sparsely explored. Therefore, studying the dynamics of G9a and H3K9me2 during inflammation-induced neurodegeneration can provide new aspects of gene regulation in the context of MS.

## 1.4 Aim of the study

CNS inflammation leads to neuronal loss and dysfunction that causes neurological disability in MS patients. Intrinsic neuronal stress response during immune cell invasion has been linked to transcriptional deregulation that result in the decay of injured neurons. Thus, the modification of transcriptional regulators serves as an option for intervention to enhance neuronal resilience during inflammation-induced neurodegeneration. As epigenetic modifiers broadly regulate transcriptional profiles and have the potential to be targeted by small molecules, the investigation of epigenetic modifiers might reset transcriptional deregulation and improve neuronal survival. In order to study the impact of epigenetic dysregulation in inflammation-induced neurodegeneration, the following aims were addressed:

- 1) Identifying epigenetic modifiers in a mouse model of neuroinflammation
- 2) Establishing cell culture assays to study epigenetic modulation of neuronal function and survival under inflammatory conditions
- 3) Translating an epigenetic therapy approach into a mouse model of neuroinflammation
- 4) Exploring the effects of epigenetic therapy on transcriptional deregulation in neuroinflammation
- 5) Translating findings into a human neuronal cell culture system

This approach will gain insights into the regulation of the epigenome during inflammation-induced neurodegeneration and will propose strategies to develop neuroprotective treatments for neurodegenerative disorders.

## 2 Material and Methods

### 2.1 Material

#### 2.1.1 Laboratory animals

All animals were housed and bred under specific pathogen-free conditions at the central animal facility of the University Medical Center Hamburg-Eppendorf (UKE). Mice were kept at 55 – 65 % humidity at 18 - 23 °C with a 12 h light / dark cycle and were provided with food and water ad libitum. Two weeks before an experiment started, mice were transferred into the experimental barrier. All experiments were approved by the local ethics committee (Behörde für Soziales, Familie, Gesundheit und Verbraucherschutz in Hamburg), Tierversuchsantrag Nr. 122/17 and ORG 713 or ORG 946.

Table 2.1: Mouse strains

Mouse strain	Official symbol	Origin
C57BL/6J	C57BL/6J	The Jackson Laboratory, stock number 000664
<i>G9α<sup>fl/fl</sup></i>	Ehmt2tm1.1Tara	The Rockefeller University, New York, Dr. Tarakhovsky
<i>Snap25-Cre</i>	B6;129S-Snap25tm2.1(cre)Hze/J	The Jackson Laboratory, stock number 023525

#### 2.1.2 Clinical data of brain specimens

Experiments with human material were performed in the laboratories of Prof. Dr. Doron Merkler in Geneva.

Table 2.2: Clinical data of brain specimens

Sample	Group	Details	Age	Sex	Region	Note	Analysis
C1	Control	NND	55	F	Frontal cortex		IF
C2	Control	NND	43	M	Frontal cortex		IF
C3	Control	NND	45	F	Frontal cortex		RNAscope; IF
C4	Control	NND	68	F	Frontal cortex		RNAscope; IF
C6	Control	NND	64	M	Occipital cortex		IF
C7	Control	NND	45	F	Cingular cortex		IF
C8	Control	NND	45	F	Frontal cortex		IF
C9	Control	NND	55	F	Frontal cortex		RNAscope
MS1	MS	RRMS	50	F	Frontal cortex - inferior frontal gyrus		RNAscope; IF
MS2	MS	RRMS	50	F	Frontal cortex - superior frontal gyrus	Same patient as MS1 but different lesion	RNAscope; IF
MS3	MS	RRMS	53	F	Cingular cortex		RNAscope; IF

MS4	MS	RRMS	57	F	Parietal cortex		RNAscope; IF
NAGM 1	NAGM	RRMS	54	M	Occipital cortex		RNAscope; IF
NAGM 2	NAGM	RRMS	54	M	Occipital cortex	Same patient as NAGM1	RNAscope; IF
NAGM 3	NAGM	RRMS	45	M	Posterior parietal cortex		IF
NAGM 4	NAGM	RRMS	50	F	Frontal cortex - inferior frontal gyrus	Same patient as MS1 but NAGM – different block	RNAscope; IF
NAGM 5	NAGM	RRMS	50	F	Frontal cortex - superior frontal gyrus	Same patient as MS1 but NAGM – different block	RNAscope; IF

### 2.1.3 Chemicals and reagents

Table 2.3: Reagents for animal experiments

Reagent	Company
CO <sub>2</sub> gas (100%)	SOL Deutschland
CO <sub>2</sub> /O <sub>2</sub> gas mixture (80% CO <sub>2</sub> , 20% O <sub>2</sub> )	SOL Deutschland
DietGel Recovery	Clear H <sub>2</sub> O
Incomplete Freund's adjuvant	BD Biosciences
Ketanest® S 25mg/ml (Ketamine)	Pfizer Pharma
MOG <sub>35-55</sub> peptide	Peptides & elephants
Mycobacterium tuberculosis	BD Biosciences
PBS (1x)	Pan-Biotech
Pertussis toxin (Bordetella pertussis)	Calbiochem (Merck)
Rompun® 2% (Xylazine)	Bayer
UNC0642	Sigma-Aldrich
Dimethyl sulfoxide (DMSO)	Merck

Table 2.4: Reagents for genotyping

Reagent	Company
Agarose Ultra Pure	Life Technologies (Merck)
ddH <sub>2</sub> O	Generated in house
dNTP Mix (10 mM)	Thermo Fisher Scientific
DreamTaq GREEN Hot Start Buffer 10x	Thermo Fisher Scientific
DreamTaq Hot Start Green DNA Polymerase	Thermo Fisher Scientific
GeneRuler 1 kb DNA Ladder	Thermo Fisher Scientific
Genotyping master mix (2x)	Thermo Fisher Scientific
QuickExtract DNA Extraction Solution	Lucigen
RotiSafe	Carl Roth
Tris Ultrapure	Applichem

Table 2.5: Reagents for flow cytometry and fluorescence-activated cell sorting

Reagent	Company
123 Counting eBeads™ Counting Beads	Invitrogen
BD FACS Clean Solution	BD Biosciences
BD FACS Flow	BD Biosciences
BD FACS Rinse Solution	BD Biosciences
Bovine serum albumin (BSA)	Merck
Brilliant Stain Buffer	BD Biosciences
Collagenase A	Roche
ddH <sub>2</sub> O	Generated in house
DNase I	Merck
EtOH reagent	Th.Geyer
Fetal calf serum (FCS)	Biochrome (Merck)
Hoechst 33342	Thermo Fisher Scientific
Methanol	Carl Roth
PBS (1×)	Pan-Biotech
Percoll (1.13 g ml <sup>-1</sup> )	GE Healthcare
Propidium Iodide	BioLegend
RPMI 1640 medium	Pan-Biotech
Sodium azide (NaN <sub>3</sub> )	Carl Roth
UltraComp eBeads (compensation beads)	Thermo Fisher Scientific
V500 live/dead stain	Thermo Fisher Scientific

Table 2.6: Reagents for immunocytochemistry, immunohistopathology and RNAscope

Reagent	Company
High Precision Microscope Cover Glasses	Marienfeld
Hoechst 33342	Thermo Fisher Scientific
Hs-GPX4 probe for RNAscope	Advanced Cell Diagnostics (ACD)
Hs-Snap25 probe for RNAscope	Advanced Cell Diagnostics (ACD)
Microscope Slides	Carl Roth
Normal Donkey Serum (NDS)	Merck
Paraformaldehyde (PFA)	Sigma-Aldrich
PBS (1×)	Pan-Biotech
Peroxidase-blocking solution	Dako
RNAscope® Multiplex Fluorescent Reagent Kit v2	Advanced Cell Diagnostics (ACD)
ROTI®Mount FluorCare	Carl Roth
Triton-X®100	Carl Roth

Table 2.7: Compounds for cell culture experiments

Compound	Chemical name	Company	Catalogue no.	Concentration used <i>in vitro</i>	Function
AP5	D-(-)-2-amino-5-phosphonopentanoic acid	Abcam	ab120003	100 $\mu$ M	Inhibitor of NMDA glutamate receptor
Coenzyme Q <sub>10</sub>		Sigma-Aldrich	C9538	0.25 $\mu$ M	Antioxidant
DFMO	DL- $\alpha$ -Difluoromethylornithine hydrochloride hydrate	Sigma-Aldrich	D193	75 $\mu$ M	Iron chelator
EGTA	Ethylene glycol-bis(2-aminoethylether)-N,N,N',N'-tetraacetic acid	Sigma-Aldrich	E3889	2 mM	Calcium chelator
Erastin		Selleckchem	S7242	30 $\mu$ M (mouse) 500 $\mu$ M (human)	Ferroptosis activator
Ferrostatin-1	3-Amino-4-cyclohexylaminobenzoic acid ethylester	Sigma-Aldrich	SML0583	0.3 $\mu$ M	Antioxidant
Glutamate	L-Glutamic acid monosodium salt monohydrate	Sigma-Aldrich	49621	20 $\mu$ M	Excitatory amino acid and neurotransmitter
H <sub>2</sub> O <sub>2</sub>	Hydrogen peroxide	Sigma-Aldrich	216763	200 $\mu$ M (ICC) 1 mM (Ca imaging)	Induction of oxidative damage
IFN- $\gamma$	Interferon-gamma	Peprtech	315-05	200 ng/mL	Cytokine
Ionomycin	Ionomycin calcium salt	Alomone Labs	I-700	8 $\mu$ M	Ionophore
LCL-161		Selleckchem	S7009	20 $\mu$ M	Second mitochondrial activator of caspase (SMAC)
NBQX	2,3-Dioxo-6-nitro-1,2,3,4-tetrahydrobenzo[f]quinoxaline-7-sulfonamide disodium salt	Abcam	ab120046	20 $\mu$ M	Inhibitor of AMPA and kainate glutamate receptors
RSL3	1S,3R-RSL 3	Sigma-Aldrich	SML2234	5 $\mu$ M	Ferroptosis activator
Shikonin		Sigma-Aldrich	S7576	1 $\mu$ M	Necroptosis activator
STS	Staurosporine	Sigma-Aldrich	11055682001	100 nM	Apoptosis induction
TNF $\alpha$	Tumour necrosis factor-alpha	Peprtech	315-01A	200 ng/mL	Cytokine
TTX	Tetrodotoxin	Tocris	1078	1 $\mu$ M	Silencing of neurons
UNC0642		Sigma-Aldrich	SML1037	1 $\mu$ M	Selective inhibitor of G9a (EHMT2) and GLP (EHMT1)
Z-VAD-FMK	Z-VAD(OMe)-FMK	Selleckchem	S7023	20 $\mu$ M	Pan caspase inhibitor

Table 2.8: Assays and plasmids for cell culture experiments

Assay	Company
CellROX™ Green Reagent	Thermo Fisher Scientific
CellTox™ Green Cytotoxicity Assay	Promega
GSH-Glo™ Glutathione Assay	Promega
pAAV-Syn-GCamp6f-WPRE-SV40	Addgene
RealTime™ MT Cell Viability Assay	Promega

Table 2.9: Reagents for nuclei extraction

Reagent	Company
Bovine serum albumin (BSA)	Merck
EDTA 0.5 M	Thermo Fisher Scientific
Glycerol	Sigma-Aldrich
Magnesium Chloride	Merck
Nonident® P40	Sigma-Aldrich
Potassium Chloride	Merck
RiboLock RNase Inhibitor (40 U $\mu\text{l}^{-1}$ )	Thermo Fisher Scientific
Sodium Chloride	Sigma-Aldrich
Succrose	Sigma-Aldrich
Tris Ultrapure	Applichem
$\beta$ -Glycerophosphat Dinatriumsalz Hydrat	Sigma-Aldrich

Table 2.10: Reagents for RNA isolation and quantitative real-time PCR

Reagent	Company
RNeasy® Mini Kit	Qiagen
$\beta$ -Mercaptoethanol	Sigma-Aldrich
Ethanol, absolute, $\geq 99.8\%$	Sigma-Aldrich
RevertAid First Strand cDNA Synthesis Kit	Thermo Fisher Scientific
TaqMan™ Gene Expression Master Mix, 2 $\times$	Thermo Fisher Scientific
RNase-Free water	Thermo Fisher Scientific
TaqMan™ Primers	Thermo Fisher Scientific

#### 2.1.4 Primer, antibodies, and Taqman probes

Table 2.11: Primer for genotyping

Primer	Sequence	Mouse line	Company
G9a fwd1	cacgctgcctagatggagcatgcc	<i>G9a<sup>fl/fl</sup></i> <i>G9a<sup>fl/fl</sup>;Snap25-Cre</i>	Biomers
G9a fwd2	cgaggctatgagaatgtaccatcccctg	<i>G9a<sup>fl/fl</sup></i> <i>G9a<sup>fl/fl</sup>;Snap25-Cre</i>	Biomers
G9a rev	gtgtgagcctgtgttctggggatta	<i>G9a<sup>fl/fl</sup></i> <i>G9a<sup>fl/fl</sup>;Snap25-Cre</i>	Biomers
Snap25-Cre fwd common	aacgtgcaacaagatgctg	<i>G9a<sup>fl/fl</sup>;Snap25-Cre</i>	Biomers
Snap25-Cre rev MT	ctgcaaagggtcgctacag	<i>G9a<sup>fl/fl</sup>;Snap25-Cre</i>	Biomers

Snap25-Cre rev WT      aatgggggtgactgactctg      *G9a<sup>fl/fl</sup>;Snap25-Cre*      Biomers

Table 2.12: Primary antibodies

Antigen	Host species	Company	Catalogue no.	Clone	Ig fraction	Fluorophore	Dilution ICC	Dilution IHP	Dilution FACS
4-HNE	Rabbit	Abcam	ab46545					1:50	
CD11b	Rat	BioLegend	101228	M1/70	IgG	PerCP-Cy5.5			1:400
CD11c	Armenian hamster	BioLegend	117318	N418	IgG	PE-Cy7			1:300
CD19	Rat	BioLegend	115539	6D5	IgG	BV650			1:400
CD3	Rabbit	Abcam	Ab16669		IgG			1:100	
CD3e	Armenian hamster	BioLegend	100305	145-2C11	IgG	FITC			1:100
CD317	Rat	BioLegend	127015	927	IgG	APC			1:100
CD45	Rat	BioLegend	103127	30-F11	IgG	AF700			1:200
CD8a	Rat	BioLegend	100750	53-6.7	IgG	BV785			1:200
COX-2	Rabbit	Abcam	ab179800	EPR12012			1:200		
DNMT3a	Rabbit	Abcam	ab188470	EPR18455			1:1000		
F4/80	Rat	BD	565411	T45-2342	IgG	BV421			1:100
G9a	Rabbit	Abcam	ab185050	EPR18894			1:500		1:500
H3K27ac	Rabbit	Abcam	ab177178	EP16602			1:8000		
H3K27me3	Rabbit	Abcam	ab192985	EPR18607			1:1000		
H3K9me1	Rabbit	Abcam	ab176880	EPR16989			1:2000		
H3K9me2	Mouse	Abcam	Ab1220				1:500		1:200
Ly6G	Rat	BioLegend	127623	1A8	IgG	APC-Cy7			1:200
Map2	Chicken	Abcam	Ab5392		IgY		1:3000		
MHCII	Rat	BioLegend	107643	M5/14.15.2	IgG	BV711			1:400
NeuN	Chicken	Millipore	ABN91		IgG		1:1000		1:200
NeuN	Rabbit	Abcam	Ab190565		IgG	AF647			1:500
NeuN	Rabbit	Abcam	ab190195			AF488		1:50	
NK1.1	Mouse	eBioscience	12-5941-82	PK136	IgG	PE			1:100

Table 2.13: Secondary antibodies

Antigen	Host species	Company	Catalogue no.	Fluorophore	Dilution
Ig chicken	Donkey	Jackson Immuno Research	703-545-155	AF488	1:500
Ig chicken	Donkey	Jackson Immuno Research	703-606-155	AF647	1:500
Ig chicken	Goat	Abcam	Ab97145	Cy3	1:500
Ig mouse	Donkey	Jackson Immuno Research	715-605-151	AF647	1:200
Ig mouse	Donkey	Abcam	Ab150111	AF647	1:500
Ig mouse	Donkey	Abcam	Ab175658	AF647	1:500
Ig rabbit	Donkey	Abcam	Ab150105	AF647	1:500

Table 2.14: Taqman assays

Gene	Target species	Assay ID	Amplification length
AcsL4	Mouse	Mm00490331_m1	96 bp
ACSL4	Human	Hs00244871_m1	86 bp
AIFM2	Human	Hs01097300_m1	82 bp
Cbs	Mouse	Mm00460654_m1	125 bp
CBS	Human	Hs00163925_m1	59 bp
Ehmt2	Mouse	Mm01132260_m1	75 bp
Fsp1	Mouse	Mm00464061_m1	82 bp
Gclc	Mouse	Mm00802655_m1	98 bp
GCLC	Human	Hs00155249_m1	92 bp
Gpx4	Mouse	Mm00515041_m1	103 bp
GPX4	Human	HS00157812_m1	123 bp
Gss	Mouse	Mm00515065_m1	67 bp
Gsta4	Mouse	Mm00494803_m1	87 bp
Gstm1	Mouse	Mm00833915_g1	177 bp
Gstm4	Mouse	Mm01203622_g1	62 bp
Gstm5	Mouse	Mm00515890_m1	66 bp
Gstm6	Mouse	Mm01200184_m1	89 bp
Gstp1	Mouse	Mm00496606_m1	68 bp
Gstt2	Mouse	Mm00494804_g1	62 bp
Nfe2l2	Mouse	Mm00477784_m1	61 bp
Slc3a2	Mouse	Mm00441483_m1	87 bp
Slc7a11	Mouse	Mm00442530_m1	66 bp
SLC7A11	Human	Hs00921938_m1	57 bp
Tbp	Mouse	Mm01277042_m1	65 bp
TBP	Human	Hs00427620_m1	91 bp

## 2.1.5 Buffers, solutions, and media

Table 2.15: Media and supplements for cell culture

Name	Ingredients	Company
CultureOne		Stem Cell Technologies
Cyclopamin		Stem Cell Technologies
Cytosine $\beta$ -D-arabinofuranoside (AraC)		Sigma-Aldrich
DMEM/F-12 (Dulbecco's Modified Eagle Medium/Nutrient Mixture F-12)	500 ml DMEM/F-12 50 ml FCS	Thermo Fisher Scientific
Hanks' Balanced Salt Solution (HBSS)		Thermo Fisher Scientific
Hibernate™ -E Medium		Thermo Fisher Scientific
L-glutamic acid		Sigma-Aldrich
mTeSR1 medium		Stem Cell Technologies
Neural differentiation medium	Neurobasal™ Plus medium 10 ml B27 Plus Supplement 1× N2 Supplement-A 1× MEM non-essential amino acids 1 $\mu$ g ml <sup>-1</sup> laminin 1 $\mu$ M dibutyryl-cAMP 10 ng ml <sup>-1</sup> L-ascorbic acid 10 ng ml <sup>-1</sup> brain-derived neurotrophic factor 10 ng ml <sup>-1</sup> glial-derived neurotrophic factor	Gibco Gibco Stem Cell Technologies Gibco Sigma-Aldrich Stem Cell Technologies Stem Cell Technologies Stem Cell Technologies
Neurobasal plus feeding medium	500 ml Neurobasal™ Plus 5 ml Penicillin-Streptomycin (100 U ml <sup>-1</sup> ) 5 ml GlutaMAX™ (100×) 10 ml B-27™ Supplement	Gibco Thermo Fisher Scientific Gibco Gibco
Neurobasal plus plating medium	500 ml Neurobasal™ Plus 5 ml Penicillin-Streptomycin (100 U ml <sup>-1</sup> ) 5 ml GlutaMAX™ (100×) 10 ml B-27™ Supplement 12.5 $\mu$ l 1 M glutamate	Gibco Thermo Fisher Scientific Gibco Gibco Sigma-Aldrich
Neuronal Progenitor Medium		Stem Cell Technologies
Poly-D-Lysine hydrobromide		Sigma-Aldrich
SMADi Neural Induction Medium	250 ml SMADi Neural Induction Medium 10 $\mu$ M Y-27632	Stem Cell Technologies Stem Cell Technologies
Trypsin-EDTA (0.05%), phenol red		Gibco

Table 2.16: Buffers and solutions

Name	Ingredients
CNS digestion solution	1 mg ml <sup>-1</sup> Collagenase A 0.1 mg ml <sup>-1</sup> DNase I In RPMI 1640
FACS Buffer	0.5 % BSA

	0.02 % NaN <sub>3</sub> In 1x PBS
Nuclei incubation buffer	340 mM Succrose 2 mM MgCl <sub>2</sub> 25 mM KCl 65 mM Glycerophosphate 5 % Glycerol 1 mM EDTA 1 % BSA In H <sub>2</sub> O
Nuclei lysis buffer	10 mM Tris 10 mM NaCl 5 mM MgCl <sub>2</sub> 0.5 % NP-40 In H <sub>2</sub> O
Tris-acetate EDTA (TAE) Buffer, 50×	5.7 % Acetic acid 0.05 M EDTA 2 M Tris In H <sub>2</sub> O

### 2.1.6 Consumables

Table 2.17: Consumables

Name	Company
Butterfly Cannula	Sarstedt
Cell Culture Dishes (10 cm)	Thermo Fisher Scientific
Cell scrapers, 16 cm handle length	Sarstedt
Cellstar EasyStrainer (100 μm)	Greiner
Disposable hemocytometer	NanoEntek
Micro tubes (0.5 ml, 1.5 ml, 2 ml, 5 ml)	Sarstedt
FACS tubes 5 ml	Sarstedt
Falcon tubes	Greiner
Filter tips	Sarstedt
MACS® SmartStrainers (30 μm)	Miltenyi Biotec
Micor-Amp® Optical 384-well reaction plate	Applied biosystems
Multiwell plates (96-well, 24-well, 12-well, 6-well)	Greiner
Parafilm N	Carl Roth
PCR plate sealing tape	Sarstedt
Pipette tips	Sarstedt
Pre-Separation Filters (30 μm)	Miltenyi Biotec
Reservoir for multichannel pipettes	Integra
RNase Zap™	Invitrogen
RNase-free Microfuge tubes	Applied biosystems
Serological pipettes (5 ml, 10 ml, 25 ml)	Greiner, Sarstedt
StarGard® Comfort gloves	Starlab
Syringes and cannulas	Braun, BD Biosciences
μ-Dish 35 mm Quad	Ibidi

## 2.1.7 Equipment and devices

Table 2.18: Equipment and devices

<b>Name</b>	<b>Company</b>
BD FACS Aria III cell sorter	BD Biosciences
BD FACS LSR II analyser	BD Biosciences
Bench Top Micocentrifuge	Eppendorf
Binocular Stereo Microscope	Leica
Biometra Low Voltage Power supply	Analytik Jena
Biometra Thermocycler	Analytik Jena
Centrifuge	Heraeus
Computer	HP
Epifluorescence Microscope Eclipse	Nikon
Eppendorf® Thermomixer Compact	Eppendorf
Freezer (- 20 °C)	Liebherr
Freezer (- 80 °C)	Sanyo
Fridge (4 °C)	Liebherr
Fume hood	Belec Vario Lab
Gel documentary device	INTAS Science Imaging
Glass douncer	Sigma-Aldrich
Incubator	Thermo Fisher Scientific
Light Microscope	Olympus
LSM700 confocal laser scanning microscope	Zeiss
NanoDrop™ 1000 Spectrophotometer	Thermo Fisher Scientific
NanoZoomer 2.0-RS digital slide scanner	Hamamatsu
Pannoramic 250 FLASH II	3DHISTECH
Perfusion System	Ismatec
Picus® Electronical Pipettes	Picus® Electronical Pipettes
Pipettes	Gilson
QuantStudio™ 6 Flex Real-Time PCR Instrument	Thermo Fisher Scientific
SevenCompact pH-meter	Mettler-Toledo
Spark™ 10M Multimode microplate reader	Tecan
Sterile hood	Thermo Fisher Scientific
Surgical instruments	FST Fine Scientific Tools
Tabletop centrifuge	Thermo Fisher Scientific
Water bath	GFL

### 2.1.8 Software

Table 2.19: Software

<b>Name</b>	<b>Company</b>
Adobe Illustrator (version 25.4.1)	Adobe Inc.
Cognition Network Language	Definiens Cognition Network Technology; Definiens Developer XD software
FACS Diva™	BD Biosciences
Fiji (ImageJ)	Open source ( <a href="https://imagej.nih.gov/ij/index.html">https://imagej.nih.gov/ij/index.html</a> )
FlowJo v10	BD Biosciences
MATLAB	TheMathWorks
Microsoft Office	Microsoft
NDP.view2 software	Hamamatsu
Prism v9.2.0	Graph Pad Software
QuantStudio	Applied Biosystems
R Studio v.1.4	<a href="https://rstudio.com">https://rstudio.com</a>
TBase Client 4Dv12sql	MacKeeper
Zen black	Zeiss

## 2.2 Methods

### 2.2.1 Genotyping

Genetically modified mice were genotyped by polymerase chain reaction (PCR). Mouse tail biopsies from newborn mice were taken by the animal facilities at the UKE, ear biopsies were taken from experimental mice to verify the genotype, and brain tissue was taken from embryos of transgenic mice for primary neuronal cultures. Tissue samples were lysed in 50  $\mu$ l QuickExtract™ DNA extraction solution for 6 min at 65 °C, followed by heat inactivation at 98 °C for 2 min and extracted DNA was used as a template for following PCR.

*G9a<sup>fl/fl</sup>* mice were genotyped using the primers G9a fwd1, G9a fwd2, and G9a rev. This PCR detects the wildtype allele, the floxed allele, and the deleted allele by 400 bp, 504 bp, and 680 bp amplicon, respectively. For the reaction 2  $\mu$ l of DNA was added to a master mix containing 18.75  $\mu$ l ddH<sub>2</sub>O, 2.5  $\mu$ l Dream Green Hotstart Taq Buffer (10 $\times$ ), 0.5  $\mu$ l dNTPs (10 mM), 0.25  $\mu$ l Dream Green Hotstart Taq polymerase, and 0.5  $\mu$ l of each primer (10  $\mu$ M). PCR amplification was done in a thermal cycler at following conditions: 94 °C for 5 min, 35 cycles of 94 °C, 63 °C, and 72 °C steps for 30, 60, and 60 seconds, respectively, 72 °C for 10 min.

The presence of synaptosome associated protein 25 (*Snap25*) Cre was confirmed by using the primers Snap25-Cre fwd common, Snap25-Cre rev WT, and Snap25-Cre rev MT, which resulted in a 195 bp amplicon in Cre-negative mice and a 308 bp amplicon in Cre-positive mice. The PCR was performed by mixing 2  $\mu$ l of DNA with a master mix containing 16.83  $\mu$ l ddH<sub>2</sub>O, 2.5  $\mu$ l Dream Green Hotstart Taq Buffer (10 $\times$ ), 0.5  $\mu$ l dNTPs (10 mM), 0.17  $\mu$ l Dream Green Hotstart Taq Polymerase, and 1.0  $\mu$ l of each primer (10  $\mu$ M). Amplification of DNA was done in a thermal cycler using following program: 95 °C for 5 min, 12 cycles of 95 °C, 66 °C, and 72 °C steps for 30 seconds each, 17 cycles of 95 °C, 54 °C, and 72 °C steps for 30 seconds each, 72 °C for 10 min.

PCR products were resolved by agarose gel electrophoreses on a 1.5 % gel containing RotiSafe (diluted 1:500) and visualized on a UV transilluminator.

### 2.2.2 Experimental autoimmune encephalomyelitis

For EAE induction mice were actively immunized<sup>273</sup> with 200  $\mu$ g MOG<sub>35-55</sub> peptide. Therefore, mice were anesthetized with isoflurane and thereby received two subcutaneous injections of 50  $\mu$ l of a 1:1 mixture of MOG<sub>35-55</sub> peptide in phosphate buffered saline (PBS) (4 mg ml<sup>-1</sup>) and complete Freund's adjuvant with 4 mg ml<sup>-1</sup> *Mycobacterium tuberculosis* into the flanks of the hind limbs. In addition, 300 ng pertussis toxin solved in ddH<sub>2</sub>O and diluted in PBS was injected intraperitoneally on the day of immunization and 48 hours later. Animals were scored daily for clinical signs by the following system: 0, no clinical deficits; 1, tail weakness; 2, hind limb paresis; 3, partial hind limb paralysis; 3.5, full hind

limb paralysis; 4, full hind limb paralysis and fore limb paresis; 5, premonitory or dead. Animals reaching a clinical score  $\geq 4$  were euthanized according to the regulations of the local Animal Welfare Act. Where indicated, animals were injected intraperitoneally with  $5 \text{ mg kg}^{-1}$  UNC0642 starting from day of disease onset. UNC0642 was prediluted in DMSO ( $5 \text{ mg ml}^{-1}$ ) and the final injection contained 10 % DMSO  $\pm$  UNC0642 and 90 % PBS. For treatment EAEs female C57BL/6J mice were used, and for genotype EAEs littermate mice from both genotypes and sexes were used. Animals which did not get sick were excluded from statistical analysis.

### 2.2.3 Candidate gene identification

The previously generated RNA-Seq dataset of spinal cord motor neuronal transcriptomes during CNS inflammation in the EAE model<sup>274</sup> was reanalyzed by Dr. Dr. Jan Broder Engler to extract known epigenetic regulators (dbEM - a Database of Epigenetic Modifiers) that were differentially expressed in inflamed vs. healthy motor neurons. Differential expression analysis was performed with DESeq2 (v.1.14.1) calling genes with a minimal twofold change and false discovery rate (FDR)-adjusted  $P < 0.05$  differentially expressed.

### 2.2.4 Isolation of CNS-infiltrating immune cells and flow cytometry

For isolation of CNS infiltrating cells, mice were anesthetized with a mixture of 80 %  $\text{CO}_2$  and 20 %  $\text{O}_2$  and consecutively sacrificed with 100 %  $\text{CO}_2$ . Mice were subsequently intracardially perfused with 10 ml ice-cold PBS to remove leucocytes from intracranial blood vessels. Brain and spinal cord were prepared with sterile instruments, minced with a scalpel, and incubated with agitation in 10 ml CNS digesting solution containing  $1 \text{ mg ml}^{-1}$  Collagenase A and  $0.1 \text{ mg ml}^{-1}$  DNase I in RPMI 1640 medium at  $37^\circ\text{C}$  for 45 min. Tissue was triturated through a  $100 \mu\text{m}$  cell strainer and washed with 40 ml PBS (pellet was centrifuged at 300g for 10 min at  $4^\circ\text{C}$ ) to obtain a single cell suspension. Cells were resuspended in 4 ml 30 % isotonic Percoll solution diluted in RPMI 1640 and carefully underlaid with 78 % isotonic Percoll solution in PBS. After gradient centrifugation (2,500 g for 30 min at  $4^\circ\text{C}$ , acceleration 1, deceleration 1), CNS-infiltrating immune cells were recovered from the gradient interphase and washed in 15 ml ice-cold PBS (1,800 g for 10 min at  $4^\circ\text{C}$ ). Immune cells were resuspended in  $800 \mu\text{l}$  fluorescence activated cell sorting (FACS) buffer and were stained for different immune cell subsets. Therefore, cell suspension was transferred to a 5 ml FACS tube and centrifuged (1,500 rpm for 5 min) followed by incubation in PBS supplemented with Fc block (1:250) to reduce unspecific binding of antibodies and V500 live/dead stain for 10 min at  $4^\circ\text{C}$ . Afterwards, a cocktail of directly labeled antibodies diluted in BD Brilliant Stain Buffer was added and incubated for 20 min at  $4^\circ\text{C}$  (Table 2.12, Table 2.20). Cell suspension was washed with 2 ml FACS buffer (1,500 rpm for 5 min)

and resuspended in 300  $\mu$ l FACS buffer. The exact volume was measured for further analysis of absolute cell count. Finally, 50  $\mu$ l of 123 counting beads diluted at 1:1 ratio in FACS buffer was added to the stained cell suspension to quantify the absolute cell count of immune cells.

Table 2.20: BD FACS LSR II analyzer configuration and staining panel

Laser	Detector	Dichroic Mirror	Bandpass Filter	Fluorochrome	Antigen	Dilution
488 nm (blue)	E	505 LP	530/30 513/17	FITC	CD3e	1:100
	D	550 LP	575/26	PE	NK1.1	1:300
	C	600 LP	610/20	PE-TxRed		
	B	685 LP 635 LP	695/40 670/14	PerCP/Cy5.5	CD11b	1:400
	A	735 LP	780/60	PE-Cy7	CD11c	1:300
405 nm (violet)	F		450/50	BV421	F4/80	1:100
	E	505 LP	525/50	V500	L/D	1:1000
	D	600 LP	610/20	BV605		
	C	630 LP	660/20	BV650	CD19	1:400
	B	690 LP	710/50	BV711	MHC II	1:400
	A	750 LP	780/60	BV786	CD8	1:200
633 nm (red)	C		660/20	APC	CD317	1:100
	B	710 LP	730/45	Alexa700	CD45	1:200
	A	755 LP	780/60	APC-Cy7	Ly6G	1:200

The acquisition of single cell events was obtained at the BD FACS LSR II analyzer and events recorded by FACSDiva™ software. Further analysis and manual gating were performed by using FlowJo v10 software.

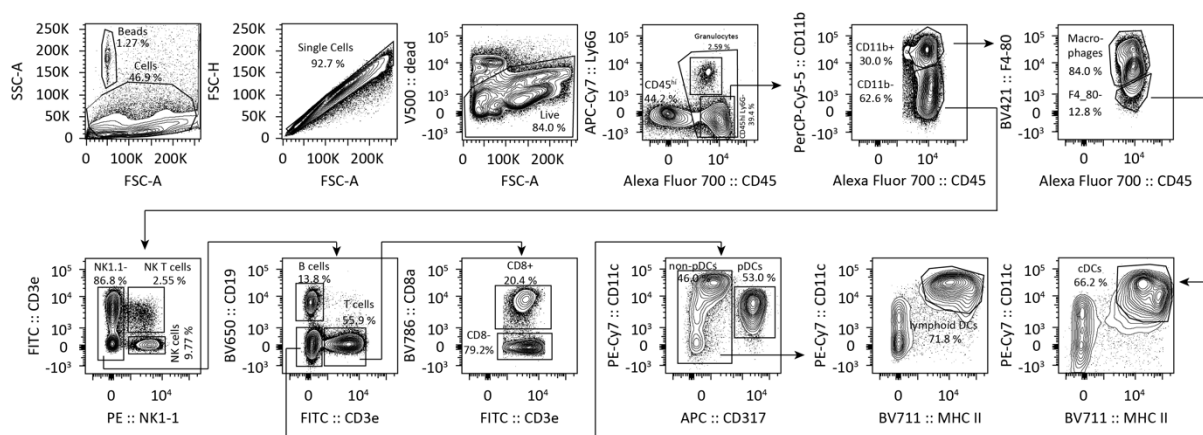


**Figure 2.1: Gating strategy for immune cell subsets.** Lymphocytes were identified according to their size and granularity (SSC and FSC) and were discriminated from counting beads. Doublets were excluded by gating height against area of the forward scatter. Dead cells were excluded by V500 live/dead stain and living lymphocytes were further analyzed by gating CD45<sup>high</sup> cells. Granulocytes were identified as CD45<sup>high</sup>/Ly6G<sup>+</sup>. For macrophages CD45<sup>high</sup>/Ly6G<sup>-</sup>/CD11b<sup>+</sup>/F4\_80<sup>+</sup> surface markers were used. NK cells and NK T cells were gated in the CD11b<sup>-</sup> negative fraction. NK1.1<sup>-</sup> cells were separated into B cells (CD3e<sup>-</sup>/CD19<sup>+</sup>) and T cells (CD19<sup>-</sup>/CD3e<sup>+</sup>). T cells were further discriminated into CD8<sup>+</sup> and CD8<sup>-</sup> (CD4) populations. DCs were analyzed by either gating F4\_80<sup>-</sup> cells to identify conventional DCs (MHCII<sup>+</sup>/CD11c<sup>+</sup>) or by discriminating NK1.1<sup>-</sup>/CD19<sup>-</sup>/CD3e<sup>-</sup> cells to gate plasmacytoid DCs as CD317<sup>+</sup> and lymphoid DCs as CD317<sup>-</sup>/CD11c<sup>+</sup>/MHCII<sup>+</sup>.

### 2.2.5 Mouse Immunohistopathology

Mice were anesthetized by an intraperitoneal injection of Ketamine/Xylazine (12 mg ml<sup>-1</sup>/1.6 mg ml<sup>-1</sup>) in NaCl. For immunohistopathology (IHP) mice were first perfused with PBS followed by perfusion with ice-cold 4 % paraformaldehyde (PFA) solution diluted in PBS by using a perfusion system. Spinal cord tissue was dissected and post-fixed in 4 % PFA solution for 24 h. Following fixation, tissue was decalcified, dehydrated, cast in paraffin, and stained according to the standard procedures of the UKE Mouse Pathology Facility. The tissue was stained with hematoxylin (blue color) for orientation, followed by immunolabeling, that was visualized using the avidin–biotin complex technique with 3,3'-diaminobenzidine (brown stain). Antibodies and used concentrations are summarized in Table 2.12. Slides were analyzed with a NanoZoomer 2.0-RS digital slide scanner and NDP.view2 software. CD3-positive cells were manually quantified in the white matter tract of the spinal cord and NeuN-positive cells (neurons) were manually counted in the ventral horn outflow tract of the spinal cord. Area of 4-hydroxynonenal (4-HNE) and Iba1 staining's were analyzed with a customized mask using Fiji. Analysis conditions were standardized across all groups. At least three images were analyzed per animal and the mean per animal was used for subsequent statistical comparisons.

### 2.2.6 Human Immunohistochemistry

Human tissue was stained by immunohistochemistry (IHC) in the laboratory of Prof. Dr. Doron Merkler in Geneva. Clinical data about the brain specimen are in detail described in Table 2.2. CNS tissues were fixed with 4 % PFA and embedded in paraffin. After deparaffination and antigen retrieval (Tris ethylenediaminetetraacetic acid (EDTA) pH 9.0), the 2 µm sections were incubated with a peroxidase-blocking solution to inactivate endogenous peroxidases and unspecific binding was blocked in PBS supplemented with 10 % goat serum. Tissue sections were incubated overnight with primary antibodies (H3K9me2 and NeuN-AF488, for details Table 2.12) and H3K9me2 bound antibodies were visualized using a donkey anti-mouse secondary antibody. Immunostained human samples were scanned using the Panoramic 250 FLASH II (3DHISTECH) Digital Slide Scanner at 20× magnification. Mean fluorescence intensity (MFI) of H3K9me2 from NeuN-positive cells was quantified using Fiji software.

### 2.2.7 RNAscope *in situ* hybridization

RNAscope *in situ* hybridization on human brain tissue was performed in the laboratory of Prof. Dr. Doron Merkler in Geneva. Clinical data about the brain specimen are in detail described in Table 2.2. RNAscope was performed by using RNAscope Fluorescent Multiplex V2 Kit according to the manufacturer standard protocol for PFA fixed tissue. The human probe Hs-*GPX4* and Hs-*SNAP25* were

commercially available from ACD. RNAscope human samples were scanned using the Panoramic 250 FLASH II (3DHISTECH) Digital Slide Scanner at 20× magnification. *GPX4+ SNAP25+* neurons were quantified by a blinded experimenter using a custom-made script, which was based on Cognition Network Language (Definiens Cognition Network Technology; Definiens Developer XD software).

### 2.2.8 Primary mouse neuronal culture

For primary cortical cultures pregnant C57BL/6J or *G9α<sup>fl/fl</sup>;Snap25-Cre* mice were anesthetized with a mixture of 80 % CO<sub>2</sub> and 20 % O<sub>2</sub> and sacrificed with 100 % CO<sub>2</sub>. 15.5 days old embryos were used for all experiments. Embryos were removed from the cavity and were decapitated in a cell culture dish containing HBSS. Brains were removed under a binocular and cortices were either directly dissected (C57BL/6J mice) for further processing, or brains were stored in Hibernate-E medium (*G9α<sup>fl/fl</sup>;Snap25-Cre* mice) until genotyping of brain tissue was finished before cortices were separated. Cortices from the same genotype were collected in a 15 ml tube containing HBSS. For dissociation, HBSS was removed, and cortices were incubated in 1 ml 0.05 % Trypsin EDTA solution for 6 min at 37 °C. Next, the Trypsin EDTA solution was removed, and cortices were washed with 5 ml DMEM/F-12 medium to stop the enzymatic reaction. Cortices were resuspended in 1 ml Neurobasal plus plating medium for mechanical dissociation. Therefore, the suspension was carefully pipetted up and down with a 1000 µl filter tip followed by a narrowed Pasteur pipette. The single cell suspension was diluted with 10 ml Neurobasal plus plating medium and cell number was determined in a hemocytometer in a 1:1 ratio with trypan blue. 100,000 cells per cm<sup>2</sup> were plated in Poly-D-Lysine coated plates containing Neurobasal plus plating medium in an incubator at 37 °C and 5 % CO<sub>2</sub>. One day after seeding, 1 µM AraC was added to the culture to avoid proliferation of non-neuronal cells. From day seven on, 50 % of the medium was replaced with fresh Neurobasal plus feeding medium until neurons were used for experiments (between day 16 and 21). G9a inhibitor UNC0642 was used in a concentration of 1 µM and cultures were pre-treated 24 hours before further experimental procedures.

### 2.2.9 Human induced pluripotent stem cell-derived neurons

The cultivation and maintenance of human induced pluripotent stem cells (iPSCs) was done by Undine Haferkamp in the Fraunhofer Institute for Translational Medicine and Pharmacology ITMP in Hamburg. Therefore, human iPSCs (ZiPi013-B)<sup>275</sup> were maintained under feeder-free conditions on Matrigel (Corning)-coated plates in mTeSR1 medium. For neuronal induction, iPSCs were dissociated with Accutase and seeded at a density of 3 × 10<sup>6</sup> cells per well on AggreWell800 plates (10,000 cells per embryoid body) in SMADi Neural Induction Medium supplemented with 10 µM Y-27632. On day 6, embryoid bodies were harvested and cultivated on Matrigel-coated plates in SMADi NIM for 12 days.

Newly formed neural rosettes were manually picked and cultured for another 4 days. In order to release neural precursor cells (NPCs), neural rosettes were dissociated with Accutase and were maintained for several passages at high density in Neural Progenitor Medium on Matrigel-coated plates. Human iPSC-derived NPCs were differentiated into neurons as previously described<sup>276,277</sup> with some modifications. Briefly, NPCs were seeded at a density of  $1 \times 10^5$  cells per  $\text{cm}^2$  in Neural Progenitor Medium onto Matrigel-coated plates. After 24 hours, the medium was replaced by neural differentiation medium (day 0 of differentiation). To promote a glutamatergic neuronal cell type, 5  $\mu\text{M}$  cyclopamine was additionally added to the medium during the first week of differentiation. On day 14, the cells were detached using Accutase and reseeded onto 24-well or 96-well poly-L-ornithine/laminin-coated plates suited for confocal microscopy. Thereafter, cells were maintained in neural differentiation medium supplemented with CultureOne for up to 30 weeks to increase maturity. Human iPSCs were pre-treated with 1  $\mu\text{M}$  UNC0642 24 h before stimulation with 500  $\mu\text{M}$  erastin for 24 h and were further processed for either confocal microscopy or gene expression analysis.

#### 2.2.10 Immunocytochemistry

Mouse primary cortical neurons or human iPSC-neurons were cultivated for immunocytochemistry (ICC) on 12 mm diameter coverslips or on 96-well plates suited for confocal microscopy. Following experimental procedures, cells were washed with PBS and subsequently fixed with 4 % PFA for 10 min at room temperature. After incubation time, cells were washed two times with PBS and kept at 4 °C until staining. Therefore, cells were incubated with PBS containing 0.25 % Triton-X-100 and 10 % normal donkey serum (NDS) for permeabilization and blocking of unspecific binding, respectively, for 30 min at room temperature. Next, primary antibodies were added to the same solution in the appropriate concentration (Table 2.12) for 1 h at room temperature. After 3 washing steps in PBS for 5 min each, secondary antibodies (Table 2.13) were applied in PBS supplemented with 0.25 % Triton-X-100 and 10 % NDS for 30 min at room temperature. Cells were washed with PBS and mounted with ROTI®Mount FluorCare. Immunostainings were analyzed with a 40× or 63× objective on a Zeiss LSM 700 confocal microscope.

#### 2.2.11 RealTime-Glo™ MT Cell Viability Assay

For RealTime-Glo (RTG) experiments, neurons were seeded in 96-well plates and one day before the experiment the medium was adjusted to 150  $\mu\text{l}$  per well. In addition, conditioned medium was transferred into empty wells and was used as a background control. NanoLuc® Luciferase and MT Cell Viability substrate were mixed in 4.5 ml Neurobasal plus feeding medium and 50  $\mu\text{l}$  of the mixture was added to each well. Neuronal cultures were incubated for 5 h for equilibration of luminescence signal

before the glutamate treatment was applied. The MT Cell Viability Substrate diffuses into cells and only metabolically active cells can reduce the substrate in a form that can be used by NanoLuc Luciferase to generate a luminescence signal, which is proportional to the number of live cells. Luminescence was acquired with a Spark 10M multimode microplate reader (Tecan) at 37 °C and 5 % CO<sub>2</sub> every 30 min over a total time period of 24 h. At least five technical replicates per condition were used. For analysis background signal was subtracted and every well's data point was normalized to its last value before the stressor was added and then normalized to the mean of the control wells for every time point using a customized MATLAB script. Thereby, it was normalized for well-to-well seeding variability.

#### 2.2.12 Calcium imaging

Neurons were cultured in  $\mu$ -Dish 35 mm Quad dishes (Ibidi) suitable for live cell imaging. On day *in vitro* (div) 7-9 primary neurons were transduced with an adeno-associated virus (AAV) 7 containing pAAV-Syn-GCamp6f-WPRE-SV40 by direct addition into the culture with a 20,000-fold multiplicity of infection. The plasmid for vector production was purchased from Addgene and package into AAVs was done at the UKE vector facility. Images were acquired with a confocal LSM 700 laser scanning confocal microscope every 0.48 sec with a 20 $\times$  magnification in an imaging chamber maintaining 37 °C and 5 % CO<sub>2</sub>. After 5 - 10 min baseline recording, 20  $\mu$ M glutamate or 1 mM H<sub>2</sub>O<sub>2</sub> was added to the medium and acute responses were acquired for 20 - 30 min. At the end of the experiment, 8  $\mu$ M ionomycin was applied to induce the maximum cellular calcium response that was used for normalization. For data analysis, mean fluorescence values of every cell were measured using Fiji software and normalized to the maximal calcium response after ionomycin challenge. For each cell, mean area under the curve (AUC) of the calcium response was calculated using a customized R script.

#### 2.2.13 Oxidative stress detection

To determine the production of oxidative stress in response to glutamate treatment, CellROX™ Green Reagent was used. Neuronal cultures were seeded in  $\mu$ -Dish 35 mm Quad dishes (Ibidi) and stimulated with 20  $\mu$ M glutamate or vehicle control for 1 h. CellROX reagent was added to each well in a final concentration of 5  $\mu$ M for 30 min at the end of the incubation time with the stressor. In addition, Hoechst 33342, a cell permeant nuclear counterstain, was added for 10 min. Cells were washed two times with PBS and subsequently imaged in culture medium. Images were taken on a Zeiss LSM 700 confocal microscope using 20 $\times$  magnification. The MFI of the nuclear CellROX dye was quantified in all cells by using Hoechst 33342 staining to define regions of interest with Fiji software.

#### 2.2.14 Cell death induction

For the induction of cell death pathways, neurons were cultured on black 96-well plates with a glass bottom, which are suitable for confocal microscopy. Primary neurons were subjected to dedicated compounds initiating either apoptosis (staurosporine (STS)), necroptosis (TNF $\alpha$  + LCL-161 + Z-VAD-FMK, or shikonin), or ferroptosis (RSL3, or erastin) for 48 h. Specific details about the compounds are summarized in table 2.7. Together with the cell death inducing compounds, CellTox™ Green Cytotoxicity Assay was added to primary neurons (1:2000). For each condition, five technical replicates were used. Before fixation with 4% PFA, cells were counterstained with Hoechst 33342 for 10 min. CellTox™ reagent binds the DNA of cells with impaired membrane integrity which are displayed by bright green nuclear fluorescence and defined as dead cells. Neurons were imaged on a Zeiss LSM 700 confocal microscope using 20 $\times$  magnification. The percentage of dead cells was quantified using Fiji by normalization to the number of total cells, measured by Hoechst 33342 positive nuclei.

#### 2.2.15 Glutathione measurement

Glutathione concentrations in response to glutamate stress in primary neurons were determined using GSH-Glo™ Glutathione Assay. Therefore, neurons were seeded on 96-well plates and stressed with glutamate for 2 h. Afterwards, cells were washed two times with PBS followed by the addition of 50  $\mu$ l GSH-Glo™ Reagent 1 $\times$ , consisting of GSH-Glo™ Reaction buffer supplemented with Luciferin-NT substrate (1:100) and GST (1:100). The plate was subsequently mixed on a plate shaker and incubated for 30 min at room temperature. During this reaction luciferin is generated from a luminogenic substrate, which is catalyzed by the GST in the presence of glutathione. Next, 50  $\mu$ l of reconstituted luciferin detection reagent, which was prepared by mixing the reconstitution buffer with esterase to the lyophilized luciferin detection reagent, was added to each well, mixed on a plate shaker, and incubated for 15 min at room temperature. Thereby, luciferin is detected as a luminescent signal by the luciferase and by applying luciferin detection reagent, GSH-Glo™ reaction is stopped and a luminescent signal that is proportional to the amount of formed luciferin is generated. Following incubation time, luminescence was measured at a Spark 10M multimode microplate reader.

#### 2.2.16 Neuronal nuclei isolation and sorting

Mice were anesthetized with a mixture of 80 % CO<sub>2</sub> and 20 % O<sub>2</sub> and subsequently sacrificed with 100 % CO<sub>2</sub>. Afterwards, mice were perfused with 10 ml ice-cold PBS and whole spinal cords were removed. The tissue was dissociated with a scalpel on a petri dish placed on a cooled metal block. Next, the tissue was added to 2 ml of nuclei lysis buffer and homogenized using a glass douncer with a loose and a tight pestle. After 5 min incubation on ice, homogenate was centrifuged (500 g for 5 min at 4 °C)

and the pellet was washed in 2 ml of nuclei lysis buffer (500 g for 5 min at 4 °C), followed by two washing steps in 2 ml nuclei incubation buffer (500 g for 5 min at 4 °C). Nuclei pellet was resuspended in 500 µl nuclei incubation buffer supplemented with RiboLock (1:200), filtered with MACS® SmartStrainers (30 µm), and directly stained with primary labelled rabbit NeuN-AF647 (1:500) antibody and propidium iodide (1:2000). Stained nuclei were used for sorting on a BD AriaIII cell sorter (BD Bioscience). Neuronal nuclei were identified by their high expression of NeuN and sorted into cooled 5 ml tubes containing PBS with 0.02 % BSA and RiboLock (1:200). Purity of sorted NeuN-positive nuclei was routinely above 96 %. After sorting, nuclei were centrifuged (1,500 g at 4 °C for 10 min) and the pellet was directly lysed for RNA extraction.

#### 2.2.17 Intra-nuclear staining and flow cytometry

Nuclei of mouse spinal cords were isolated as described above and whole lymph nodes were used after surface staining (30 min, 4 °C). After filtering of the suspension, nuclei were fixed with 100 % ice-cold methanol for 10 min followed by two washing steps with 2 ml of nuclei incubation buffer (1,500 rpm for 5 min). For intra-nuclear staining, nuclei were permeabilized with nuclei incubation buffer supplemented with 0.5 % Triton-X-100 and incubated for 15 min on ice. Nuclei were washed with nucleus incubation buffer (1,500 rpm for 5 min) and unspecific binding of antibodies was blocked with nucleus incubation buffer containing 10 % NDS for 10 min at room temperature. Primary antibodies for NeuN (Millipore) and H3K9me2 (Abcam) were added to the blocking solution for 1 h at room temperature and after a washing step with nucleus incubation buffer (1,500 rpm for 5 min), secondary antibodies (chAF-647, msAF-488) were added in nucleus incubation buffer + 10 % NDS together with Hoechst 33342 for 30 min at room temperature. Finally, nuclei suspension was washed (1,500 rpm for 5 min) and resuspended in 300 µl nuclei incubation buffer. Immunofluorescence (IF) was acquired on a LSR II FACS analyzer (BD Biosciences). Frequencies of NeuN-positive nuclei and MFI of H3K9me2 signal in NeuN-positive nuclei was analyzed using the FlowJo v10 software.

#### 2.2.18 RNA isolation, cDNA synthesis, and quantitative real-time PCR

RNA was isolated using RNeasy Mini Kit according to manufacturer's instructions. For cell culture experiments, cells plated on 12- (primary mouse neurons) or 24-well plates (human iPSCs) were washed two times with ice-cold PBS and 350 µl RLT lysis buffer containing β-Mercaptoethanol (1:100) was directly added to the cells. Sorted neuronal nuclei were centrifuged and the pellet was lysed in 350 µl RLT lysis buffer containing β-Mercaptoethanol (1:100). Further processing of lysed cell or nuclei samples was similar. An equal volume of 70 % ethanol was gently mixed with the samples by pipetting up and down. The mixture was transferred to an RNA isolation column and spun down (8,000 g for

20 sec). The flow-through was discarded and the column-bound RNA was consecutively washed with 700  $\mu$ l RW1 buffer (8,000 g for 20 sec) and two times with 500  $\mu$ l RPE buffer (8,000 g for 20 sec). The column was dried by centrifugation (20,000 g for 1 min) and finally the RNA was eluted in 30  $\mu$ l RNase-free water into a fresh RNase-free collection tube. RNA concentration was measured photometrically by Nanodrop and was stored at -80 °C until further processing.

For cDNA synthesis RevertAid First Strand cDNA Synthesis Kit was used. Therefore 11  $\mu$ l of RNA were mixed with 1  $\mu$ l of random hexamer primers and denatured at 65 °C for 5 min in a thermal cycler. Then a master mix containing 4  $\mu$ l 5 $\times$  Reaction buffer, 1  $\mu$ l RiboLock RNase inhibitor, 2  $\mu$ l dNTPmix, and 1  $\mu$ l RevertAid H Minus reverse transcriptase was added. Samples were mixed and incubated in a thermal cycler with the following program: 25 °C for 5 min, 42 °C for 60 min, 70 °C for 5 min. Transcribed cDNA was diluted with RNase-free water 1:5 and stored at -20°C.

Gene expression was analyzed by quantitative real-time PCR (qPCR) on a QuantStudio™ 6 Flex Real-Time PCR Instrument with indicated Taqman Assays (table 2.14) which contain a pair of primers and a FAM reporter probe. The cDNA samples were run in triplicates and for each Taqman Assay a control containing RNase-free water instead of cDNA was done to verify the purity of used reagents. For a single reaction, 2  $\mu$ l cDNA were added to master mix consisting of 0.5  $\mu$ l 20 $\times$  Taqman Assay, 5  $\mu$ l 2 $\times$  TaqMan gene expression master mix, and 2.5  $\mu$ l RNase-free water. Reaction was initiated by 50 °C for 2 min and 95 °C for 10 min, followed by 40 cycles with 95 °C for 15 sec and 60 °C for 60 sec. The housekeeping gene Tbp was used as an endogenous control. Gene expression was calculated as  $2^{-\Delta Ct}$  relative to Tbp expression. For analysis QuantStudio software was used.

### 2.2.19 Computational and statistical analysis

Flow cytometric data were analyzed by FlowJo v10. Images were analyzed using Fiji software (NIH). Experimental data obtained from RealTime-Glo™ MT Cell Viability Assay was analyzed with a customized MATLAB script and calcium imaging data were processed using a customized R script. Statistical analysis was performed with Prism v9.2.0 software for Mac and data are presented as means  $\pm$  standard error of the mean (s.e.m.) Unless otherwise stated, differences between two experimental groups were determined using an unpaired, two-tailed Student's t-test; differences between three or more experimental groups were determined using one-way analysis of variance (ANOVA) with Tukey's post hoc test; differences between two or more experimental groups depending on two different variables were analyzed using two-way ANOVA with Tukey's post hoc test. Statistical analysis for EAE experiments was performed by using a Mann–Whitney U-test to determine differences between the groups. Outliers were examined by Grubb's outlier test ( $\alpha = 0.05$ ), and the statistical outliers were excluded from the result. All data significant results are indicated by \* $P < 0.05$ , \*\* $P < 0.01$  and \*\*\* $P < 0.001$ .

### 3 Results

#### 3.1 Neuroinflammation promotes G9a-mediated H3K9me2 induction

##### 3.1.1 H3K9me2 regulation during EAE time course

In order to investigate neuronal responses during inflammation, a previously generated dataset from our lab that used targeted translome profiling of motor neurons by bacterial artificial chromosome translating ribosome affinity purification (bacTRAP)<sup>274</sup> was reanalyzed to extract candidates that modify the epigenetic landscape (Fig. 3.1 A). Most of the genes that were differently regulated during EAE encode for enzymes that convert post-translational histone modifications including methylation and acetylation of lysine residues (e. g. *Kdm1b*, *Ehmt2*, *Hdac7*). Moreover, some dysregulated genes modify the chromatin accessibility and thereby control gene expression (e. g. *Smarcd2*, *Smarcd1*, *Arid1a*). Only one gene, *Dnmt1*, that have an impact on overall DNA methylation maintenance showed an upregulation during neuroinflammation (Fig. 3.1 A). Among the top candidates, *Ehmt2* was chosen to study the influence of epigenetic transcriptional control during neuroinflammation due to the availability of specific chemical inhibitors with *in vivo* efficacy that enables a therapeutic approach in the preclinical mouse model of MS. *Ehmt2* encodes for the histone lysine methyltransferase G9a, which showed a robust induction in inflamed motor neurons in the acute phase of EAE (Fig. 3.1 B).

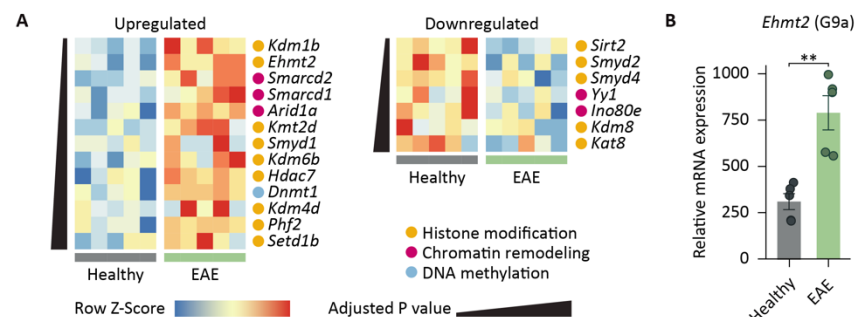


**Figure 3.1: Regulation of epigenetic modifiers during neuroinflammation. (A)** Gene expression heat map of top up- and downregulated epigenetic modifiers in inflamed motor neurons during EAE. Candidates were identified by DESeq2 and adjusted for multiple comparison by FDR ( $n = 5$  biologically independent samples per group each pooled from 3 mice,  $\log_2(\text{fold change}) > 1$ ; FDR-adjusted  $P < 0.05$ ). **(B)** Normalized RNA-Seq expression of *Ehmt2* in healthy and inflamed motor neurons. Statistical testing by DESeq2, using negative binomial generalized linear models adjusted for multiple comparisons by FDR;  $n = 5$  biologically independent samples per group, each pooled from 3 mice, motor neurons versus inflamed motor neurons. Data are shown as mean values  $\pm$  s.e.m. \*\* $P < 0.01$ .

To validate elevated *Ehmt2* levels during EAE, neuronal nuclei were extracted from healthy and EAE spinal cords and sorted by flow cytometry according to NeuN expression (Fig. 3.2 A). Therefore, the purity of sorted neuronal nuclei was analyzed by the quantification of neuronal and non-neuronal marker genes in NeuN-positive and NeuN-negative nuclei by qPCR. The neuronal marker gene RNA binding protein fox-1 homolog 3 (*Rbfox3*) showed an eight-fold enrichment in NeuN positive nuclei,

whereas glial marker genes including glial fibrillary acidic protein (*Gfap*), 2',3'-cyclic-nucleotide 3'-phosphodiesterase (*Cnp*), and C-X3-C motif chemokine receptor 1 (*Cx3cr1*) were de-enriched (Fig. 3.2 B). In addition, endothelial and immune cell marker genes platelet and endothelial cell adhesion molecule 1 (*Pecam*) and protein tyrosine phosphatase receptor type C (*Ptprc*), respectively, were de-enriched in neuronal compared to non-neuronal samples (Fig. 3.2 B), confirming the specificity of cell sorting by using NeuN as a neuronal marker. The mRNA expression of *Ehmt2* was measured in NeuN-positive nuclei and showed a strong induction during EAE, confirming the results of the bacTRAP approach (Fig. 3.2 C). Moreover, to assess G9a activity, the G9a-mediated histone modification H3K9me2 was quantified by antibody staining of neuronal nuclei and subsequent flow cytometric measurement (Fig. 3.2 D). Thereby, an increased activity of G9a was detected during the acute (day 15), and chronic phase (day 30) of EAE, but not prior to disease onset (day 11) (Fig. 3.2 D). Elevated

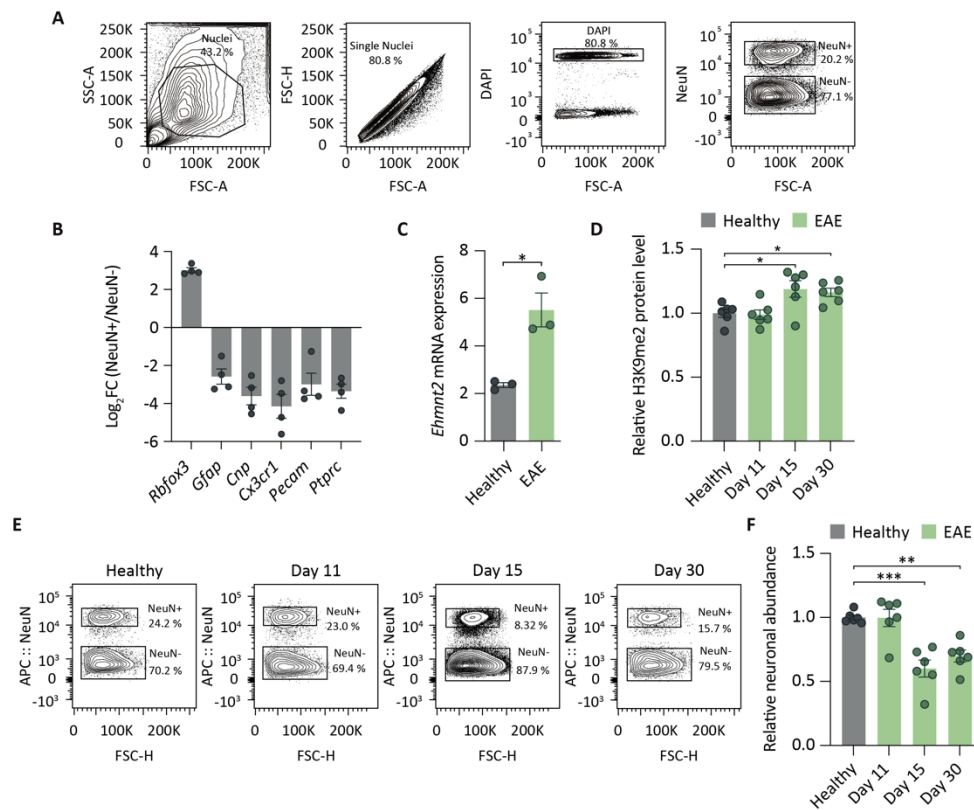


**Figure 3.2: Neuronal upregulation of G9a-mediated H3K9me2 during EAE. (A)** Representative gating strategy of neuronal nuclei from mouse spinal cord stained with NeuN. **(B)** mRNA expression of marker genes of neuronal and non-neuronal cell types from NeuN+ spinal cord nuclei compared to NeuN- spinal cord nuclei displayed by Log<sub>2</sub>FC **(C)** mRNA expression level of *Ehmt2* from sorted spinal cord neuronal nuclei of healthy vs. EAE mice (two-tailed Student's t-test,  $n = 3$  mice per group,  $P = 0.0118$ ). **(D)** Flow cytometry of H3K9me2 IF in spinal cord neuronal nuclei from healthy and EAE mice 11, 15, or 30 days after immunization (one-way ANOVA with Dunnett's post hoc test:  $n = 6$  per group,  $F_{(3,20)} = 5.802$ ,  $P = 0.0051$ ; Dunnett's post hoc test: Healthy vs. day 11  $P = 0.9961$ ; healthy vs. day 15  $P = 0.0164$ ; healthy vs. day 30  $P = 0.0421$ ). **(E)** Representative FACS plots showing neuronal loss during EAE from healthy and EAE mice on day 11, 15, and 30. **(F)** Percentage of neuronal loss in spinal cord nuclei from healthy and EAE mice 11, 15, or 30 days after immunization (one-way ANOVA with Dunnett's post hoc test:  $n = 6$  per group,  $F_{(3,20)} = 14.90$ ,  $P < 0.0001$ ; Dunnett's post hoc test: Healthy vs. day 11  $P > 0.9999$ ; healthy vs. day 15  $P < 0.0001$ ; healthy vs. day 30  $P = 0.0019$ ). Data are shown as mean values  $\pm$  s.e.m. \* $P < 0.05$ , \*\* $P < 0.01$ , \*\*\* $P < 0.001$ .

H3K9me2 levels were accompanied by a loss of neuronal nuclei as quantified by the percentage of NeuN-positive nuclei (Fig. 3.2 E, F), indicating increased G9a activity during the induction of neuronal cell death.

### 3.1.2 Glutamate-induced control of H3K9me2 induction

To establish an *in vitro* model that reflects excitotoxicity during neurodegeneration, glutamate was applied to primary neuronal cultures<sup>121,278</sup>. Mimicking the *in vivo* situation, glutamate exposure of primary cortical cultures resulted in an upregulation of H3K9me2 (Fig. 3.3 A) and simultaneously decreased cell viability as measured by the redox potential of the cells using RTG reagents (Fig. 3.3 B). Importantly, inflammatory substances such as IFN $\gamma$  or TNF $\alpha$  did not induce H3K9me2 levels (Fig. 3.3 C). Moreover, to exclude if the upregulation of epigenetic marks is an unspecific phenomenon during

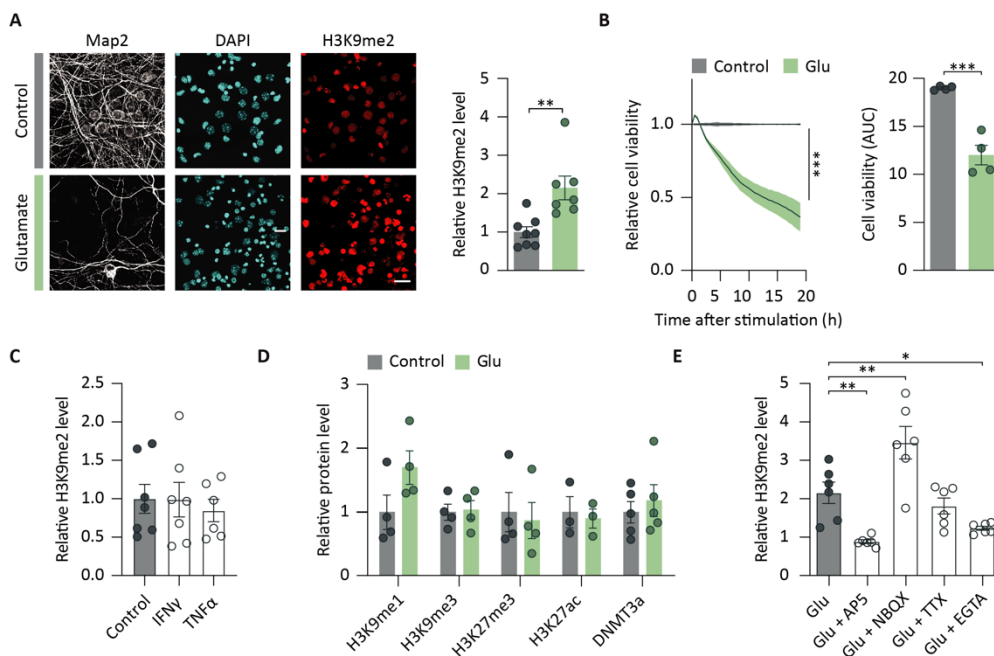


**Figure 3.3: H3K9me2 regulation in response to glutamate stress *in vitro*.** (A) Representative image and quantification of H3K9me2 staining 5 h after 20  $\mu$ M glutamate stimulation (two-tailed Student's t-test,  $n = 8$  Control vs.  $n = 7$  Glu,  $P = 0.0033$ ). Scale bar, 50  $\mu$ m. (B) Cell viability assay of cortical neurons stimulated with 20  $\mu$ M glutamate, time course (left; two-way ANOVA;  $n = 4$  independent experiments;  $F_{(1,6)} = 45.30$ ;  $P = 0.0005$ ) and AUC (right; two-tailed Student's t-test  $n = 4$  independent experiments;  $P = 0.0031$ ) 19 hours after glutamate application. (C) Quantification of H3K9me2 levels by immunostaining in primary cortical neurons stimulated with indicated substances for 48 hours (one-way ANOVA with Dunnett's post hoc test:  $F_{(2,17)} = 0.1849$ ,  $P = 0.8329$ . Dunnett's post hoc test: Control vs. IFN $\gamma$ , Control  $n = 7$ , IFN $\gamma$   $n = 7$ ,  $P = 0.9990$ ; Ctrl vs. TNF $\alpha$ , Control  $n = 7$ , TNF $\alpha$   $n = 6$ ,  $P = 0.8085$ ). (D) IF staining of indicated epigenetic modifications in primary cortical neurons treated with glutamate (two-way ANOVA with Bonferroni's post hoc test:  $F_{(4,30)} = 1.011$ ,  $P = 0.4175$ ; Bonferroni's post hoc test: H3K9me1: Control  $n = 4$ , Glu  $n = 4$ ,  $P = 0.2147$ ; H3K9me3: Control  $n = 4$ , Glu  $n = 4$ ,  $P > 0.9999$ ; H3K27me3: Control  $n = 4$ , Glu  $n = 4$ ,  $P > 0.9999$ ; H3K27ac: Control  $n = 3$ , Glu  $n = 3$ ,  $P > 0.9999$ ; DNMT3a: Control  $n = 5$ , Glu  $n = 5$ ,  $P > 0.9999$ ). (E) IF quantification of H3K9me2 of primary cortical neurons pretreated with AP5, NBQX, TTX, or EGTA and stressed with glutamate. Data are normalized to untreated control (one-way ANOVA with Dunnett's post hoc test:  $n = 6$  per group,  $F_{(4,25)} = 16.09$ ,  $P < 0.0001$ . Dunnett's post hoc test: Glu vs. Glu + AP5,  $P = 0.0049$ ; Glu vs. Glu + NBQX,  $P = 0.0037$ ; Glu vs. Glu + TTX,  $P = 0.7304$ ; Glu vs. Glu + EGTA,  $P = 0.0488$ ). Data are shown as mean values  $\pm$  s.e.m. \* $P < 0.05$ , \*\* $P < 0.01$ , \*\*\* $P < 0.001$

excitotoxicity, IF of other repressive (H3K9me1, H3K9me3, H3K27me3) or permissive (H3K27ac) epigenetic marks as well as DNMT3a was assessed which does not show any changes upon glutamate stimulation (Fig. 3.3 D). Only H3K9me1, which is also catalyzed by G9a, showed a trend towards being induced by glutamate exposure (Fig. 3.3 D).

For the determination of the upstream mechanism of H3K9me2 induction during glutamate exposure, neuronal cultures were pretreated with AP5, NBQX, TTX, or EGTA before glutamate stimulation to either block NMDA or AMPA receptors, silence signal transduction, or prevent extracellular calcium influx, respectively. AP5 as well as EGTA prevented the induction of glutamate induced upregulation of H3K9me2, indicating a NMDA receptor mediated calcium influx from the extracellular space as an inducer of G9a activity (Fig. 3.3 E). In contrast, blocking AMPA receptors, which have a low conductivity for calcium ions and rather mediate the influx of sodium ions, resulted in even higher levels of H3K9me2, whereas TTX-induced silencing of neurons by blocking sodium channels had no effect on H3K9me2 levels (Fig 3.3 E), substantiating a specific activation of G9a by calcium ions.

Together, these results demonstrate an upregulation of H3K9me2 during neuroinflammation *in vivo* and upon glutamate excitotoxicity in primary neuronal cultures that depends on calcium influx via NMDA receptors.

## 3.2 G9a interference regulates neuronal survival during excitotoxicity

### 3.2.1 *In vitro* models of G9a perturbation

To explore the effect of G9a on neuronal survival during glutamate excitotoxicity, pharmacological inhibition by the small molecule inhibitor UNC0642<sup>279</sup>, and genetic disruption of G9a in *G9a<sup>fl/fl</sup>;Snap25-Cre* primary neurons was used. Therefore, either primary neuronal cultures from wildtype mice or from *G9a<sup>fl/fl</sup>;Snap25-Cre* mice were prepared to test the efficacy of G9a perturbation by immunocytochemical staining's of G9a and H3K9me2. UNC0642 was applied to wildtype neurons in a concentration of 1  $\mu$ M for 24 h before fixation and subsequent staining. Application of UNC0642, which inactivates the catalytic domain of G9a, did not alter G9a protein levels but reduced its target H3K9me2 to 55 % (Fig. 3.4 A). Genetic disruption of G9a decreased G9a protein levels by 76 % and H3K9me2 levels by 67 % (Fig. 3.4 B). Quantification of *Ehmt2* mRNA levels resulted in a reduction of 90 % in *G9a<sup>fl/fl</sup>;Snap25-Cre* primary neuronal cultures (Fig. 3.4 C). As both interventions resulted in a sufficient reduction of H3K9me2, both are suitable for studying G9a dependent mechanisms in primary neurons.

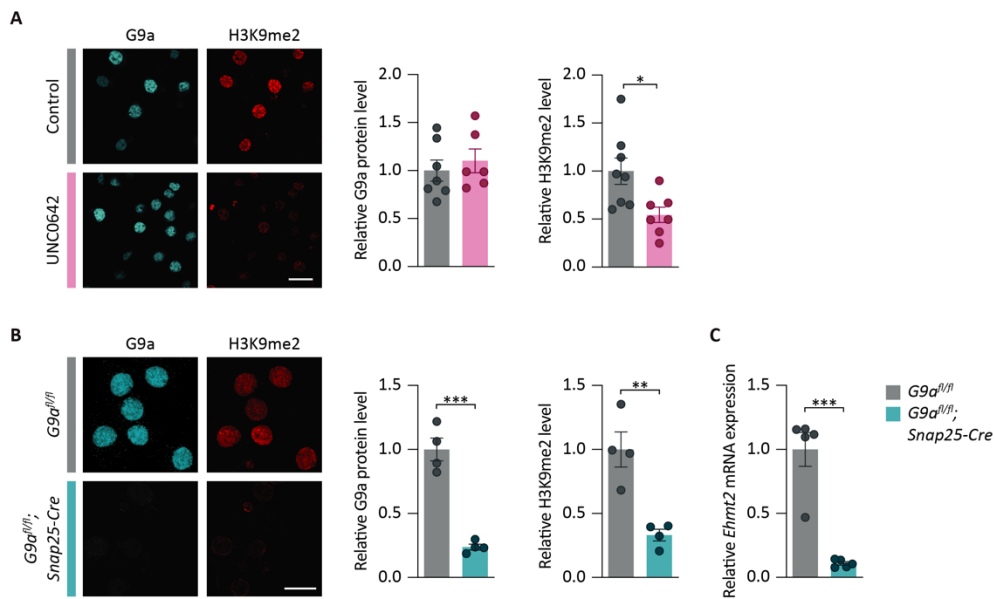


**Figure 3.4: Characterization of pharmacological and genetic perturbation of G9a in primary neurons. (A)** Representative image (left) and quantification (right) of IF staining's of G9a and H3K9me2 from UNC0642 pre-treated primary neuronal cultures compared to respective controls (two-tailed Student's t-test, G9a: DMSO n = 7, UNC0642 n = 6, P = 0.5479; H3K9me2: DMSO n = 8, UNC0642 n = 7, P = 0.0164). Scale bars, 20  $\mu$ m. **(B)** Representative image (left) and quantification (right) of IF staining's of G9a and H3K9me2 from  $G9a^{fl/fl}; Snap25-Cre$  primary neuronal cultures compared to controls (two-tailed Student's t-test, n = 4 independent experiments, G9a: P = 0.0002; H3K9me2: P = 0.0037). Scale bars, 20  $\mu$ m. **(C)** *Ehmt2* gene expression of  $G9a^{fl/fl}$  and  $G9a^{fl/fl}; Snap25-Cre$  primary cortical cultures (two-tailed Student's t-test: n = 5 per group, P = 0.0002). Data are shown as mean values  $\pm$  s.e.m. \*P < 0.05, \*\*P < 0.01, \*\*\*P < 0.001

### 3.2.2 Neuroprotection by G9a interference during glutamate stress

To measure neuronal survival during glutamate stress, wildtype primary neurons treated with UNC0642 and  $G9a^{fl/fl}; Snap25-Cre$  knockout neurons were exposed to glutamate and cellular survival was measured over a time period of 20 h by assessing the redox potential via RTG compounds. As a second readout, toxic calcium overload in response to glutamate stress was recorded in cultures transduced with AAV7 containing the genetically encoded calcium indicator GCamp6f. Pharmacological inactivation of G9a by UNC0642 24 h before glutamate stress resulted in an increased neuronal viability (Fig. 3.5 A) and less toxic calcium accumulation (Fig. 3.5 B) in response to glutamate compared to DMSO treated controls. Those findings could be validated in  $G9a^{fl/fl}; Snap25-Cre$  neuronal knockout cultures, which showed a similar rescue of glutamate toxicity measured by cell viability (Fig. 3.5 C) and calcium upload (Fig. 3.5 D). Moreover, to determine the specificity of UNC0642, G9a-deficient neurons from  $G9a^{fl/fl}; Snap25-Cre$  mice were treated with UNC0642 or DMSO control and cell viability (Fig. 3.5 E) as well as cytosolic calcium influx (Fig. 3.5 F) were measured during glutamate stress. The absence of an additional rescue supported a specific effect of UNC0642 on G9a activity. These findings demonstrate the potential value of small molecule G9a inhibitors for the treatment of neurodegeneration in inflammation-induced excitotoxicity.

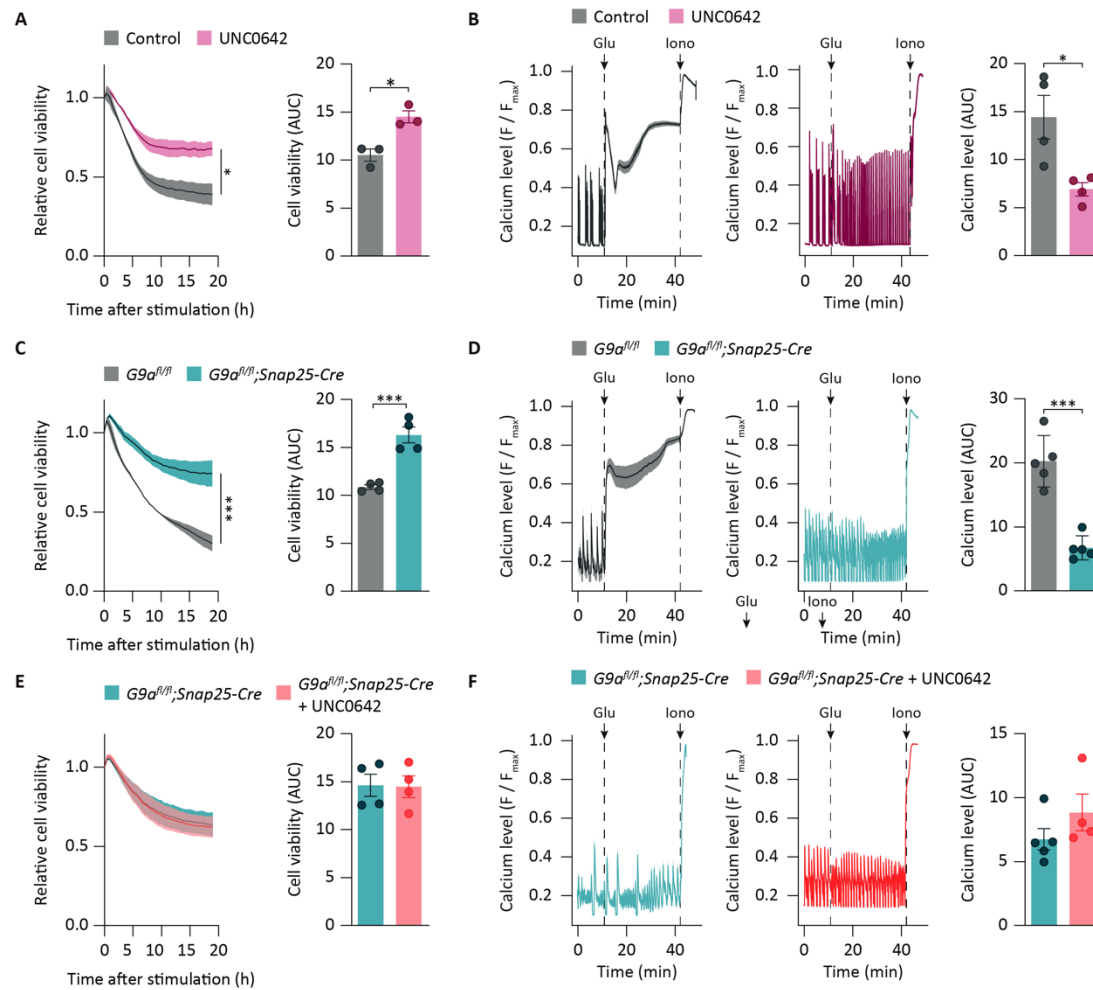


**Figure 3.5: G9a perturbation results in neuroprotection during glutamate exposure.** (A) Time course (left; two-way ANOVA;  $n = 3$  independent experiments;  $F_{(1,4)} = 19.37$ ;  $P = 0.0117$ ) and quantification of the AUC (right; two-tailed Student's t-test,  $n = 3$  independent experiments,  $P = 0.0115$ ) of cell viability from DMSO- vs. UNC0642-treated primary cortical cultures. (B) Cytosolic calcium recordings of glutamate-exposed neuronal cultures treated with DMSO or UNC0642 (two-tailed Student's t-test,  $n = 4$  independent experiments,  $P = 0.0193$ ). (C) Time course (left; two-way ANOVA;  $n = 4$  independent experiments;  $F_{(1,6)} = 38.19$ ;  $P < 0.0001$ ) and quantification of the AUC (right; two-tailed Student's t-test,  $n = 4$  independent experiments,  $P = 0.0008$ ) of cell viability from *G9a<sup>fl/fl</sup>* vs. *G9a<sup>fl/fl</sup>;Snap25-Cre* primary cortical cultures. (D) Cytosolic calcium recordings of glutamate-exposed *G9a<sup>fl/fl</sup>* and *G9a<sup>fl/fl</sup>;Snap25-Cre* neuronal cultures (two-tailed Student's t-test,  $n = 5$  independent experiments,  $P = 0.0001$ ). (E) Time course (left; two-way ANOVA;  $n = 4$  independent experiments;  $F_{(38,228)} = 0.1206$ ;  $P > 0.9999$ ) and quantification of the AUC (right; two-tailed Student's t-test,  $n = 4$  independent experiments,  $P > 0.9301$ ) of cell viability from *G9a<sup>fl/fl</sup>;Snap25-Cre* primary cortical cultures  $\pm$  UNC0642. (F) Cytosolic calcium recordings of glutamate-exposed neuronal cultures from *G9a<sup>fl/fl</sup>;Snap25-Cre* mice  $\pm$  UNC0642 (two-tailed Student's t-test, *G9a<sup>fl/fl</sup>;Snap25-Cre*  $n = 5$ , *G9a<sup>fl/fl</sup>;Snap25-Cre + UNC0642*  $n = 4$ ,  $P = 0.2278$ ). Data are shown as mean values  $\pm$  s.e.m. \* $P < 0.05$ , \*\* $P < 0.01$ , \*\*\* $P < 0.001$

### 3.2.3 G9a perturbation protects neurons from glutamate-induced oxidative stress

Besides the involvement of excessive levels of glutamate to the progression of neurodegeneration, oxidative stress has been shown to drive neuronal loss in many neurodegenerative conditions<sup>107</sup>. As glutamate neurotoxicity increases intracellular ROS levels<sup>97,280</sup>, the G9a mediated responses to oxidative stress was determined. Therefore, CellROX™ green reagent was used to detect oxidative stress in primary neurons in response to glutamate exposure. This cell-permeant dye is weakly fluorescent in a reduced state but exhibits bright green photostable fluorescence upon oxidation by ROS and subsequent binding to DNA. Glutamate stimulation of primary neurons resulted in oxidative stress within 1 h, whereas pre-treatment with UNC0642 almost completely abolished the generation of ROS (Fig. 3.6 A). Similarly, in *G9a<sup>fl/fl</sup>;Snap25-Cre* knockout neurons, the glutamate induced generation of oxidative stress was close to baseline levels as seen in *G9a<sup>fl/fl</sup>* controls (Fig. 3.6 B). To also explore the neuroprotective potential of G9a perturbation in a dedicated model of high oxidative stress, the involvement of G9a activity during H<sub>2</sub>O<sub>2</sub> exposure in primary neuronal cultures was studied.

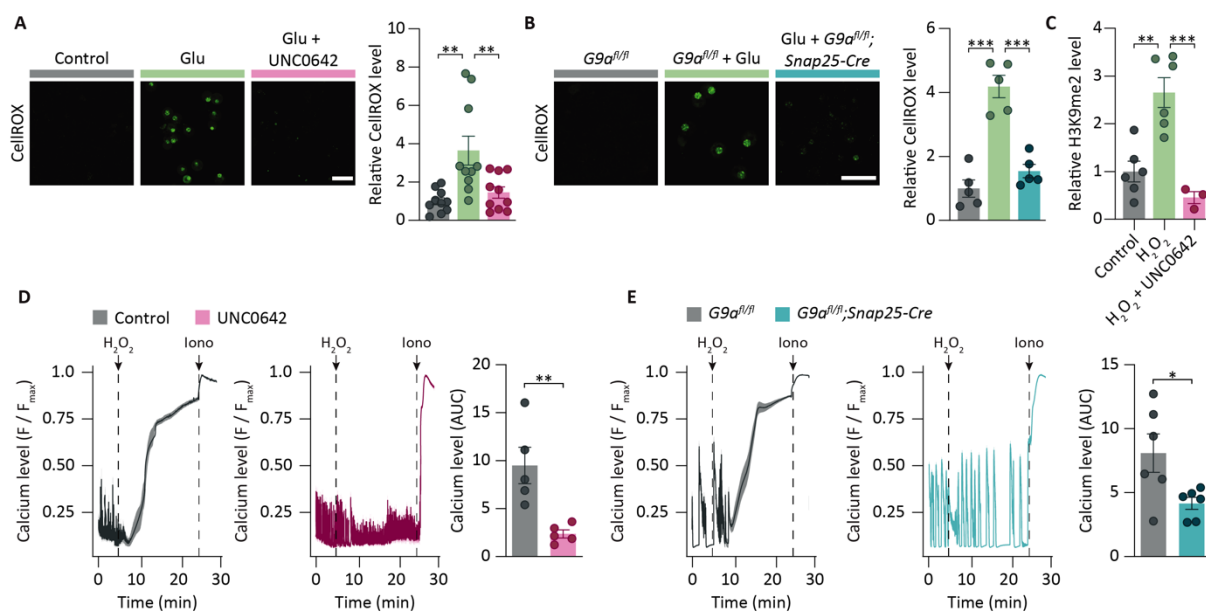


**Figure 3.6: G9a perturbation protects neurons from oxidative stress.** (A) Representative images (left) and quantification (right) of CellROX green reagent in DMSO- vs. UNC0642-treated cultures after glutamate stress (one-way ANOVA:  $n = 10$  independent experiments,  $F_{(2,27)} = 8.614$ ,  $P = 0.0013$ . Tukey's post hoc test: Control vs. Glu,  $P = 0.0017$ ; control vs. UNC0642 + Glu,  $P = 0.7783$ ; Glu vs. UNC0642 + Glu,  $P = 0.0093$ ). Scale bar, 40  $\mu\text{m}$ . (B) Representative images (left) and quantification (right) of immunostaining of oxidative stress with CellROX green reagent in *G9a<sup>fl/fl</sup>* vs. *G9a<sup>fl/fl</sup>;Snap25-Cre* cultures after glutamate stress (one-way ANOVA:  $n = 5$  independent experiments,  $F_{(2,12)} = 36.59$ ,  $P < 0.0001$ , Tukey's post hoc test: Control vs. *G9a<sup>fl/fl</sup>* + Glu,  $P < 0.0001$ ; control vs. *G9a<sup>fl/fl</sup>;Snap25-Cre* + Glu,  $P = 0.3929$ ; *G9a<sup>fl/fl</sup>* + Glu vs. *G9a<sup>fl/fl</sup>;Snap25-Cre* + Glu,  $P < 0.0001$ ); Scale bar, 40  $\mu\text{m}$ . (C) IF quantification of H3K9me2 in response to H<sub>2</sub>O<sub>2</sub> exposure for 5 hours  $\pm$  UNC0642 (one-way ANOVA: Control  $n = 6$ , H<sub>2</sub>O<sub>2</sub>  $n = 6$ , H<sub>2</sub>O<sub>2</sub> + UNC0642  $n = 3$ ,  $F_{(2,12)} = 17.59$ ,  $P = 0.0003$ . Tukey's post hoc test: Control vs. H<sub>2</sub>O<sub>2</sub>,  $P = 0.0012$ ; control vs. UNC0642 + H<sub>2</sub>O<sub>2</sub>,  $P = 0.4310$ ; H<sub>2</sub>O<sub>2</sub> vs. H<sub>2</sub>O<sub>2</sub> + UNC0642,  $P = 0.0006$ ). (D) Cytosolic calcium recordings of H<sub>2</sub>O<sub>2</sub>-exposed neuronal cultures treated with DMSO or UNC0642 (two-tailed Student's t-test,  $n = 5$  independent experiments,  $P = 0.0062$ ). (E) Cytosolic calcium recordings of H<sub>2</sub>O<sub>2</sub>-exposed *G9a<sup>fl/fl</sup>* and *G9a<sup>fl/fl</sup>;Snap25-Cre* neuronal cultures (two-tailed Student's t-test,  $n = 6$  independent experiments,  $P = 0.0315$ ). Data are shown as mean values  $\pm$  s.e.m. \* $P < 0.05$ , \*\* $P < 0.01$ , \*\*\* $P < 0.001$ .

Importantly, H<sub>2</sub>O<sub>2</sub> treatment itself led to a pronounced upregulation of H3K9me<sub>2</sub>, which could be counteracted by pre-treatment with UNC0642 (Fig. 3.6 C). Moreover, acute H<sub>2</sub>O<sub>2</sub> stress induced a progressive neuronal calcium overload that was prevented by both, G9a inhibition by UNC0642 pre-treatment and genetic disruption in *G9a<sup>fl/fl</sup>;Snap25-Cre* cultures in comparison to respective controls (Fig. 3.6 D, E). In conclusion, G9a interference enhanced neuronal resilience during the exposure to toxic levels of ROS.

### 3.3 Neuronal cell death *in vitro* is induced via ferroptosis by G9a

#### 3.3.1 G9a activity is induced by ferroptosis

As G9a perturbation interfered with neuronal ROS production and supported neuronal viability, the implication of G9a in a central form of PCD was investigated. To do so, different forms of PCD that have been shown to be implicated in neurodegeneration and oxidative stress were induced in primary

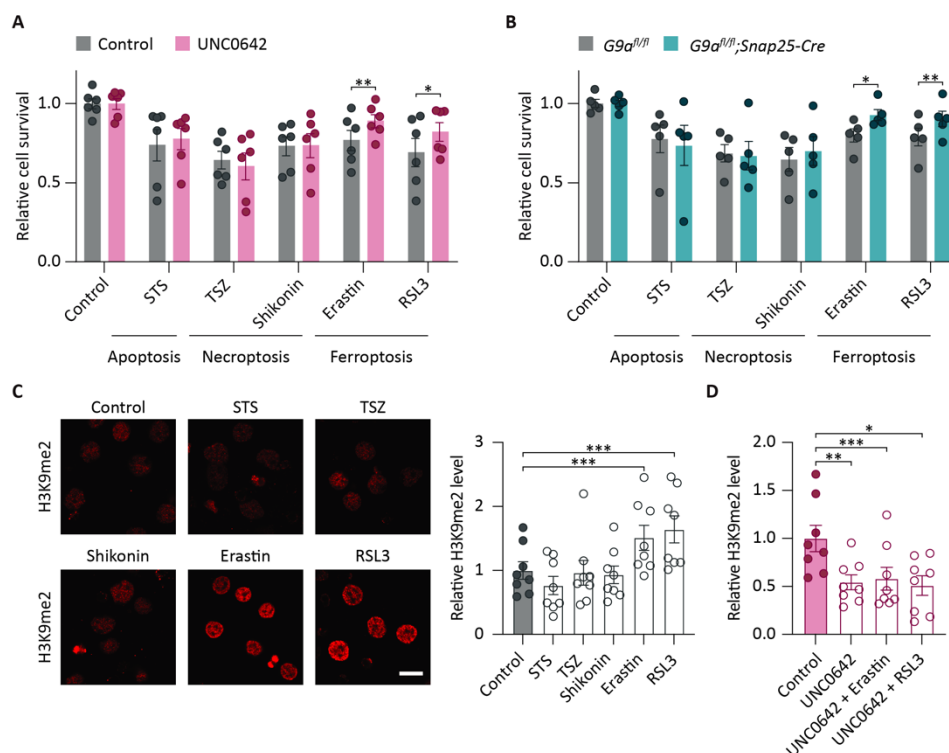


**Figure 3.7: G9a perturbation counteracts ferroptosis.** (A) Quantification of dead neurons with CellTox green reagent in response to induction of different cell death pathways in cultures  $\pm$  UNC0642 (two-tailed paired Student's t-test,  $n = 6$  independent experiments; Control:  $P > 0.999$ ; STS:  $P = 0.3786$ ; TSZ:  $P = 0.4790$ ; Shikonin:  $P = 0.8992$ ; Erastin:  $P = 0.0039$ ; RSL3:  $P = 0.0498$ ). (B) Quantification of dead neurons with CellTox green reagent in response to induction of different cell death pathways in *G9a<sup>fl/fl</sup>* vs. *G9a<sup>fl/fl</sup>;Snap25-Cre* cultures (two-tailed paired Student's t-test,  $n = 5$  independent experiments; Control:  $P > 0.999$ ; STS:  $P = 0.4885$ ; TSZ:  $P = 0.8128$ ; Shikonin:  $P = 0.2156$ ; Erastin:  $P = 0.0140$ ; RSL3:  $P = 0.0043$ ). (C) IF of H3K9me<sub>2</sub> in primary cortical neurons after treatment with indicated compounds (repeated measures one-way ANOVA:  $n = 8$  independent experiments,  $F_{(5,35)} = 26.91$ ,  $P < 0.0001$ . Dunnett's post hoc test: Control. vs. STS,  $P = 0.0752$ ; control. vs. TSZ,  $P = 0.9952$ , control vs. Shikonin,  $P = 0.9327$ , control. vs. erastin,  $P < 0.0001$ , control. vs. RSL3,  $P < 0.0001$ ). Scale bar 20  $\mu$ m. (D) IF quantification of H3K9me<sub>2</sub> in response to ferroptosis induction in cortical cultures pre-treated with UNC0642 (repeated measures one way ANOVA:  $n = 8$  independent experiments,  $F_{(1,676,11.73)} = 12.63$ ,  $P = 0.0017$ . Dunnett's post hoc test: Control vs. UNC0642,  $P = 0.0020$ ; control vs. UNC0642 + Erastin,  $P = 0.0007$ , control vs. UNC0642 + RSL3,  $P = 0.0151$ ). Data are shown as mean values  $\pm$  s.e.m. \* $P < 0.05$ , \*\* $P < 0.01$ , \*\*\* $P < 0.001$ .

neurons and cell survival was quantified with and without G9a perturbation. Induction of apoptotic cell death by using the protein kinase inhibitor STS was neither affected by UNC0642 treatment nor in *G9a<sup>fl/fl</sup>;Snap25-Cre* neurons. Similarly, neither necroptotic cell death triggered by a combination of TNF $\alpha$ , Smac mimetics and the caspase inhibitor z-VAD-fmk (TSZ), nor necroptosis induced by shikonin was rescued by G9a perturbation (Fig. 3.7 A, B).

By contrast, ferroptosis induction either by erastin or RSL3 resulted in a significant higher cell survival upon G9a interference measured by Celltox green reagent (Fig. 3.7 A, B). Moreover, G9a activity was analyzed by H3K9me2 IF in response to the induction of the different cell death cascades. There were no changes in H3K9me2 signal while triggering apoptosis (STS) or necroptosis (TSZ, shikonin) in primary neurons (Fig. 3.7 C), but the induction of ferroptosis via erastin or RSL3 resulted in a significant upregulation of H3K9me2 (Fig. 3.7 C). Notably, upregulation of H3K9me2 in response to ferroptosis inducing agents could be prevented by pre-treatment with UNC0642 (Fig. 3.7 D).

### 3.3.2 G9a interference diminish glutamate-induced ferroptotic cell death

To corroborate the involvement of ferroptosis in glutamate-induced cell death, cyclooxygenase-2 (COX-2), encoded by the gene prostaglandin-endoperoxide synthase 2 (*Ptgs2*), was investigated as a widely used biomarker of ferroptosis<sup>182</sup>. Glutamate excitotoxicity led to a markedly higher percentage of COX-2-positive cells, whereas the pharmacological inhibition of G9a almost completely abolished its induction (Fig. 3.8 A). Since ferroptosis is induced in response to glutamate excitotoxicity, the impact of ferroptosis on acute cytosolic calcium responses during glutamate stimulation was investigated. Therefore, the ferroptosis inhibitors ferrostatin-1, DFMO, and CoQ10, which have lipophilic radical-trapping, iron chelating, or antioxidant functions, respectively, were used. The inhibition of ferroptosis by using those compounds led to a significant decrease of cytosolic calcium levels after glutamate stimulation (Fig. 3.8 B). Of note, pre-treatment with the G9a inhibitor UNC0642 did not further potentiate the rescue effects of these ferroptosis inhibitors suggesting a direct effect of G9a inhibition on ferroptosis (Fig. 3.8 C). In addition, glutathione levels were assessed in response to glutamate stress after G9a perturbation, as glutathione has a central function in the regulation of ferroptosis via its antioxidant properties. In UNC0642 pre-treated neurons as well as in *G9a<sup>fl/fl</sup>;Snap25-Cre* neurons, glutathione levels were significantly higher during glutamate stress as compared to controls (Fig. 3.8 C, D). Together, these findings demonstrate a specific role of G9a in regulating ferroptotic cell death in neurons.

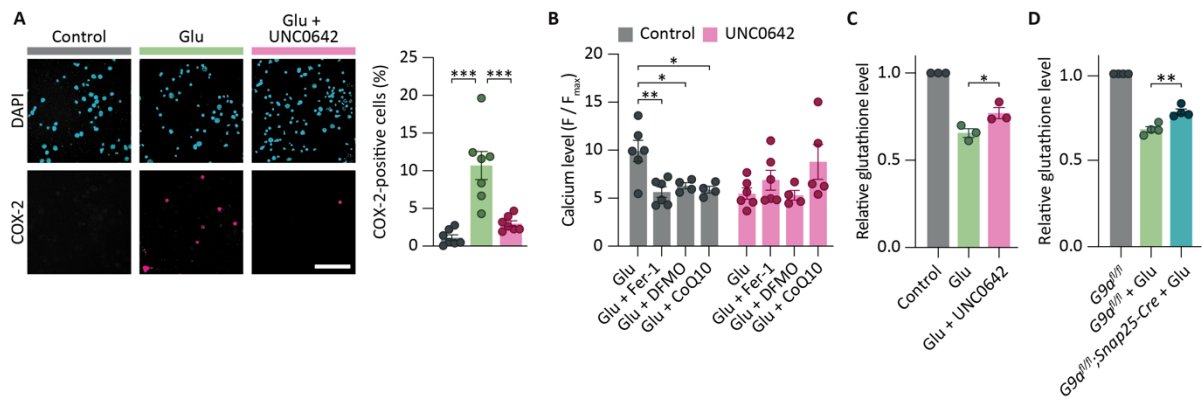


**Figure 3.8: Prevention of ferroptosis induction by G9a interference.** (A) Representative images (left) and quantification (right) of COX-2 immunostaining after glutamate stimulation in neuronal cultures  $\pm$  UNC0642 (one-way ANOVA:  $n = 7$  independent experiments,  $F_{(2,18)} = 20.31$ ,  $P = 0.0001$ ; Tukey's post hoc test: Control vs. Glu,  $P < 0.0001$ ; control vs. UNC0642 + Glu,  $P = 0.4834$ ; Glu vs. UNC0642 + Glu,  $P = 0.0004$ ). Scale bar, 40  $\mu\text{m}$ . (B) Quantification of  $F_{\text{max}}$ -normalized cytosolic calcium responses after glutamate treatment  $\pm$  UNC0642. Cultures were stimulated 10 min prior to glutamate treatment with ferrostatin-1, DMFO, or CoQ10 (two-way ANOVA with Bonferroni's post hoc test,  $n = 6$  per group;  $F_{(3,33)} = 5.599$ ,  $P = 0.0032$ ; Bonferroni's post hoc test: Control + Glu vs. Control + Glu + Fer-1,  $P = 0.0059$ ; Control + Glu vs. Control + Glu + DFMO,  $P = 0.0467$ ; Control + Glu vs. Control + Glu + CoQ10,  $P = 0.0234$ ; UNC0642 + Glu vs. UNC0642 + Glu + Fer-1,  $P = 0.414$ ; UNC0642 + Glu vs. UNC0642 + Glu + DFMO,  $P > 0.9999$ ; UNC0642 + Glu vs. UNC0642 + Glu + CoQ10,  $P = 0.0569$ ). (C, D) Glutathione measurement in UNC0642-treated (C; two-tailed Student's t-test,  $n = 4$  independent experiments,  $P = 0.0469$ ) or  $G9a^{\text{fl/fl}}$  vs.  $G9a^{\text{fl/fl}}; \text{Snap25-Cre}$  (D; two-tailed Student's t-test,  $n = 3$  independent experiments,  $P = 0.0042$ ) cortical neurons in response to glutamate. Data are normalized to untreated controls. Data are shown as mean values  $\pm$  s.e.m. \* $P < 0.05$ , \*\* $P < 0.01$ , \*\*\* $P < 0.001$ .

### 3.3.3 Transcriptional regulation of ferroptosis-relevant genes upon G9a inhibition *in vitro*

G9a activity leads to the modulation of gene expression by repressing gene transcription. As G9a interference diminished ferroptosis induction in neurons, the transcript level of ferroptosis-relevant genes was investigated upon pharmacological G9a inhibition in the presence of ferroptosis inducing substances. Therefore, primary neurons pretreated with UNC0642 were exposed to various stimuli that induce ferroptosis either by generating oxidative stress via glutamate and  $\text{H}_2\text{O}_2$  or by blocking system Xc<sup>-</sup> through erastin, which regulates glutathione levels.

Several genes showed a strong dysregulation during ferroptosis induction that was further potentiated by G9a inhibition. Among them is the subunit *Slc7a11* of system Xc<sup>-</sup> which showed a prominent induction upon glutamate or erastin treatment and a mild upregulation after  $\text{H}_2\text{O}_2$  exposure. G9a inhibition resulted in a significantly higher expression of *Slc7a11* exclusively during erastin treatment. Moreover, genes regulating glutathione via metabolizing cystine including glutamate-cysteine ligase catalytic subunit (*Gclc*), and *Gss* showed a mild induction during ferroptosis. *Gss* was further potentiated by the inhibition of G9a activity during  $\text{H}_2\text{O}_2$  and erastin stress, but controversially *Gclc* was downregulated to basal levels during glutamate stress in UNC0642 treated cultures. This indicates a role of G9a in balancing intracellular glutathione. On the contrary, *Cbs*, which generates glutathione via the transsulfuration pathway, was upregulated during glutamate stress, but downregulated upon  $\text{H}_2\text{O}_2$  or erastin exposure. G9a inactivation resulted in a mild repression of *Cbs*

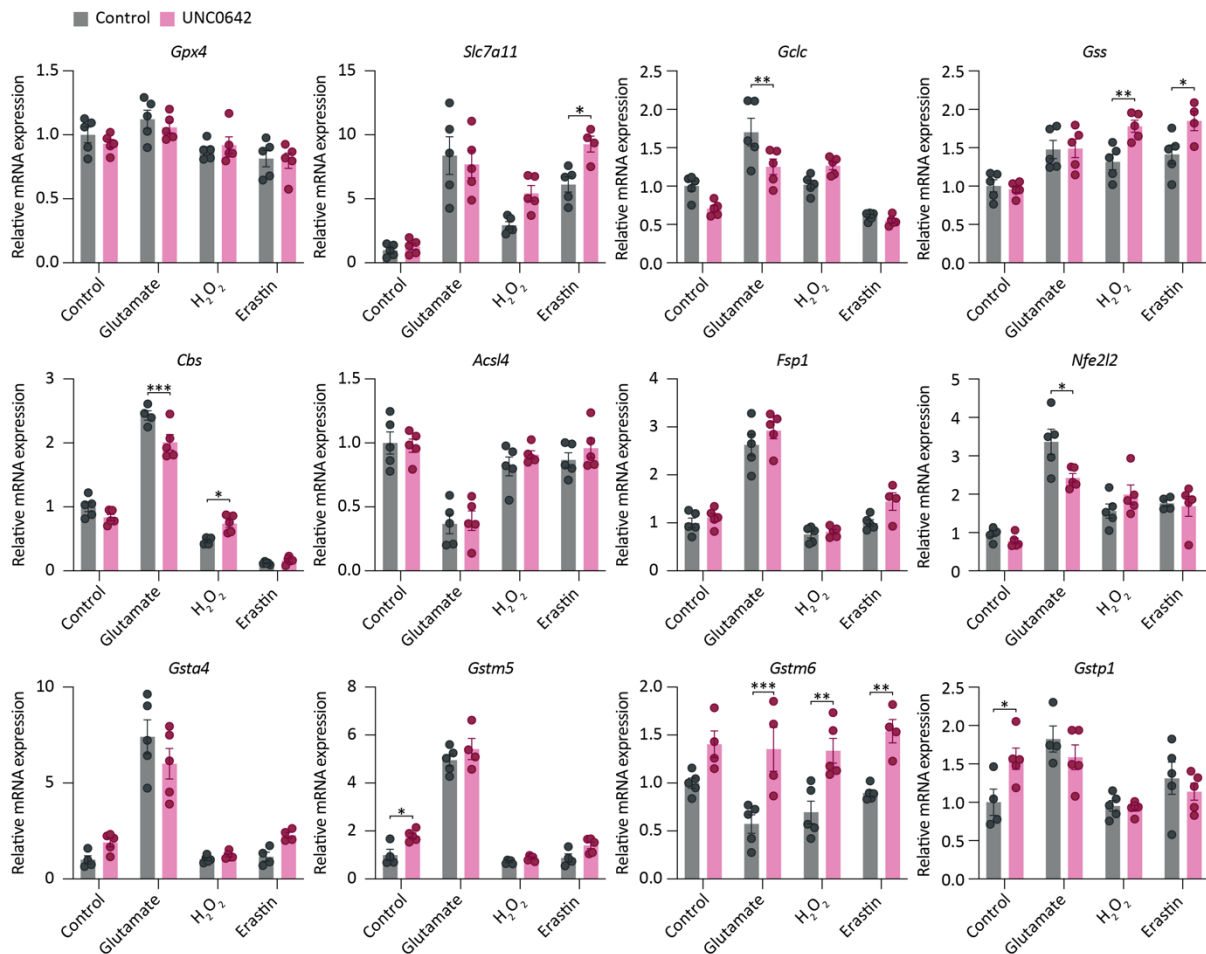


**Figure 3.9: Ferroptosis-relevant genes during induction of ferroptosis in primary neurons treated with UNC0642.** mRNA expression of selected genes from primary cortical neurons in response to indicated stressors  $\pm$  UNC0642 treatment (two-way ANOVA  $n = 4 - 5$  per group: *Gpx4*  $F_{(3,32)} = 0.4197$   $P = 0.7401$ , Sidak's post hoc test: Control  $P = 0.8705$ , Glutamate  $P = 0.8942$ ,  $H_2O_2$   $P = 0.9727$ , Erastin  $P = 0.9989$ ; *Slc7a11*:  $F_{(3,31)} = 2.740$   $P = 0.0600$ , Sidak's post hoc test: Control  $P = 0.9983$ , Glutamate  $P = 0.9534$ ,  $H_2O_2$   $P = 0.0995$ , Erastin  $P = 0.0365$ ; *Gclc*:  $F_{(3,32)} = 6.614$   $P = 0.0013$ , Sidak's post hoc test: Control  $P = 0.0698$ , Glutamate  $P = 0.0023$ ,  $H_2O_2$   $P = 0.1683$ , Erastin  $P = 0.0779$ ; *Gss*:  $F_{(3,31)} = 3.563$   $P = 0.0253$ , Sidak's post hoc test: Control  $P = 0.9960$ , Glutamate  $P > 0.9999$ ,  $H_2O_2$   $P = 0.0099$ , Erastin  $P = 0.0263$ ; *Cbs*:  $F_{(3,30)} = 9.640$   $P = 0.0001$ , Sidak's post hoc test: Control  $P = 0.2687$ , Glutamate  $P = 0.0005$ ,  $H_2O_2$   $P = 0.0311$ , Erastin  $P = 0.9784$ ; *Acs4*:  $F_{(3,32)} = 0.3330$   $P = 0.8015$ , Sidak's post hoc test: Control  $P = 0.9990$ , Glutamate  $P = 0.9980$ ,  $H_2O_2$   $P = 0.8231$ , Erastin  $P = 0.8118$ ; *Fsp1*:  $F_{(3,31)} = 0.8994$   $P = 0.4526$ , Sidak's post hoc test: Control  $P = 0.9545$ , Glutamate  $P = 0.3678$ ,  $H_2O_2$   $P = 0.9968$ , Erastin  $P = 0.1092$ ; *Nfe2l2*:  $F_{(3,31)} = 4.039$   $P = 0.0156$ , Sidak's post hoc test: Control  $P = 0.9345$ , Glutamate  $P = 0.0086$ ,  $H_2O_2$   $P = 0.4473$ , Erastin  $P = 0.9984$ ; *Gsta4*:  $F_{(3,29)} = 2.845$   $P = 0.0540$ , Sidak's post hoc test: Control  $P = 0.5937$ , Glutamate  $P = 0.1546$ ,  $H_2O_2$   $P = 0.9968$ , Erastin  $P = 0.4486$ ; *Gstm5*:  $F_{(3,29)} = 0.9917$   $P = 0.4105$ , Sidak's post hoc test: Control  $P = 0.0288$ , Glutamate  $P = 0.3615$ ,  $H_2O_2$   $P = 0.9682$ , Erastin  $P = 0.2569$ ; *Gstm6*:  $F_{(3,29)} = 0.8182$   $P = 0.4972$ , Sidak's post hoc test: Control  $P = 0.1015$ , Glutamate  $P = 0.0004$ ,  $H_2O_2$   $P = 0.0018$ , Erastin  $P = 0.0032$ ; *Gstp1*:  $F_{(3,30)} = 3.195$   $P = 0.0376$ , Sidak's post hoc test: Control  $P = 0.0401$ , Glutamate  $P = 0.7028$ ,  $H_2O_2$   $P = 0.9998$ , Erastin  $P = 0.8531$ ). Data are shown as mean values  $\pm$  s.e.m. \* $P < 0.05$ , \*\* $P < 0.01$ , \*\*\* $P < 0.001$ .

while glutamate treatment but was higher expressed upon  $H_2O_2$  stimulation compared to vehicle treated controls. The main regulator of the ferroptosis pathway, GPX4<sup>182</sup>, did not show any changes on the transcriptional level when triggering ferroptosis induction or in response to pharmacological G9a inhibition. In addition, G9a did not affect the gene expression of the ferroptosis promoting gene *Acs4*, that shows a prominent downregulation during glutamate stress, indicating the prevention of lipid peroxidation in the presence of toxic glutamate levels to enhance neuronal survival. Furthermore,

the gene *Fsp1* that regulates the initiation of ferroptosis in a glutathione independent manner, showed a strong induction during glutamate treatment, but was not differently expressed in G9a inactivated neurons. The transcription factor *Nfe2l2* (NRF2), which has been shown to drive the transcription of several antioxidant genes including *Gclc*<sup>281-283</sup>, displayed a marked upregulation upon glutamate treatment and also a mild induction during H<sub>2</sub>O<sub>2</sub> or erastin exposure. In line with the downregulation of *Gclc* and *Cbs* gene expression during glutamate exposure in UNC0642 treated neurons, *Nfe2l2* showed a significant repression upon G9a inhibition during glutamate stress. Moreover, several GSTs that have antioxidant functions were strongly upregulated especially after glutamate treatment including *Gsta4*, *Gstm5*, and *Gstp1*, whereas *Gstm6* was downregulated upon glutamate and H<sub>2</sub>O<sub>2</sub> treatment. UNC0642 pre-treatment boosted the levels of *Gstm6* in all stress conditions but had no effect on other GSTs during ferroptosis induction. Interestingly, G9a inactivation increased the gene expression levels of *Gstm5* and *Gstp1* already in unstressed neurons, enhancing their antioxidant defense system. Together, G9a inhibition altered the transcription level of some ferroptosis-regulating genes in primary neurons that are mainly involved in glutathione metabolism or have detoxifying functions by catalyzing the conjugation of glutathione.

### 3.4 G9a induces neuronal cell death during inflammation-induced neurodegeneration *in vivo*

#### 3.4.1 Pharmacological G9a inhibition as neuroprotective treatment in CNS inflammation

In order to translate the findings from *in vitro* experiments back into the animal model and explore the concept of G9a inhibition as pharmacological strategy, EAE mice were injected once daily with 5 mg kg<sup>-1</sup> body weight UNC0642 or vehicle control, starting at symptom onset. In accordance with the *in vitro* findings, treatment with UNC0642 resulted in a significantly ameliorated EAE disease course compared to vehicle-treated mice (Fig. 3.10 A), which was reflected by a significantly lower cumulative score during the chronic phase (Fig. 3.10 B). Animals treated with UNC0642 had a similar disease onset and did not show differences in body weight change in comparison to vehicle treated mice (Fig. 3.10 C, D). G9a inhibition further led to a reduced loss of neurons in the ventral horn of the spinal cord as quantified by histopathological NeuN staining (Fig. 3.10 E). Moreover, immune cell infiltration as well as microglia activation, analyzed by CD3 and Iba1 staining's respectively, were not altered in UNC0642 treated mice (Fig. 3.10 F, G). To investigate the potential of UNC0642 to suppress the EAE-driven induction of H3K9me2 as observed earlier (Fig. 3.2 D), neuronal nuclei of healthy mice, healthy mice treated with UNC0642, EAE mice, and EAE mice treated with UNC0642 were stained for H3K9me2 and analyzed by flow cytometry. Indeed, UNC0642 treatment led to a complete suppression of H3K9me2 induction in EAE mice, whereas UNC0642 in healthy mice did not alter H3K9me2 levels (Fig. 3.10 H). In

order to visualize ferroptosis in CNS inflammation, 4-HNE was stained and quantified as a byproduct of lipid peroxidation that is used as a biomarker of ferroptosis. A significant increase in 4-HNE positive area was detected in cervical spinal cord sections of EAE mice during the acute phase compared to healthy controls (Fig. 3.10 I), confirming the induction of ferroptosis-related lipid peroxidation during neuroinflammation. Importantly, G9a inhibition by UNC0642 reduced 4-HNE levels during the chronic phase of EAE compared to vehicle treated mice (Fig. 3.10 J).

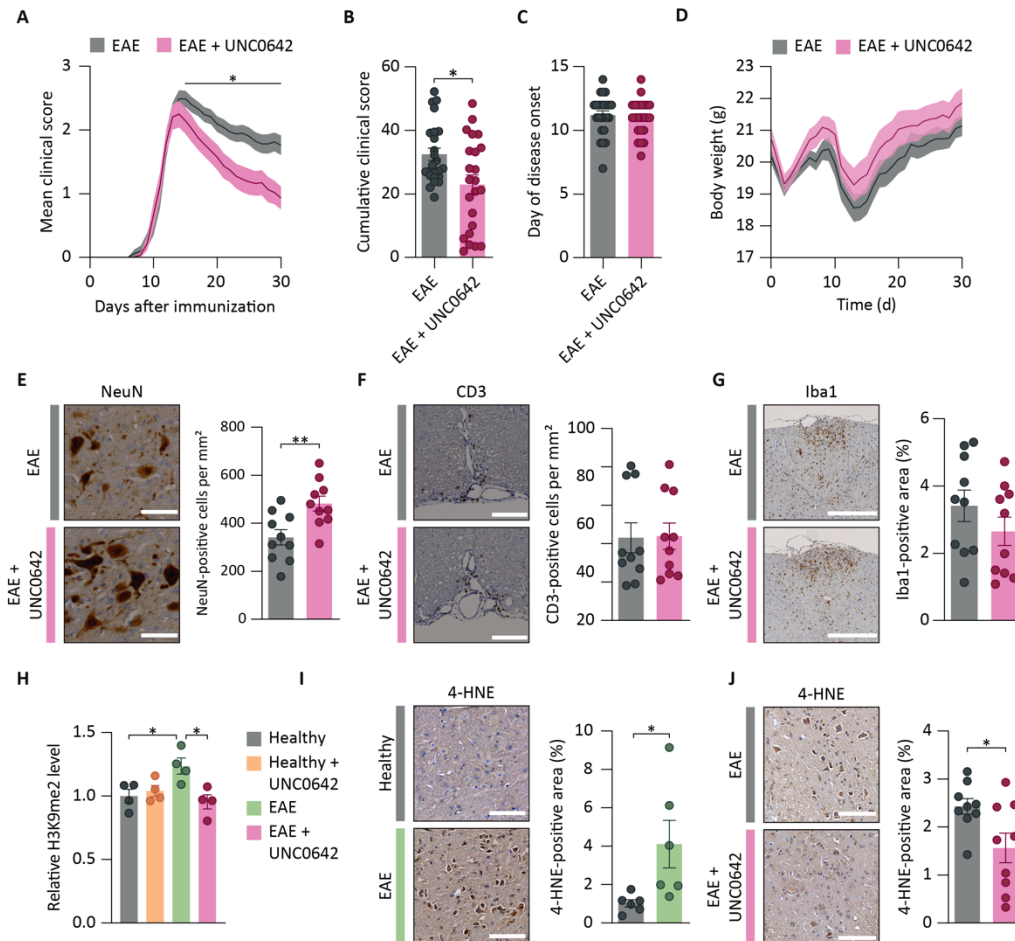


**Figure 3.10: Pharmacological inhibition of G9a ameliorated EAE symptoms.** (A) Disease course of mice subjected to EAE, which were treated with either DMSO or 5 mg kg<sup>-1</sup> body weight UNC0642 beginning at disease onset. Data are pooled from two independent experiments. DMSO, n = 24; UNC0642, n = 23. (B) Quantification of cumulative EAE score from day 15 to day 30 (two-tailed Mann–Whitney U-test: DMSO n = 24; UNC0642 n = 23; P = 0.0294). (C) Analysis of day of disease onset in EAE mice treated with 5 mg kg<sup>-1</sup> UNC0642 or vehicle (two-tailed Mann–Whitney U-test: DMSO n = 2, UNC0642 n = 23, P = 0.4842). (D) Body weight change of EAE mice treated with 5 mg kg<sup>-1</sup> UNC0642 or vehicle. (E) Histopathological staining and quantification of neuronal loss in the spinal cord of EAE mice ± UNC0642 at day 30 (two-tailed Mann–Whitney U-test: n = 10 per group; P = 0.0068). Scale bars, 100 μm. (F) Histopathological staining and quantification of T cells (CD3) in the spinal cord of EAE mice ± UNC0642 at day 30 (two-tailed Mann–Whitney U-test: n = 10 per group; P = 0.7959). Scale bars, 100 μm. (G) Histopathological staining of activated microglia (Iba1) in cervical spinal cord sections from EAE mice treated with 5 mg kg<sup>-1</sup> UNC0642 or vehicle (two-tailed Mann–Whitney U-test; n = 10 animals per group, P = 0.2176). (H) Flow cytometry of H3K9me2 IF of spinal cord neuronal nuclei from healthy, EAE, and UNC0642-treated EAE mice (one-way ANOVA: n = 4 mice each group, F<sub>(3,12)</sub> = 5.131, P = 0.0164. Tukey’s post hoc test: Healthy vs. EAE, P = 0.0436; healthy vs. healthy + UNC0642, P = 0.9502; healthy vs. EAE + UNC0642, P = 0.9324; EAE vs. healthy + UNC0642, P = 0.1071; EAE vs. EAE + UNC0642, P = 0.0155; healthy + UNC0642 vs. EAE + UNC0642, P = 0.6834). (I) Representative images and quantification of anti-4-HNE staining of cervical spinal cord sections from healthy vs. EAE mice during the acute phase (two-tailed Mann–Whitney U-test: n = 6 animals per group, P = 0.0043). Scale bars, 100 μm. (J) Representative images and quantification of cervical spinal cord section from chronic EAE treated with vehicle or 5 mg kg<sup>-1</sup> body weight UNC0642 (two-tailed Mann–Whitney U-test: n = 12 animals per group, P = 0.0279). Scale bars, 100 μm. Data are shown as mean values ± s.e.m. \*P < 0.05, \*\*P < 0.01, \*\*\*P < 0.001.

To explore whether the observed milder EAE disease course upon G9a inhibition was driven by differences in CNS infiltration, EAE mice subjected to UNC0642 or DMSO were immunophenotyped 18 days after immunization by flow cytometry. Absolute numbers of infiltrating immune cells were quantified by using 123 counting beads. No significant differences between UNC0642 treatment and vehicle control in all analyzed immune cell subsets, including granulocytes, macrophages, natural killer (NK) cells, T cells, B cells, and DCs were observed (Fig. 3.11). Therefore, UNC0642 treatment did not influence the amount and composition of infiltrating immune cells in the inflamed CNS.

Together, these findings demonstrate a neuroprotective effect of pharmacological G9a inhibition, displayed by a reduced neuronal loss and improvement of motor function in the EAE model. Additionally, G9a inhibition in EAE rescued in the induction of H3K9me2 and suppressed ferroptosis as measured by 4-HNE.

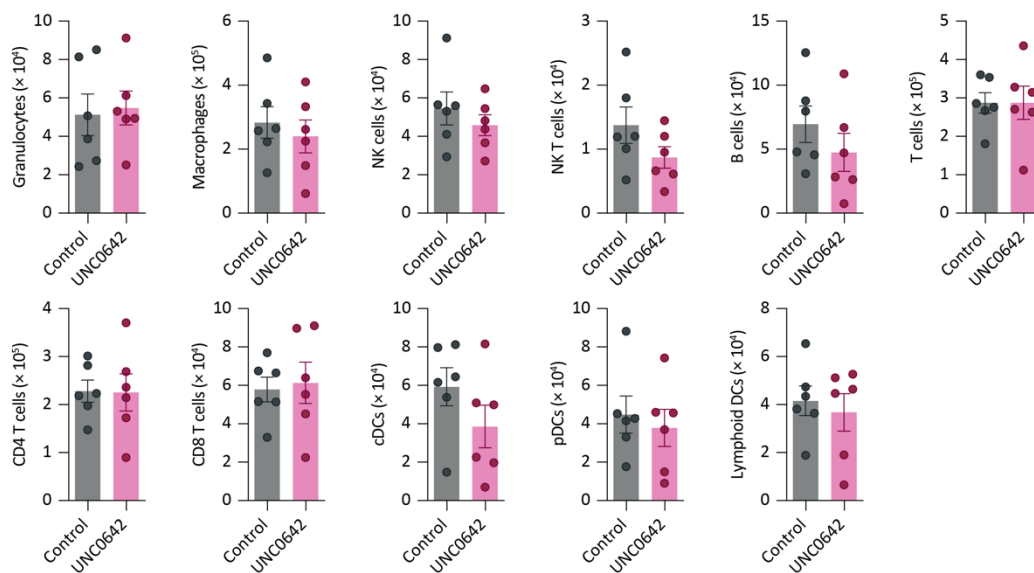


**Figure 3.11: Immune cell infiltration is not affected by UNC0642 treatment during EAE.** Quantification of absolute numbers of CNS-infiltrating immune cell populations in the CNS of mice that were treated with UNC0642 or vehicle during the acute phase of EAE, 18 days after immunization (two-tailed Mann–Whitney U-test:  $n = 6$  mice per group; granulocytes  $P = 0.6991$ ; macrophages  $P = 0.6991$ ; NK cells  $P = 0.4848$ ; NK T cells  $P = 0.3095$ ; B cells  $P = 0.2403$ ; T cells  $P = 0.9372$ ; CD4 T cells  $P = 0.9372$ ; CD8 T cells  $P = 0.9372$ ; cDCs  $P = 0.2403$ ; pDCs  $P = 0.9372$ ; lymphoid DCs  $P = 0.9372$ ). Data are shown as mean values  $\pm$  s.e.m. \* $P < 0.05$ , \*\* $P < 0.01$ , \*\*\* $P < 0.001$ .

### 3.4.2 Genetic disruption of G9a during CNS inflammation

#### 3.4.2.1 Validation of G9a deletion in $G9a^{fl/fl};Snap25-Cre$ mice

For validating the findings of pharmacological inhibition of G9a during EAE and to elucidate the effect of G9a deletion specifically in neurons, the genetic disruption of G9a in *Snap25*-positive cells in the mouse model was used via the Cre-loxP system. Therefore, the efficiency of G9a knockout in  $G9a^{fl/fl};Snap25-Cre$  was assessed in the CNS and lymph nodes. For the quantification of G9a signal in the brain and spinal cord, nuclei were isolated and the expression of G9a was assessed in neurons and

non-neurons by co-staining with NeuN. In the cortex of  $G9a^{fl/fl};Snap25-Cre$  mice, almost 90 % of NeuN-positive nuclei had no G9a signal, whereas in the spinal cord only 57 % of NeuN-positive nuclei showed a loss of G9a signal (Fig. 3.12 A, B). In both tissues the G9a signal in the NeuN-negative fraction was not affected, showing the neuron-specific loss of G9a in  $G9a^{fl/fl};Snap25-Cre$  mice (Fig. 3.12 A, B). Moreover, to exclude a G9a-mediated effect during EAE derived from changes in its expression in immune cells, CD4 T cells, CD8 T cells, and B cells extracted from lymph nodes of  $G9a^{fl/fl};Snap25-Cre$  mice were stained for G9a. All assessed immune cell subsets did not show any changes in G9a expression after intra-nuclear staining procedure (Fig. 3.12 A, B) suggesting a neuron-specific knockout.

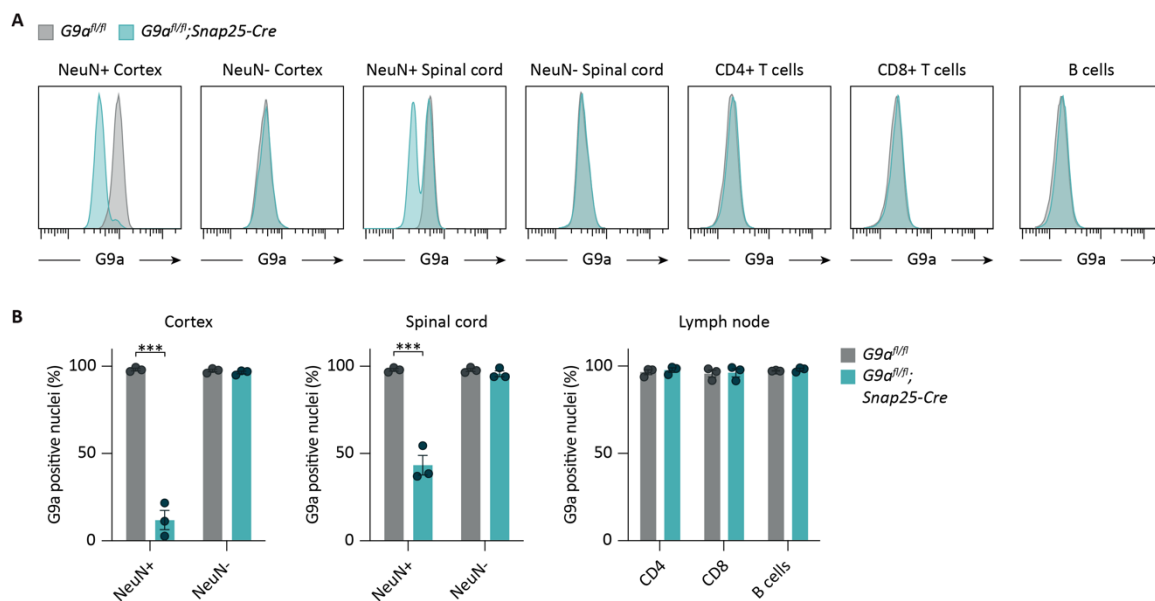


**Figure 3.12: G9a expression in brain, spinal cord, and lymph nodes of  $G9a^{fl/fl};Snap25-Cre$  mice.** (A) Representative histograms of G9a IF in NeuN-positive and NeuN-negative nuclei from cortex and spinal cord as well as in immune cell subsets from lymph nodes of  $G9a^{fl/fl}$  and  $G9a^{fl/fl};Snap25-Cre$  mice. (B) Quantification of G9a-positive events from cortex, spinal cord, and lymph nodes of  $G9a^{fl/fl}$  and  $G9a^{fl/fl};Snap25-Cre$  mice (two-way ANOVA:  $n = 3$  mice per group, Cortex:  $F_{(1,8)} = 227.8$ ,  $P < 0.0001$ , Bonferroni's post hoc test: NeuN+  $P < 0.0001$ , NeuN-  $P > 0.9999$ ; Spinal cord:  $F_{(1,8)} = 77.03$ ,  $P < 0.0001$ , Bonferroni's post hoc test: NeuN+  $P < 0.0001$ , NeuN-  $P > 0.9999$ ; Lymph node:  $F_{(2,12)} = 0.02491$ ,  $P = 0.9755$ , Bonferroni's post hoc test: CD4  $P > 0.9999$ , CD8  $P > 0.9999$ , B cells  $P > 0.9999$ ). Data are shown as mean values  $\pm$  s.e.m. \* $P < 0.05$ , \*\* $P < 0.01$ , \*\*\* $P < 0.001$ .

To check whether the downstream target of G9a, H3K9me2, is similarly affected by a deletion of G9a in *Snap25*-positive cells, the histone modification H3K9me2 was stained in nuclei of brain and spinal cord as well as in immune cells from lymph nodes of  $G9a^{fl/fl};Snap25-Cre$  mice. The H3K9me2 signal in the NeuN-positive fraction showed a reduction of more than 90 % in the cortex and about 58 % within the spinal cord (Fig. 3.13 A, B) like it has been observed for the G9a expression. In agreement with the results of G9a expression in non-neuronal nuclei in the cortex and spinal cord as well as in immune cell subsets from lymph nodes, the H3K9me2 expression was not altered in  $G9a^{fl/fl};Snap25-Cre$  mice (Fig. 3.13 A, B). In conclusion, this mouse model showed a neuron-specific deletion of G9a and suppression of its target H3K9me2. The cortical tissue displayed a highly efficient

reduction of the target protein, but in the spinal cord, which is mainly affected during EAE, the disruption of G9a occurs only in a subpopulation of neuronal nuclei.

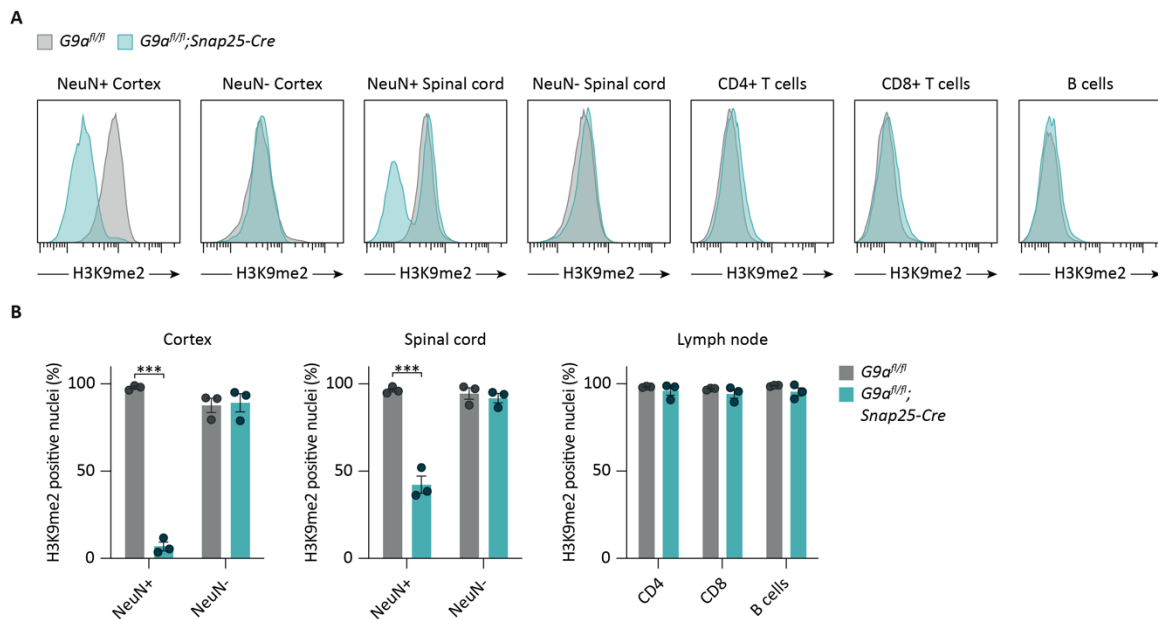


**Figure 3.13: H3K9me2 expression in brain, spinal cord, and lymph nodes of  $G9a^{fl/fl};Snap25-Cre$  mice. (A)** Representative histograms of H3K9me2 IF in NeuN-positive and NeuN-negative nuclei from cortex and spinal cord as well as in immune cell subsets from lymph nodes of  $G9a^{fl/fl}$  and  $G9a^{fl/fl};Snap25-Cre$  mice. **(B)** Quantification of H3K9me2-positive events from cortex, spinal cord, and lymph nodes of  $G9a^{fl/fl}$  and  $G9a^{fl/fl};Snap25-Cre$  mice (two-way ANOVA:  $n = 3$  mice per group, Cortex:  $F_{(1,8)} = 169.4$ ,  $P < 0.0001$ , Bonferroni's post hoc test: NeuN+  $P < 0.0001$ , NeuN-  $P > 0.9999$ ; Spinal cord:  $F_{(1,8)} = 60.28$ ,  $P < 0.0001$ , Bonferroni's post hoc test: NeuN+  $P < 0.0001$ , NeuN-  $P > 0.9999$ ; Lymph node:  $F_{(2,12)} = 0.05901$ ,  $P = 0.9430$ , Bonferroni's post hoc test: CD4  $P > 0.9999$ , CD8  $P = 0.8239$ , B cells  $P = 0.5482$ ). Data are shown as mean values  $\pm$  s.e.m. \* $P < 0.05$ , \*\* $P < 0.01$ , \*\*\* $P < 0.001$ .

### 3.4.2.2 Neuronal loss in $G9a^{fl/fl};Snap25-Cre$ mice during EAE

Following the characterization of  $G9a^{fl/fl};Snap25-Cre$  mice, the functional impact of neuronal deletion of G9a on CNS inflammation was assessed. For this purpose, EAE was induced in  $G9a^{fl/fl}$  and  $G9a^{fl/fl};Snap25-Cre$  littermates. Deletion of G9a in neurons did not change the clinical disability as analyzed by the disease course (Fig. 3.14 A) and the cumulative disease score (Fig. 3.14 B). Nevertheless,  $G9a^{fl/fl};Snap25-Cre$  mice had a slightly earlier disease onset compared to controls (Fig. 3.14 C). The body weight change, histopathological NeuN count in the ventral horn of the spinal cord on day 30, and CD3 cell infiltration on day 30 of the EAE did not differ between the groups (Fig. 3.14 D, E, F). Due to the observed neuroprotective phenotype during EAE in response to pharmacological inhibition of G9a, a milder disease course after genetic deletion of G9a in neurons would have been expected. However, the incomplete knockout of G9a in spinal cord neurons, might attenuate an effect of G9a on motor function during inflammation.

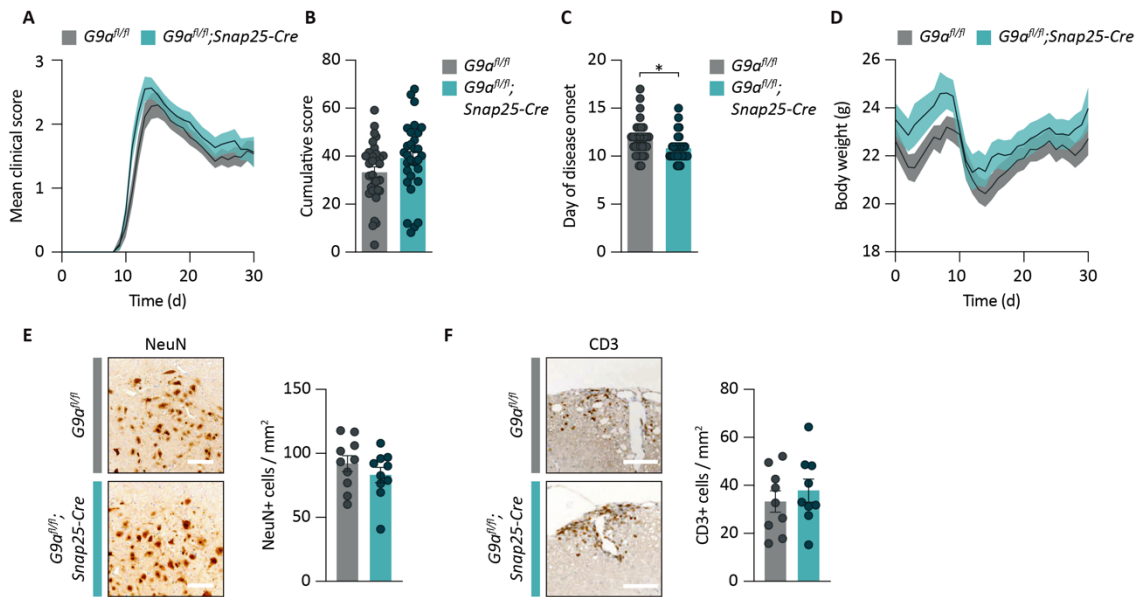


**Figure 3.14: Impact of genetic disruption of G9a in  $G9a^{fl/fl};Snap25-Cre$  mice during CNS inflammation. (A)** Disease course of  $G9a^{fl/fl}$  and  $G9a^{fl/fl};Snap25-Cre$  mice subjected to EAE. Data are pooled from three independent experiments.  $G9a^{fl/fl}$ , n = 31;  $G9a^{fl/fl};Snap25-Cre$ , n = 30. **(B)** Quantification of cumulative EAE score from day 15 to day 30 (two-tailed Mann–Whitney U-test:  $G9a^{fl/fl}$ , n = 31;  $G9a^{fl/fl};Snap25-Cre$ , n = 30, P = 0.0706). **(C)** Analysis of day of disease onset in  $G9a^{fl/fl}$  and  $G9a^{fl/fl};Snap25-Cre$  mice subjected to EAE (two-tailed Mann–Whitney U-test:  $G9a^{fl/fl}$ , n = 31;  $G9a^{fl/fl};Snap25-Cre$ , n = 30; P = 0.0111). **(D)** Body weight change of  $G9a^{fl/fl}$  and  $G9a^{fl/fl};Snap25-Cre$  during EAE.  $G9a^{fl/fl}$ , n = 31;  $G9a^{fl/fl};Snap25-Cre$ , n = 30. **(E)** Histopathological staining and quantification of neuronal loss in the spinal cord of  $G9a^{fl/fl}$  and  $G9a^{fl/fl};Snap25-Cre$  mice during EAE at day 30 (two-tailed Mann–Whitney U-test: n = 10 per group; P = 0.3930). Scale bars, 100  $\mu$ m. **(F)** Histopathological staining and quantification of T cells (CD3) in the spinal cord of  $G9a^{fl/fl}$  and  $G9a^{fl/fl};Snap25-Cre$  mice at day 30 of EAE (two-tailed Mann–Whitney U-test: n = 10 per group; P = 0.6665). Scale bars, 100  $\mu$ m. Data are shown as mean values  $\pm$  s.e.m. \*P < 0.05, \*\*P < 0.01, \*\*\*P < 0.001.

To determine whether neuronal loss is more pronounced within the neuronal population of the spinal cord where G9a is not deleted, the abundance of neuronal nuclei in the G9a-positive fraction was compared to the G9a-negative fraction from  $G9a^{fl/fl};Snap25-Cre$  mice. First, the overall percentage of NeuN-positive nuclei was assessed in  $G9a^{fl/fl}$  and  $G9a^{fl/fl};Snap25-Cre$  mice 30 days after immunization with MOG peptide. Thereby, no differences in NeuN+ nuclei frequencies between the groups were detected (Fig. 3.15 A). Next, to assess the impact of G9a deletion on neuronal survival in spinal cords during CNS inflammation, the percentage of NeuN-positive events from G9a-positive as well as from G9a-negative nuclei in  $G9a^{fl/fl};Snap25-Cre$  mice were compared in healthy and EAE mice. Notably, a reduction of NeuN-positive nuclei was observed in the population that did not lose its G9a signal in healthy vs. EAE nuclei from  $G9a^{fl/fl};Snap25-Cre$  mice. However, in the fraction that had a deletion of G9a, the NeuN nuclei-count was not altered in healthy or EAE  $G9a^{fl/fl};Snap25-Cre$  mice (Fig. 3.15 B). Therefore, consistently with our *in vitro* and *in vivo* pharmacological results the genetic deletion of G9a has a neuroprotective effect in the EAE model, but due to the insufficient frequency of G9a-deleted neurons in the spinal cord, this effect was concealed in overall NeuN counts and the disease course.

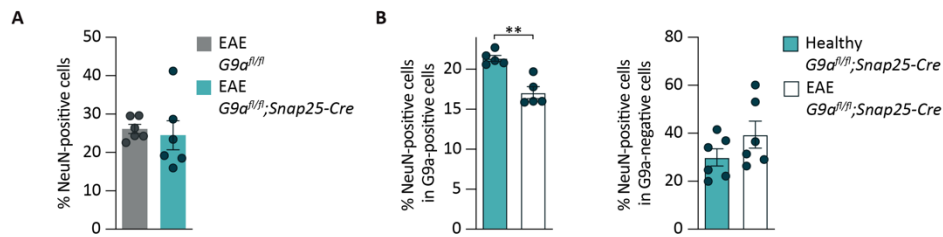


**Figure 3.15: Neuronal loss in spinal cords of *G9a<sup>fl/fl</sup>;Snap25-Cre* mice during inflammation.** (A) Quantification of NeuN-positive spinal cord nuclei from *G9a<sup>fl/fl</sup>* and *G9a<sup>fl/fl</sup>;Snap25-Cre* mice subjected to EAE (two-tailed Mann–Whitney U-test:  $n = 6$  per group;  $P = 0.3095$ ). (B) Quantification of the percentage of neuronal nuclei from spinal cords of *G9a<sup>fl/fl</sup>;Snap25-Cre* mice that were subjected to EAE or healthy controls in the G9a-negative (left; two-tailed Mann–Whitney U-test:  $n = 5$  per group;  $P = 0.0079$ ) or G9a-positive (right; two-tailed Mann–Whitney U-test:  $n = 6$  per group;  $P = 0.3095$ ) fraction. Data are shown as mean values  $\pm$  s.e.m. \* $P < 0.05$ , \*\* $P < 0.01$ , \*\*\* $P < 0.001$ .

### 3.5 G9a inhibition enhances expression of ferroptosis-related genes in neurons during CNS inflammation *in vivo*

For the validation of G9a-mediated neuroprotection via the ferroptosis pathway, neuronal nuclei from spinal cord of healthy and EAE animals treated with UNC0642 or vehicle controls were analyzed for their expression of relevant ferroptosis genes. Therefore, nuclei were sorted upon their NeuN expression and mRNA was extracted followed by quantification of the target gene expression via qPCR. Interestingly, UNC0642 treatment in healthy mice resulted already in an induction of several target genes (Fig. 3.16, 3.17), indicating the efficacy of G9a inhibition on transcriptional regulation in the CNS.

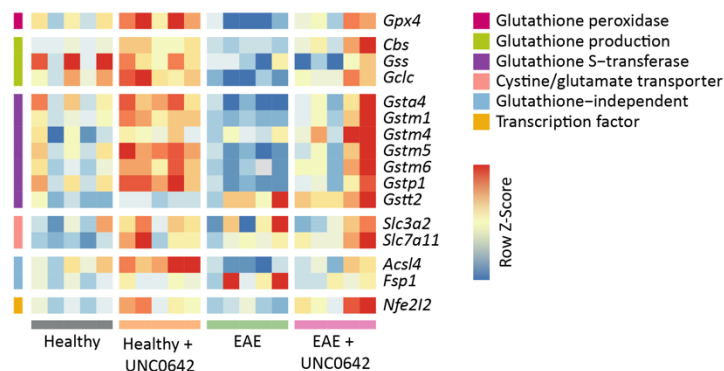


**Figure 3.16: G9a-mediated transcriptional regulation of ferroptosis regulated genes during EAE.** Gene expression heatmap of qPCR data from sorted spinal cord neuronal nuclei of healthy, EAE, and UNC0642-treated EAE mice.  $n = 5$  mice per group.

Moreover, most of the genes with anti-ferroptotic properties showed a downregulation during EAE, among them key regulators of ferroptosis like *Cbs*, a marker of transsulfuration pathway activity that synthesizes glutathione from methionine, as well as the lipid hydroperoxidase GPX4 (*Gpx4*). Both genes showed a prominent upregulation upon G9a inhibition in healthy mice and a rescue to above healthy

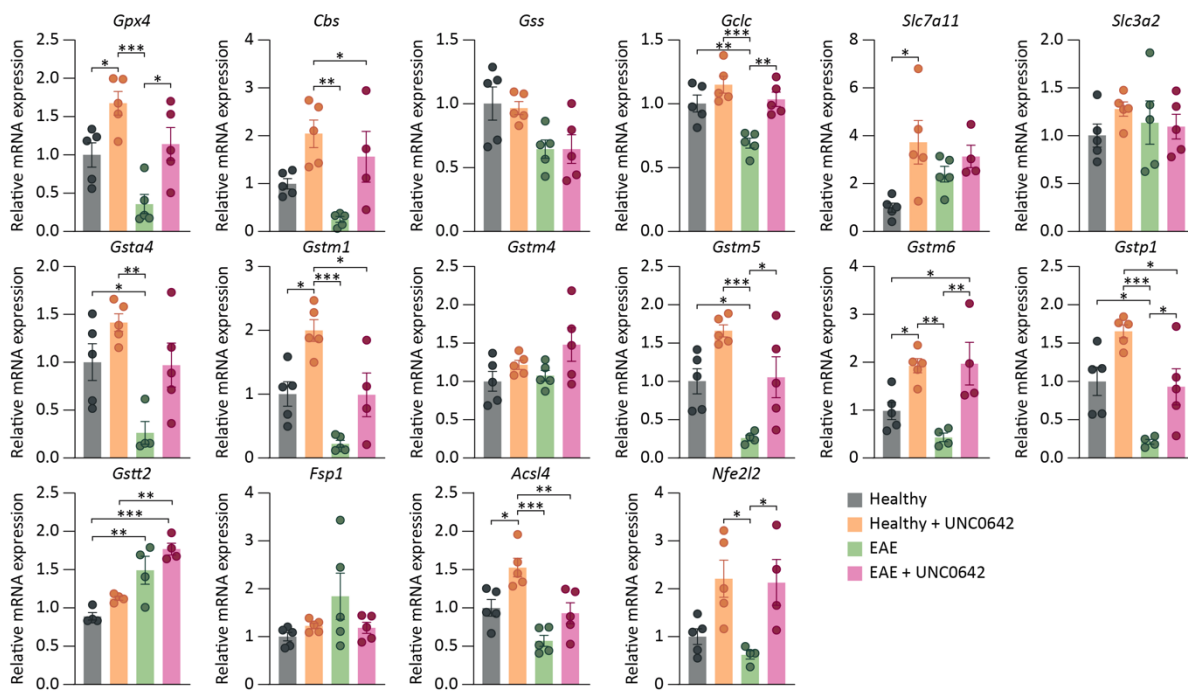


**Figure 3.17: Gene expression analysis of ferroptosis-related genes during EAE upon UNC0642 treatment.** Transcriptional level of selected ferroptosis-relevant genes in healthy and EAE animals  $\pm$  UNC0642 treatment (one-way ANOVA:  $n = 4 - 5$  per group; **Gpx4**:  $F_{(3,16)} = 10.61$ ,  $P = 0.0004$ , Tukey's post hoc test: Healthy vs. EAE  $P = 0.0645$ , Healthy vs. Healthy + UNC0642  $P = 0.049$ , Healthy vs. EAE + UNC0642  $P = 0.9273$ , EAE vs. Healthy + UNC0642  $P = 0.0002$ , EAE vs. EAE + UNC0642  $P = 0.0196$ , Healthy + UNC0642 vs. EAE + UNC0642  $P = 0.1492$ ; **Gclc**:  $F_{(3,16)} = 11.46$ ,  $P = 0.0003$ , Tukey's post hoc test: Healthy vs. EAE  $P = 0.0080$ , Healthy vs. Healthy + UNC0642  $P = 0.2998$ , Healthy vs. EAE + UNC0642  $P = 0.9757$ , EAE vs. Healthy + UNC0642  $P = 0.0002$ , EAE vs. EAE + UNC0642  $P = 0.0035$ , Healthy + UNC0642 vs. EAE + UNC0642  $P = 0.5113$ ; **Cbs**:  $F_{(3,15)} = 8.225$ ,  $P = 0.0018$ , Tukey's post hoc test: Healthy vs. EAE  $P = 0.0606$ , Healthy vs. Healthy + UNC0642  $P = 0.2394$ , Healthy vs. EAE + UNC0642  $P = 0.5102$ , EAE vs. Healthy + UNC0642  $P = 0.0013$ , EAE vs. EAE + UNC0642  $P = 0.0234$ , Healthy + UNC0642 vs. EAE + UNC0642  $P = 0.6324$ ; **Slc7a11**:  $F_{(3,15)} = 4.671$ ,  $P = 0.0170$ , Tukey's post hoc test: Healthy vs. EAE  $P = 0.2899$ , Healthy vs. Healthy + UNC0642  $P = 0.0132$ , Healthy vs. EAE + UNC0642  $P = 0.0793$ , EAE vs. Healthy + UNC0642  $P = 0.3364$ , EAE vs. EAE + UNC0642  $P = 0.8006$ , Healthy + UNC0642 vs. EAE + UNC0642  $P = 0.8809$ ; **Nfe2l2**:  $F_{(3,14)} = 6.209$ ,  $P = 0.0066$ , Tukey's post hoc test: Healthy vs. EAE  $P = 0.8330$ , Healthy vs. Healthy + UNC0642  $P = 0.0568$ , Healthy vs. EAE + UNC0642  $P = 0.1035$ , EAE vs. Healthy + UNC0642  $P = 0.0159$ , EAE vs. EAE + UNC0642  $P = 0.0306$ , Healthy + UNC0642 vs. EAE + UNC0642  $P = 0.9980$ ; **Gss**:  $F_{(3,16)} = 4.122$ ,  $P = 0.0241$ , Tukey's post hoc test: Healthy vs. EAE  $P = 0.0807$ , Healthy vs. Healthy + UNC0642  $P = 0.9938$ , Healthy vs. EAE + UNC0642  $P = 0.0802$ , EAE vs. Healthy + UNC0642  $P = 0.1281$ , EAE vs. EAE + UNC0642  $P > 0.9999$ , Healthy + UNC0642 vs. EAE + UNC0642  $P = 0.1272$ ; **Slc3a2**:  $F_{(3,16)} = 0.1695$ ,  $P = 0.6185$ , Tukey's post hoc test: Healthy vs. EAE  $P = 0.9146$ , Healthy vs. Healthy + UNC0642  $P = 0.5600$ , Healthy vs. EAE + UNC0642  $P = 0.9694$ , EAE vs. Healthy + UNC0642  $P = 0.9037$ , EAE vs. EAE + UNC0642  $P = 0.9970$ , Healthy + UNC0642 vs. EAE + UNC0642  $P = 0.8149$ ; **Fsp1**:  $F_{(3,16)} = 2.074$ ,  $P = 0.1440$ , Tukey's post hoc test: Healthy vs. EAE  $P = 0.1301$ , Healthy vs. Healthy + UNC0642  $P = 0.9237$ , Healthy vs. EAE + UNC0642  $P = 0.9557$ , EAE vs. Healthy + UNC0642  $P = 0.3465$ , EAE vs. EAE + UNC0642  $P = 0.2955$ , Healthy + UNC0642 vs. EAE + UNC0642  $P = 0.9995$ ; **Acsl4**:  $F_{(3,16)} = 12.47$ ,  $P = 0.0002$ , Tukey's post hoc test: Healthy vs. EAE  $P = 0.0647$ , Healthy vs. Healthy + UNC0642  $P = 0.0200$ , Healthy vs. EAE + UNC0642  $P = 0.9689$ , EAE vs. Healthy + UNC0642  $P < 0.0001$ , EAE vs. EAE + UNC0642  $P = 0.1454$ , Healthy + UNC0642 vs. EAE + UNC0642  $P = 0.0081$ ; **Gsta4**:  $F_{(3,15)} = 6.980$ ,  $P = 0.0037$ , Tukey's post hoc test: Healthy vs. EAE  $P = 0.0468$ , Healthy vs. Healthy + UNC0642  $P = 0.3430$ , Healthy vs. EAE + UNC0642  $P = 0.9991$ , EAE vs. Healthy + UNC0642  $P = 0.0019$ , EAE vs. EAE + UNC0642  $P = 0.0591$ , Healthy + UNC0642 vs. EAE + UNC0642  $P = 0.2842$ ; **Gstm1**:  $F_{(3,15)} = 14.34$ ,  $P = 0.0001$ , Tukey's post hoc test: Healthy vs. EAE  $P = 0.0515$ , Healthy vs. Healthy + UNC0642  $P = 0.0110$ , Healthy vs. EAE + UNC0642  $P > 0.9999$ , EAE vs. Healthy + UNC0642  $P < 0.0001$ , EAE vs. EAE + UNC0642  $P = 0.0748$ , Healthy + UNC0642 vs. EAE + UNC0642  $P = 0.00153$ ; **Gstm4**:  $F_{(3,16)} = 2.426$ ,  $P = 0.1033$ , Tukey's post hoc test: Healthy vs. EAE  $P = 0.9810$ , Healthy vs. Healthy + UNC0642  $P = 0.6840$ , Healthy vs. EAE + UNC0642  $P = 0.0988$ , EAE vs. Healthy + UNC0642  $P = 0.8792$ , EAE vs. EAE + UNC0642  $P = 0.1893$ , Healthy + UNC0642 vs. EAE + UNC0642  $P = 0.5301$ ; **Gstm5**:  $F_{(3,15)} = 10.29$ ,  $P = 0.0006$ , Tukey's post hoc test: Healthy vs. EAE  $P = 0.0453$ , Healthy vs. Healthy + UNC0642  $P = 0.0612$ , Healthy vs. EAE + UNC0642  $P = 0.9955$ , EAE vs. Healthy + UNC0642  $P = 0.0003$ , EAE vs. EAE + UNC0642  $P = 0.0299$ , Healthy + UNC0642 vs. EAE + UNC0642  $P = 0.0931$ ; **Gstm6**:  $F_{(3,14)} = 9.490$ ,  $P = 0.0011$ , Tukey's post hoc test: Healthy vs. EAE  $P = 0.3930$ , Healthy vs. Healthy + UNC0642  $P = 0.0454$ , Healthy vs. EAE + UNC0642  $P = 0.0497$ , EAE vs. Healthy + UNC0642  $P = 0.0029$ , EAE vs. EAE + UNC0642  $P = 0.0036$ , Healthy + UNC0642 vs. EAE + UNC0642  $P = 0.9994$ ; **Gstp1**:  $F_{(3,15)} = 11.81$ ,  $P = 0.0003$ , Tukey's post hoc test: Healthy vs. EAE  $P = 0.0247$ , Healthy vs. Healthy + UNC0642  $P = 0.0533$ , Healthy vs. EAE + UNC0642  $P = 0.9888$ , EAE vs. Healthy + UNC0642  $P = 0.0001$ , EAE vs. EAE + UNC0642  $P = 0.0436$ , Healthy + UNC0642 vs. EAE + UNC0642  $P = 0.0293$ ; **Gstt2**:  $F_{(3,12)} = 14.04$ ,  $P = 0.0003$ , Tukey's post hoc test: Healthy vs. EAE  $P = 0.0069$ , Healthy vs. Healthy + UNC0642  $P = 0.4011$ , Healthy vs. EAE + UNC0642  $P = 0.0003$ , EAE vs. Healthy + UNC0642  $P = 0.1140$ , EAE vs. EAE + UNC0642  $P = 0.2833$ , Healthy + UNC0642 vs. EAE + UNC0642  $P = 0.0044$ ). Data are shown as mean values  $\pm$  s.e.m. \* $P < 0.05$ , \*\* $P < 0.01$ , \*\*\* $P < 0.001$ .

levels during EAE (Fig. 3.16, 3.17). In contrast, the anti-ferroptotic subunit *Slc7a11* of the system  $Xc^-$ , which controls intracellular glutathione levels, was upregulated upon G9a inhibition in healthy mice but also by EAE itself, indicating a potential beneficial adaptation of neurons during inflammation (Fig. 3.16, 3.17). The mRNA expression of the system  $Xc^-$  subunit *Slc3a2* was not altered by EAE or G9a inhibition (Fig. 3.16, 3.17). More generally, several genes involved in the biosynthesis and utilization of glutathione were repressed during EAE. Among them, *Gclc* and *Gss*, which are the main regulators of glutathione synthesis, as well as *Gpx4*, which prevents lipid peroxidation by using glutathione as a substrate. In addition, GSTs such as *Gsta4*, *Gstm1*, *Gstm5*, *Gstm6*, *Gstp1*, and *Gstt2* showed a downregulation during EAE. Almost all of the glutathione-dependent genes, except *Gss* and *Gstt2*, were rescued by UNC0642 treatment during neuroinflammation (Fig. 3.16, 3.17). This demonstrates a strong impact of G9a-mediated transcriptional regulation on the glutathione pathway, while *Fsp1*, a glutathione-independent anti-ferroptotic molecule showed only a slight increase during EAE and was not regulated upon UNC0642 treatment (Fig. 3.16, 3.17). On the contrary, the enzyme *Acs14* that can promote lipid peroxidation and therefore ferroptosis was upregulated in healthy UNC0642 treated animals but showed a reduced expression in EAE which was prevented by UNC0642 in EAE, indicating a rebalancing of ferroptosis-related genes (Fig. 3.16, 3.17). In addition, the transcription factor *Nfe2l2*, encoding NRF2 that suppresses lipid peroxidation<sup>284</sup> showed a significant upregulation upon G9a inactivation that persists during neuroinflammation (Fig. 3.16, 3.17).

In conclusion, G9a inhibition led to a de-repression of several anti-ferroptotic genes, many of which are implicated in the generation of the intracellular antioxidant glutathione and might thereby exert its anti-ferroptotic and neuroprotective function in CNS inflammation.

### 3.6 Mechanism of G9a-dependent neuroprotective effect in CNS inflammation

The obtained results from *in vitro* and *in vivo* experiments indicate a substantial role of G9a in the regulation of neuronal susceptibility during inflammation-induced neurodegeneration. Glutamate excitotoxicity and oxidative stress resulted in calcium influx that induced the G9a-dependent transcriptionally repressive mark H3K9me2 and thereby initiated ferroptosis. Additionally, ferroptosis itself enhanced G9a activity leading to a self-reinforcing feedback loop. During neuroinflammation, several anti-ferroptotic genes showed a downregulation, indicating the initiation of neuronal cell death via ferroptosis. Genes implicated in the synthesis of the main intracellular antioxidant glutathione were impaired during EAE. *Gclc*, the first-rate limiting enzyme of glutathione synthesis that generates glutathione from cystine, as well as *Cbs* that synthesize glutathione from homocysteine via the transsulfuration pathway in the case of a cystine restriction, were both impaired in neurons of EAE mice. Moreover, the transcript level of the lipid hydroperoxide *Gpx4*, which utilize glutathione as a substrate to prevent lipid peroxidation and finally ferroptosis, was suppressed during

neuroinflammation that resulted in neuronal cell death. Pharmacological inhibition of G9a prevented the repression of those anti-ferroptosis genes and thereby ameliorated calcium overload and neuronal loss. Together, these findings indicate the neuroprotective function of G9a in regulating ferroptosis induction via the transcriptional control of anti-ferroptosis genes (Fig. 3.18).

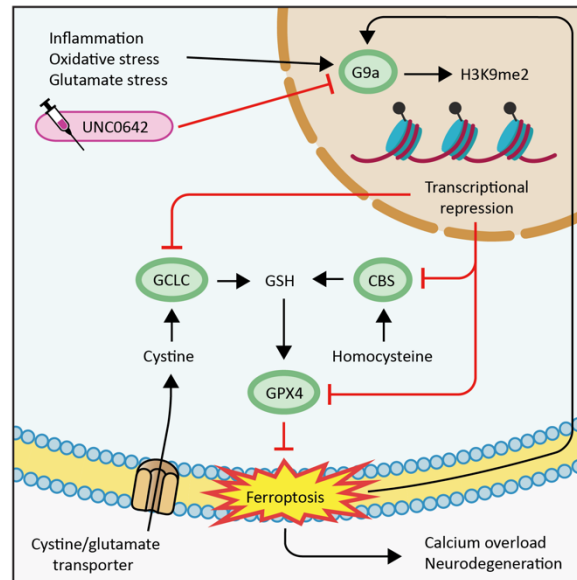


**Figure 3.18: Mechanism of G9a-dependent ferroptosis regulation.** CNS inflammation enhances oxidative stress and extracellular glutamate levels that trigger G9a activity in neurons, resulting in transcriptional repression via G9a-mediated H3K9me2 induction. Inactivation of G9a by UNC0642 enhances the transcription of the anti-ferroptotic genes *Gclc*, *Cbs*, and *Gpx4*, thereby increasing the availability of glutathione and preventing lipid peroxidation, which reduce the induction of ferroptosis. Ferroptosis itself is enhancing G9a activity leading to a self-amplifying feedforward mechanism.

### 3.7 Ferroptosis induction in MS brains and human iPSC neurons

To translate the findings from the EAE mouse model to MS, neuronal G9a activity was measured in brain sections of MS patients. Therefore, IF of G9a downstream target H3K9me2 was quantified in brains of MS patients compared to control individuals without neurological symptoms. Nuclear expression of H3K9me2 was detected in NeuN-positive cells which revealed a significant upregulation in the NAGM and in lesions of MS patients in comparison to controls (Fig. 3.19 A), manifesting the involvement of aberrant G9a-regulated gene transcription during MS. Furthermore, the induction of ferroptosis during neuroinflammation in MS brain sections was investigated by measurement of the main regulator of ferroptosis, GPX4, via RNAscope *in situ* hybridization. The amount of SNAP25 positive neurons that co-express GPX4 was significantly reduced in NAGM and lesions of MS patients compared to control patients (Fig. 3.19 B). In agreement, also the GPX4 positive dots per SNAP25 positive cells were reduced in MS NAGM and lesions (Fig. 3.19 B).

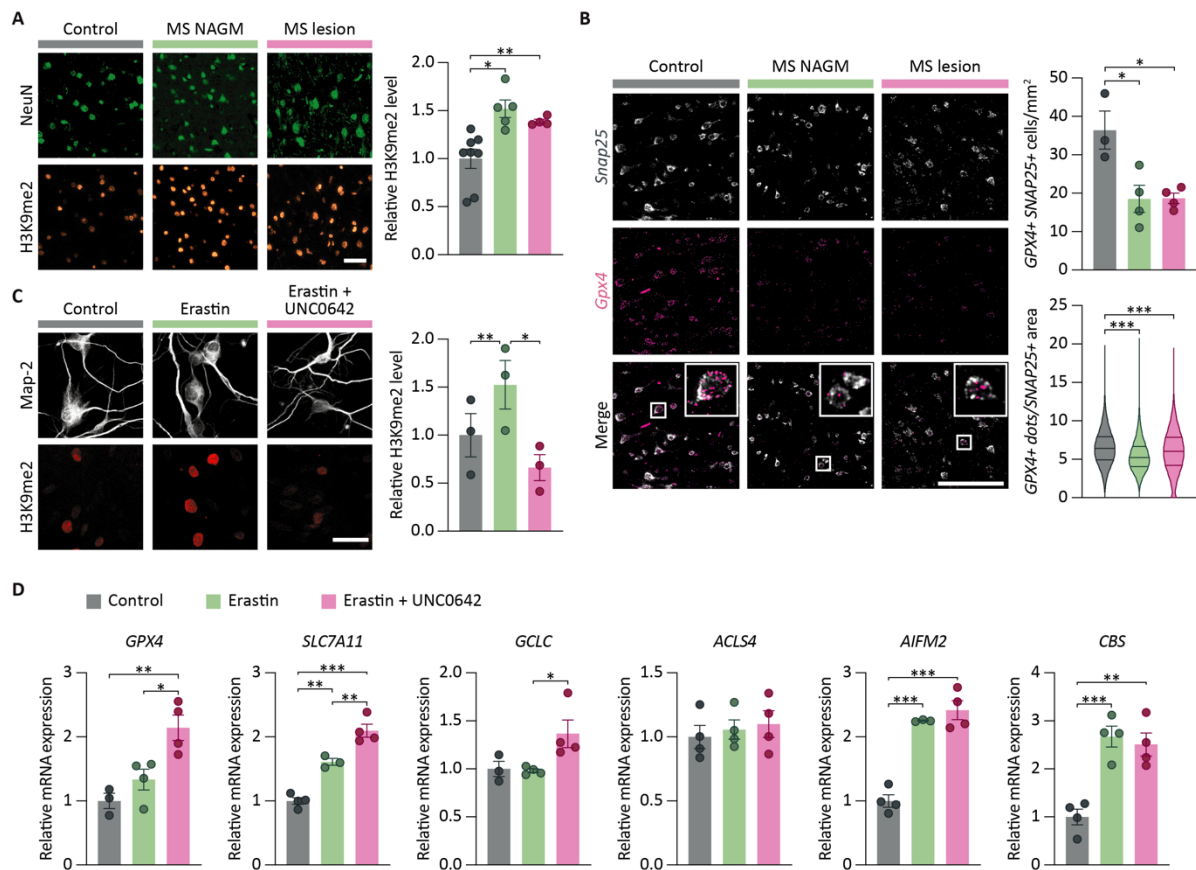


**Figure 3.19: Ferroptosis induction in MS brains and human iPSC neurons.** **(A)** Representative images and quantification of mean fluorescence of immunohistochemistry staining's from H3K9me2 in NeuN+ cells of brain sections from MS NAGM or cortical MS lesions in comparison to control individuals without neurological diseases (one-way ANOVA: Controls,  $n = 8$ ; MS NAGM,  $n = 5$ ; MS lesion,  $n = 4$ ,  $F_{(2,14)} = 9.170$ ,  $P = 0.0028$ ; Tukey's post hoc test: Control vs. NAGM  $P = 0.0034$ ; control vs. MS  $P = 0.0350$ ; NAGM vs. MS  $P = 0.6751$ ). Scale bar, 80  $\mu\text{m}$ . **(B)** RNAscope fluorescence in situ hybridization of *GPX4* transcripts in brain sections of control individuals and multiple sclerosis NAGM and cortical lesions (one-way ANOVA: above: Control  $n = 3$  patients, MS NAGM  $n = 4$  patients, MS lesion  $n = 4$  patients,  $F_{(2,8)} = 8.756$ ,  $P = 0.0097$ ; Dunnett's post hoc test: Control vs. MS NAGM  $P = 0.0104$ , Control vs. MS lesion  $P = 0.0108$ ; below: Control  $n = 79057$  neurons; MS NAGM  $n = 135305$  neurons; MS lesion  $n = 64444$  neurons;  $F_{(2,278803)} = 5362$ ,  $P < 0.0001$ , Dunnett's post hoc test: Control vs. MS NAGM  $P < 0.0001$ , Control vs. MS lesion  $P < 0.0001$ ). Scale bar, 100  $\mu\text{m}$ . **(C)** H3K9me2 immunostaining and quantification in response to ferroptosis induction with erastin in human iPSC neurons (repeated measures one-way ANOVA:  $n = 3$  independent experiments,  $F_{(1,060,2.12)} = 49.21$ ,  $P = 0.0169$ . Tukey's post hoc test: Control vs. + Erastin,  $P = 0.0082$ ; control vs. Erastin + UNC0642,  $P = 0.1136$ , Erastin vs. Erastin + UNC0642,  $P = 0.0327$ ). Scale bar, 40  $\mu\text{m}$ . **(D)** mRNA expression levels of indicated genes from hiPSC-neurons treated with erastin  $\pm$  UNC0642 vs. Control (one-way ANOVA:  $n = 3 - 4$  per group; *GPX4*:  $F_{(2,8)} = 11.43$ ,  $P = 0.0045$ . Tukey's post hoc test: Control vs. Erastin,  $P = 0.4265$ ; Control vs. Erastin + UNC0642,  $P = 0.0048$ ; Erastin vs. Erastin + UNC0642,  $P = 0.0211$ ; *SLC7A11*:  $F_{(2,8)} = 56.75$ ,  $P < 0.0001$ . Tukey's post hoc test: Control vs. Erastin,  $P = 0.0015$ ; Control vs. Erastin + UNC0642,  $P < 0.0001$ ; Erastin vs. Erastin + UNC0642,  $P = 0.0059$ ; *GCLC*:  $F_{(2,8)} = 5.039$ ,  $P = 0.0383$ . Tukey's post hoc test: Control vs. Erastin,  $P = 0.9897$ ; Control vs. Erastin + UNC0642,  $P = 0.0816$ ; Erastin vs. Erastin + UNC0642,  $P = 0.0487$ ; *ACSL4*:  $F_{(2,9)} = 0.2993$ ,  $P = 0.7484$ . Tukey's post hoc test: Control vs. Erastin,  $P = 0.8961$ ; Control vs. Erastin + UNC0642,  $P = 0.7296$ ; Erastin vs. Erastin + UNC0642,  $P = 0.9451$ ; *AIFM2*:  $F_{(2,8)} = 50.09$ ,  $P < 0.0001$ . Tukey's post hoc test: Control vs. Erastin,  $P = 0.0002$ ; Control vs. Erastin + UNC0642,  $P < 0.0001$ ; Erastin vs. Erastin + UNC0642,  $P = 0.6083$ ; *CBS*:  $F_{(2,9)} = 19.27$ ,  $P = 0.0006$ . Tukey's post hoc test: Control vs. Erastin,  $P = 0.0008$ ; Control vs. Erastin + UNC0642,  $P = 0.0017$ ; Erastin vs. Erastin + UNC0642,  $P = 0.8435$ ). Data are shown as mean values  $\pm$  s.e.m. \* $P < 0.05$ , \*\* $P < 0.01$ , \*\*\* $P < 0.001$ .

Following the validation of enhanced G9a activity and dysregulation of ferroptosis defense system, the regulation of ferroptosis relevant genes by G9a inhibition was assessed in human iPSC derived neurons. First, ferroptosis was induced in human iPSC neurons by erastin treatment and G9a activity was measured via H3K9me2 IF. In accordance with the *in vitro* data of mouse primary neurons,

H3K9me2 showed an induction in response to erastin stimulation, which was prevented by UNC0642 pre-treatment (Fig. 3.19 C), indicating the efficacy of G9a inhibitor in human cells. To confirm if G9a is repressing genes involved in the ferroptosis pathway in human iPSC neurons, mRNA expression of genes that have been shown to be regulated by G9a in neuronal nuclei of EAE mice have been investigated in human neurons upon ferroptosis induction and exposure to UNC0642. Upregulation of the anti-ferroptosis genes *GPX4*, *SLC7A11*, *AIFM2*, and *CBS* (Fig. 3.18 D) was detected in response to ferroptosis induction by erastin, suggesting an adaptation to counteract neuronal cell death by the ferroptosis pathway. In line with the findings of neuronal nuclei from EAE mice treated with UNC0642, a prominent upregulation of *GPX4* and *GCLC* was found upon erastin stimulation in UNC0642-treated neurons in comparison to vehicle-treated human iPSC neurons (Fig. 3.19 D). Moreover, *SLC7A11* expression was highly induced in response to G9a inhibition in human neurons when ferroptosis was initiated (Fig. 3.19 D).

In summary, these results demonstrate the involvement of epigenetic regulator G9a during neuroinflammation in MS patients. Moreover, an implication of ferroptosis in MS patients was detected by the downregulation of *GPX4* levels in MS brains. G9a mediated transcriptional regulation of ferroptosis relevant genes was confirmed in human neurons that opens a translational perspective.

## 4 Discussion

### 4.1 H3K9me2 regulation during neuroinflammation

The starting point of this project was to evaluate the regulation of epigenetic modulators in neurons during inflammation-induced neurodegeneration and characterize potential candidates that can be pharmacologically targeted. Several deregulated epigenetic modifiers have been identified in inflammation-exposed motor neurons during EAE in a cell-type specific isolation of translating ribosomes, that have been previously performed in our lab<sup>94</sup>. Strikingly, the majority of dysregulated genes belongs to the group of histone modifying enzymes, whereas most of them showed an induction in inflamed motor neurons rather than a repression (Fig. 3.1 A). Nevertheless, the regulation of prominent modifiers of DNA methylation (*Dnmt1*) or chromatin accessibility (e. g. *Smarcd2*, *Smarcd1*) were affected during EAE, indicating a broad influence of CNS inflammation on the epigenetic landscape in neurons. However, it seems quite obvious that the dynamic character of hPTMs is primarily altered in impaired motor neurons compared to the relatively stable methylation of DNA, at least when considering the transcript levels of the respective modifying enzymes (Fig. 3.1 A). Among the histone modifying enzymes are almost exclusively methyltransferases (*Ehmt2*, *Kmt2d*, *Smyd1*, *Setd1b*, *Smyd2*, *Smyd4*) and demethylases (*Kdm1b*, *Kdm6b*, *Kdm4d*, *Kdm8*) that can promote or suppress gene transcription by either adding activating marks or removing repressing ones and vice versa. Considering the upregulated KMTs and KDMs, there is no apparent trend of dysregulated enzymes that preferentially mediate gene activation or repression. The induction of genes like *Kmt2d*, *Smyd1d* or *Setd1b* result in the activation of transcription whereas *Kdm1b* and *Ehmt2* act repressive. Moreover, the downregulation of *Smyd2* could also result in the suppression of gene transcription as it mediates the methylation on H3K4 that enhances gene transcription<sup>224</sup>. These results indicate that impaired gene expression during neuroinflammation that is caused by dysregulated histone methylation might be counterbalanced by opposing proteins. One example is the upregulated transcript of KMT2D that add the activating methyl-mark on H3K4, whereas its counterpart KMD1B, a demethylase of H3K4, has the opposite effect. Moreover, the transcript levels of the enzymes that mediate the addition and removal of the repressive dimethylation on H3K9, EHMT2 and KDM4D respectively, are both upregulated, supporting the hypothesis that impaired gene expression in injured neurons might be compensated. Besides alterations in histone methylation, the acetylation of lysine residues seems less affected during EAE. The only transcript that is upregulated is HDAC7 that repress gene transcription, whereas SIRT2 (a HDAC) and KAT8 (a HAT) are downregulated. Nevertheless, it has been suggested that hPTMs have context dependent effects and their crosstalk may provide a code that determines the transcriptional outcome<sup>285</sup>. The interpretation of the interaction of histone modifying enzymes in terms of gene regulation is quite complex during EAE due to the various levels

of chromatin modifying enzymes that are affected. To counteract the disbalance of the epigenetic signature, a highly deregulated enzyme was chosen to study the effect of its interference on the level of gene transcription during neuroinflammation. Thereby, a master regulator of gene expression control was selected, that additionally has the potential to be pharmacologically targeted under disease conditions. Among the top candidates, only the upregulated ones were considered as they have the potential to be targeted by available small molecule inhibitors. *Ehmt2*, coding for the G9a protein, was selected as target gene, as it is an established regulator of gene repression<sup>250</sup>, and several compounds are available that inhibits its enzymatic activity and have been validated for its *in vivo* efficiency within the CNS<sup>265,268,286</sup>.

For the validation of the induction of G9a activity during CNS inflammation, the G9a-mediated histone modification H3K9me2 has been quantified. Before starting with the validation of the G9a downstream modification on isolated nuclei, the induction of G9a transcript level has been confirmed in isolated NeuN-positive nuclei from EAE mice during the acute phase (Fig. 3.2 C), as the initial finding was obtained from whole motor neurons where the actively translated mRNA was isolated. The activity of G9a as assessed by H3K9me2 levels was enhanced during the acute (day 15) and chronic phase (day 30) of the EAE but not prior to disease onset (day 11) (Fig. 3.2 D), indicating a correlation with the initiation of neuronal cell death rather than immune cell invasion, as neuronal loss is observed from day 15 on (Fig. 3.2 F), whereas immune cell infiltration starts on day 7 – 10, even before neurological symptoms can be observed<sup>287</sup>. Based on these findings, the induction of G9a activity appears to exceed the demethylase activity of KDM4D during neuroinflammation as the target modification H3K9me2 of the enzymes is enhanced. In comparison to other neurological diseases that are linked to excessive neuronal cell death, H3K9me2 have also been found to be upregulated in animal models of AD<sup>265</sup>, autism-spectrum disorder<sup>268</sup>, and posttraumatic stress disorder<sup>267</sup>. Importantly, the induction of H3K9me2 was observed in the AD mouse model 5xFAD in 5 – 6 months old mice in the prefrontal cortex where typical AD-like symptoms already appear<sup>265</sup>, whereas the increase of H3K9me2 was absent in 8 month old 5xFAD mice within the hippocampus<sup>266</sup>. Therefore, G9a activity might be either brain region dependent or increases acutely with the initiation of the stimulus but adapts during chronic exposure to the toxic environment and recovers to basal levels. Moreover, H3K9me2 have been suggested as an experience-driven mechanism of transcriptional regulation in the hippocampus. In fear conditioning paradigms, H3K9me2 showed a prominent induction 1 h after shock or context exposure, whereas 24 h after fear conditioning the shock or context exposure resulted even in a significant downregulation of H3K9me2. Interestingly, trimethylation of H3K4, an activating histone mark, was upregulated 1 h following shock exposure but not in response to the context alone, and returned to baseline levels 24 h after fear conditioning<sup>267</sup>. These findings demonstrate the highly dynamic character of H3K9me2 and H3K4me3 that might have a diverse role in the formation of

context dependent long-term memory. However, during EAE H3K9me2 induction appeared to be persistent even in the chronic stage of EAE, in which inflammation already declined (Fig. 3.2 D). To get further information about the stability of H3K9me2 in progressive neurodegeneration, its expression needs to be quantified during a longer time period in the EAE model when inflammation already diminishes and neurodegeneration predominates. Moreover, for the assessment of the dynamics of histone modifications during EAE, it would be interesting to check whether an activating mark such as H3K4me3 have the same pattern as H3K9me2 and if a perturbation of H3K9me2 also affects other hPTMs. Most important, the understanding of H3K9me2 dynamics during neuroinflammation, especially in terms of relapses, would provide meaningful information about the timing of treatment for MS patients.

#### 4.2 Neuroprotection by G9a perturbation during glutamate excitotoxicity and oxidative stress

To investigate the effect of G9a activity on neuronal survival under inflammatory conditions, primary cortical mouse neurons were used as an *in vitro* model. Neuronal cultures were exposed to different mediators that are part of the inflammatory milieu during CNS inflammation. Interestingly, increased H3K9me2 signal was specifically observed upon glutamate treatment, which also led to reduced neuronal viability (Fig. 3.3 A, B, C), supporting the hypothesis that H3K9me2 signal is linked to neuronal cell death. In addition, glutamate-mediated enhancement of G9a activity appears to be a specific phenomenon rather than an overall regulation of epigenetic mechanism as other repressive or permissive marks are not affected by glutamate treatment (Fig. 3.3 D). In the context of neuroinflammation, excessive amounts of extracellular glutamate are typically driven by a combination of release from dying cells, active secretion by immune cells<sup>278</sup>, and impaired glutamate reuptake<sup>288</sup>. These processes lead to an enhanced activity of NMDA receptors that result in toxic intracellular calcium accumulation<sup>119</sup> and oxidative stress in neurons<sup>289</sup>. By exploring the upstream mechanism that cause G9a activation, blocking NMDA receptors or chelating extracellular calcium by using AP5 or EGTA, respectively, prevented glutamate induced H3K9me2 induction (Fig. 3.3 E). These results indicate that G9a might be activated in response to NMDA receptor mediated calcium influx, as H3K9me2 levels were reduced to baseline levels when blocking the influx of calcium.

Based on the assumption that enhanced G9a activity initiates cell death cascades, the interference of the enzymatic activity of G9a might be neuroprotective. To test this hypothesis, pharmacological inhibition by using the small molecule inhibitor UNC0642 or genetic deletion of G9a in *G9a<sup>fl/fl</sup>;Snap25-Cre* mice were used. Since excessive glutamate triggers G9a activity it has been chosen as a neurotoxic stimulus to investigate the impact of G9a perturbation on cell viability and calcium overload. Both

approaches resulted in improved neuronal viability and prevented the accumulation of intracellular calcium, proposing G9a as a regulator of stress-induced coping mechanisms in neurons (Fig. 3.5 A-D). Overexcitation of neurons caused by elevated extracellular glutamate levels results in the formation of increased ROS levels within neurons, pointing out the important role of oxidative stress as a causal factor of neurodegenerative diseases<sup>290</sup>. As G9a inactivation enhances neuronal resilience during glutamate exposure, one could also assume that the glutamate induced elevated ROS levels are dependent on G9a activity. Indeed, G9a interference prevents the production of glutamate-induced generation of ROS (Fig. 3.6 A, B). Moreover, direct exposure to H<sub>2</sub>O<sub>2</sub> massively increased H3K9me2 levels, whereas the inactivation of G9a potently prevented calcium overload triggered by H<sub>2</sub>O<sub>2</sub> (Fig. 3.6 E-F). These findings underline the hypothesis that G9a is activated upon calcium influx since application of H<sub>2</sub>O<sub>2</sub> resulted in elevated intracellular calcium levels.

Together, G9a interference prevented neuronal cell death during excitotoxicity and oxidative stress probably by blocking the production of free radicals within neurons that could result in massive intracellular damage and cell lysis.

### 4.3 Pharmacological G9a inhibition as neuroprotective treatment during EAE

To test the therapeutic efficacy of G9a inhibition *in vivo*, UNC0642 was administered to mice undergoing EAE. Among several G9a inhibitors that have been used for CNS treatment<sup>265,268,286</sup>, UNC0642 was shown to possess high potency, low cell toxicity, excellent selectivity and favorable pharmacokinetic properties for *in vivo* applications<sup>279</sup>. Accordingly, the results from UNC0642 treatment were always consistent with those from genetic G9a disruption and no add-on effects were observed upon UNC0642 treatment of knockout cultures (Fig. 3.5 E, F), supporting its efficacy and specificity. To circumvent effects on early immune priming in EAE<sup>291</sup>, injections of UNC0642 were started one day after the individual disease onset in each mouse. G9a inhibition profoundly diminished disease severity reflected by a reduced loss of neurons within the spinal cord. Additionally, treatment with UNC0642 reverses the induction of repressive histone mark H3K9me2 within neuronal nuclei of EAE mice (Fig. 3.10 A, B, E). Interestingly, G9a inhibition in healthy mice did not result in a reduction of H3K9me2. Only after pathological induction of H3K9me2 in the EAE model, UNC0642 application reduced H3K9me2 levels to healthy baseline levels, indicating that G9a inhibition restores H3K9me2 levels to physiological levels, but does not lead to an exacerbated loss of H3K9me2 mark that would end up in a broad de-repression of transcription (Fig. 3.10 H). These observations also might indicate a reduced risk of UNC0642 side effects, underlining its potential as therapeutic target to prevent inflammation-induced neurodegeneration.

Regarding the route of administration, UNC0642 has the potential to affect other cell types including immune cells and glia cells. To exclude that the neuroprotective effect of UNC0642 treatment

results from a suppression of immune cell infiltration rather than neuron-intrinsic effects, the extend and composition of immune cells during EAE was analyzed. For the discrimination of different immune cell subsets in the acute phase of EAE, where the invasion of immune cells into the CNS reaches its maximum, no significant differences in the absolute number of immune cells were detected. Among the investigated subsets were macrophages, CD4 T cells, CD8 T cells, DCs, and B cells (Fig. 3.11). Moreover, immune cell infiltration as well as microglia activation in the chronic phase of EAE measured by immunohistochemical CD3 or Iba1 staining, respectively, was unaffected by UNC0642, supporting the assumption of a direct effect of UNC0642 on neurons. Pharmacological blockade of G9a activity also provided benefit in other preclinical models by counteracting transcriptional deregulation and improving clinical outcome. In a mouse model of AD<sup>265</sup> and autism spectrum disorder<sup>268</sup>, G9a inhibition led to a recovery of glutamate receptor expression and excitatory synaptic function and rescued impaired memory function or social deficits, respectively. The potential of therapeutic effects of inhibitory agents targeting epigenetic enzymes has also been evaluated by using DNMT inhibitors, such as 5-aza-deoxycytidine, and HDAC inhibitors such as valproic acid or trichostatin A, which showed a beneficial effect in the EAE model in mice and rats<sup>292-297</sup>. Most of those studies focused on the investigation of immune-mediated mechanisms that result in reduced spinal cord inflammation, demyelination, and axonal loss, but so far, knowledge about neuronal adaption is lacking.

To validate the neuroprotective effect of G9a inhibition during inflammation, the neuron-specific knockout line *G9a<sup>fl/fl</sup>/Snap25-Cre* was used for EAE induction. The correlating expression of G9a and its downstream histone modification H3K9me2, substantiates the fact that H3K9me2 is specifically mediated by G9a. Unfortunately, using *Snap25-Cre* as a driver line resulted in an insufficient knockout of G9a in the spinal cord even though the brain displays a complete knockout (Fig. 3.12). Since the used EAE model mainly affects the spinal cord, the incomplete deletion of G9a might be insufficient to pinpoint the function of G9a activity during CNS pathology. Nevertheless, the non-neuronal nuclei and immune cells did not show any differences in G9a expression, therefore this model might be a good starting point to elucidate the role of G9a in neurons during CNS inflammation. Counter-intuitively, *G9a<sup>fl/fl</sup>/Snap25-Cre* mice did not display any differences in the disease course compared to *G9a<sup>fl/fl</sup>* control mice, except for a slight difference in the day of disease onset (Fig. 3.14 A-C). Several reasons might cause the discrepancy between the pharmacological inhibition and the genetic deletion of G9a. One reason could be the incomplete knockout in spinal cord neurons, that possibly dampens a neuroprotective effect of G9a, as spinal cord neurons are the main driver of neurological symptoms in the EAE model. To check whether a sufficient knockout of G9a in spinal cord neurons ameliorates EAE symptoms, another Cre-driver line could be used. Furthermore, G9a has an impact on the development of the nervous system<sup>298</sup> and regulates neuronal subtype specification<sup>256</sup>. As *G9a<sup>fl/fl</sup>/Snap25-Cre* does not show any obvious neurological deficits, there might be compensatory mechanisms that balance

the function of G9a in neurons. It would be interesting to investigate the expression of other KMTs and their corresponding histone modification, to assess if the lack of transcriptional repression by G9a is taken over by functionally related enzymes. One opportunity to circumvent the influence of G9a on neurodevelopment is to use an inducible and neuron-specific Cre-driver line. Albeit the *G9a<sup>fl/fl</sup>/Snap25-Cre* model seems not to be suitable for *in vivo* experiments, there might be still a neuroprotective effect that is not reflected by the disease course, as the scoring system of motor functions is not directly translatable into the histological loss of neurons. Therefore, the neuronal loss within the knockout and non-knockout fraction of neurons was determined in the chronic phase of EAE mice compared to healthy mice by nuclear FACS staining of NeuN nuclei. This approach revealed a reduced neuronal loss in the G9a knockout population (Fig. 3.15 A, B), while the overall NeuN count in FACS staining and IHP was not different between the groups (Fig. 3.14 E; Fig. 3.15 A). In addition, the immune cell infiltration at the end of EAE showed no differences between *G9a<sup>fl/fl</sup>/Snap25-Cre* and *G9a<sup>fl/fl</sup>* control mice (Fig. 3.14 F). These results suggest that a genetic deletion of G9a in neurons has a protective effect during CNS inflammation that diminishes neuronal cell death. Nevertheless, it would be necessary to validate this effect in a suitable animal model which has a sufficient knockout of G9a in spinal cord neurons and might overcome compensatory developmental effects by either using an inducible Cre-line or by delivering Cre-protein via AAV injections. The implication of the immune system on the EAE outcome in response to UNC0642 treatment has already been assessed. Nevertheless, to exclude the involvement of the immune system in neuron-specific G9a-knockout mice would strengthen the finding of a neuronal effect of G9a during inflammation that enhance neuronal resilience. Additionally, to validate the specificity of UNC0642, it needs to be applied in knockout animals during EAE.

Together, pharmacological G9a inhibition has a beneficial effect on EAE symptoms, suggesting it as a potential candidate for targeted epigenetic therapy. The neuron-specific effect still needs to be validated during EAE course, but the preliminary data give already indications that neuronal G9a deletion results in a higher resilience of neurons.

#### 4.4 G9a-dependent protection from ferroptosis

Mechanistically, G9a appeared to control the initiation and execution of regulated forms of PCD pathways as H3K9me2 induction was associated with neuronal loss and reduced cell viability. Therefore, the neuroprotective effect of G9a inhibition *in vitro* and *in vivo* might be a consequence of the prevention of death signaling.

Perturbation of G9a in primary mouse neurons specifically dampened the induction of ferroptosis mediated by RSL3 or erastin, which initiates ferroptosis by the inactivation of GPX4 or system Xc<sup>-</sup>, respectively. Necroptotic or apoptotic cell death induction was not modulated by G9a inactivation confirming a specific mechanism of cell death prevention (Fig. 3.7 A, B). G9a perturbation did not

completely prevent neuronal decay in stress conditions, but especially in *G9a<sup>fl/fl</sup>/Snap25-Cre* knockout neurons cell death was almost absent after RSL3 or erastin stimulation, strengthen the selective function of G9a on ferroptosis. The incomplete rescue of neuronal cell death during glutamate and H<sub>2</sub>O<sub>2</sub> stress might be due to non-ferroptotic cell death as elevated glutamate levels can induce different forms of cell death in neurons<sup>299</sup> and the same is true for ROS<sup>300</sup>. Moreover, the activity of G9a was robustly enhanced in primary mouse neurons specifically in response to ferroptosis induction which could be prevented by G9a inhibition (Fig. 3.7 C, D). Interestingly, also vice versa, ferroptosis enhanced G9a activity, emphasizing G9a as an epigenetic amplifier that is driven by ferroptosis, but also drives ferroptosis itself.

Ferroptosis is initiated by the perturbation of metabolic pathways during acute and chronic stress that result in massive lipid peroxidation<sup>185</sup>. The contribution of ferroptosis in several physiological and pathophysiological processes, including tumor suppression, immunity<sup>188</sup> as well as tissues damage<sup>301</sup> is only recently being appreciated. An implication of ferroptosis in neurodegeneration has been postulated in different studies<sup>194,302,303</sup>, however, the exact contribution of ferroptosis to neuronal loss remains unclear. To substantiate a role of ferroptosis in inflammatory neurodegeneration, its involvement in glutamate excitotoxicity was investigated *in vitro*. Thereby, glutamate initiates ferroptosis as shown by the enhanced protein levels of COX-2, which is encoded by the gene *Ptgs2* – an accepted biomarker of ferroptosis (Fig. 3.8 A)<sup>182</sup>. The induction of ferroptosis was almost completely abolished by G9a inhibition, highlighting G9a as a main regulator of ferroptosis execution.

The high impact of ferroptotic cell death during glutamate toxicity has become more clear as commercially available ferroptosis inhibitors, which prevent ferroptosis via different routes, were able to diminish cytosolic calcium influx in primary neurons (Fig. 3.8 B). Additionally, G9a inhibition had no add-on effect when ferroptosis was blocked, substantiating a direct effect of G9a in the ferroptosis pathway. These results also indicate that increased calcium influx could subsequently initiate downstream signaling that trigger the ferroptosis cascade. Recent work already indicted that a sustained increase in cytosolic calcium levels is a hallmark of ferroptosis in several cell lines<sup>304,305</sup>. Nevertheless, ferroptosis inhibitors do not directly act on key molecules of the ferroptosis pathway, but rather have broad antioxidant or iron chelating functions. Therefore, the reduced calcium influx could also be a result of an enhanced neuronal resilience against radicals. Thus, the direct contribution of calcium induced ferroptosis in neurons still needs to be confirmed by blocking the calcium influx during RSL3 or erastin treatment, that should protect from cell death. The assumption that calcium induces ferroptosis in neurons also corroborate the finding that G9a might be activated in response to calcium influx and thereby regulate neuronal adaptation.

Another trigger of ferroptosis is the depletion of intracellular glutathione, which lead to the generation of toxic lipid ROS<sup>306</sup>. Deprivation of cysteine, which is rate-limiting in the biosynthesis of

glutathione, has been shown to cause cell death<sup>307</sup>. Glutathione is the most abundant reductant in mammalian cells and plays an important role in antioxidant defense and nutrient metabolism, where it serves as a cofactor for multiple enzymes including glutathione peroxidases and GSTs<sup>184</sup>. Exceeding extracellular glutamate concentrations halt the cystine import via the system Xc<sup>-</sup> and thereby prevent the biogenesis of glutathione<sup>183</sup>. Glutamate stress resulted in a marked reduction of the antioxidant glutathione in primary neurons whereas pharmacological and genetical G9a interference partially circumvents glutathione depletion (Fig. 3.8 C, D). These results suggest that G9a prevents the induction of ferroptosis by the enhancement of glutathione metabolism.

To validate the findings of G9a-mediated ferroptosis regulation in the mouse model, the level of lipid peroxidation was assessed during EAE. Lipids containing PUFAs are most susceptible to lipid peroxidation and necessary for the execution of ferroptosis. The main aldehyde products of lipid peroxidation are the 3-carbon dialdehyde species malondialdehyde and 4-HNE<sup>308</sup>. 4-HNE protein adducts were detected in spinal cords of EAE and healthy mice. Thereby, an increase of 4-HNE levels were obtained during the acute phase of EAE, substantiating the involvement of ferroptosis in inflammation-induced neurodegeneration. Moreover, G9a inhibition reduced lipid peroxidation in the chronic phase of EAE (Fig. 3.10), validating the finding of G9a-mediated neuroprotection via the ferroptosis pathway in the MS mouse model.

All in all, these experiments showed an essential contribution of ferroptosis in glutamate excitotoxicity and CNS inflammation. Moreover, these findings suggest that G9a enhances neuronal damage during inflammation by amplifying ferroptosis, while G9a perturbation appears as a viable approach to normalize redox homeostasis, increase glutathione levels, and rescue neuronal survival.

#### 4.5 G9a-mediated transcriptional regulation of ferroptosis-relevant genes

The consequences of G9a activation are reflected by transcriptional changes that predominantly result in the inhibition of gene expression. To reveal the mechanism of G9a-mediated neuroprotection, mRNA expression levels of ferroptosis-related genes were determined in response to pharmacological G9a inhibition in cell culture experiments as well as in neuronal nuclei from EAE mice (Fig. 3.9, 3.16, 3.17).

Several genes implicated in the ferroptosis pathway were dysregulated in stressed primary neurons and during EAE, establishing the role of ferroptosis in inflammation-induced neurodegeneration and confirming its mechanistic regulation on the level of transcription. Most of the genes with anti-ferroptotic properties were induced in primary neurons but downregulated during EAE, indicating that primary neurons enhance their defense system to counteract ferroptotic cell death, whereas neurons from EAE mice already decline due to the massive cellular damage via activated immune cells. Multiple genes coding for enzymes that regulate the biosynthesis of glutathione were differently regulated

during neuroinflammation and induced by G9a inhibition. *Gclc* and *Gss* are the key enzymes in generating glutathione from cystine, which is imported via the system  $Xc^{-184}$ . G9a induced the levels of *Gss* and *Gclc* in primary neurons and EAE spinal cord neurons, respectively, implying the homeostatic adaptation of neurons during inflammation by boosting the intracellular antioxidant pool. Supportingly, also *Slc7a11*, the subunit of the cystine/glutamate antiporter system  $Xc^{-}$ , was amplified upon G9a inhibition in primary neurons. Moreover, the transcript of CBS that generates glutathione from methionine-derived homocysteine via the transsulfuration pathway<sup>309</sup>, was prominently induced in EAE neurons and also during  $H_2O_2$  stimulation in primary neurons, substantiating the G9a-dependent glutathione-regulation. NRF2, encoded by *Nfe2l2*, is a transcription factor that regulates the expression of several proteins with antioxidant function, among them genes that regulate the abundance of glutathione<sup>281,284</sup>. G9a inhibition strongly induced the expression of *Nfe2l2* during EAE, thereby supporting the findings of G9a-mediated transcriptional regulation of glutathione synthesis. Most important for the defense of ferroptosis is the glutathione-peroxidase GPX4<sup>182</sup> that shows a very prominent downregulation during EAE indicating a poor antioxidant defense system during inflammation that initiate neurodegeneration. G9a potentially induced the expression of *Gpx4* during EAE, thereby manifesting the G9a-dependent regulation of ferroptotic cell death during CNS inflammation.

Another class of enzymes that uses glutathione for the intracellular detoxification are GSTs. In general, GSTs catalyze the conjugation of a wide variety of compounds to glutathione. Thereby, GSTs are the major regulators of intracellular 4-HNE concentration as they metabolize the majority of 4-HNE through its conjugation to glutathione. Lipid peroxidation results in a significant rise of 4-HNE and GSTs have the potential to suppress lipid peroxidation and limit 4-HNE formation<sup>310</sup>. Here, the gene expression of GSTs was strongly impaired during EAE and G9a inhibition was sufficient to restore the expression of a variety of GSTs. Of note, in cell culture experiments, the expression of *Gstm6* was reduced during ferroptosis induction via glutamate,  $H_2O_2$ , and erastin, whereas UNC0642 treatment potentially induced the expression of *Gstm6* in all conditions. *Gstm6* showed the strongest regulation in cell culture experiments when treated with G9a inhibitor, suggesting it as the main mediator of G9a-dependent neuroprotection. As *Gstm6* has a quite low mRNA expression in the CNS compared to other GSTs<sup>311</sup>, it might be specifically induced in neurons in response to stress conditions. Therefore, it would be particularly interesting to assess its G9a-dependent function in cell toxicity assays by establishing *Gstm6* knockout and overexpressing neurons. Moreover, the regulation of GSTs by G9a-mediated mechanisms has already been shown in a mouse model of acute liver injury where loss of G9a resulted in the inhibition of GSTP1<sup>312</sup>. The investigation of mouse neurons during EAE indicate that G9a inhibition upregulates the transcript level of GSTP1, showing a diverse function of G9a in different cell types.

The glutathione-independent anti-ferroptotic enzyme FSP1<sup>187</sup> showed no significant regulation during EAE and its gene expression was not affected by G9a inhibition. During glutamate stress, the transcript level of FSP1 was upregulated in primary neurons, but not boosted when G9a inhibitor UNC0642 was administered. These results demonstrate that the G9a-dependent ferroptosis regulation is mediated mainly via the induction of glutathione-dependent enzymes. Nevertheless, the pro-ferroptotic molecule ACSL4, which promotes ferroptosis by influencing the lipid composition required for the execution of ferroptosis<sup>181</sup>, showed an upregulation of gene expression upon G9a inhibition in EAE neurons, indicating a rebalancing of ferroptotic enzymes by G9a.

However, there are some discrepancies of the results between *in vitro* and *in vivo* experiments. One example is the transcript level of *Gclc*, which showed a downregulation upon G9a inhibition in glutamate stressed neurons but was induced during EAE in UNC0642 treated mice. The *in vitro* situation displays an isolated system where definite signaling pathways are turned on according to the stimulus, whereas neuroinflammation *in vivo* constitutes a combination of different known and unknown neurotoxic factors that can have a divergent effect on the transcriptional regulation. Moreover, *Gpx4* did not show any changes in cell culture experiments, neither in response to the toxic stimuli, nor upon G9a inhibition, although it has been shown that *Gpx4* is highly induced in primary cortical neurons when treated with the glutamate analog homocysteate<sup>302</sup>. One opportunity might be that the applied concentrations or the incubation time were not sufficient to induce the transcript level of *Gpx4* in the setting here. Therefore, the G9a-dependent regulation of *Gpx4* during ferroptosis induction cannot be determined in the *in vitro* experiment.

In conclusion, gene expression data from cell culture and EAE experiments revealed that G9a activity regulates neuronal resilience during inflammation via the induction of genes coding for glutathione dependent enzymes. These findings highlight the pharmacological inhibition of G9a as a valuable therapeutic approach to counteract inflammation-driven neurodegeneration in MS by preventing the induction of ferroptosis.

#### 4.6 Ferroptosis regulation in MS patients and therapeutic potential of UNC0642

According to the observed findings, epigenetic dysregulation might be a main contributing factor to accelerate the progression of neurodegenerative diseases. To translate the findings from mouse *in vitro* and *in vivo* experiments to humans, MS brain sections were used for validation and human iPSC derived neurons were used to assess the applicability of UNC0642.

In line with the data from the EAE model, H3K9me2 levels were elevated in MS NAGM and lesions (Fig. 3.19 A). H3K9me2 has also been found to be regulated in human diseases associated with excessive neuronal cell death like AD. In the prefrontal cortex of AD patients, H3K9me2 was significantly induced<sup>265</sup>, whereas another study detected a decline in the CA1 and dentate gyrus region

of AD patients with disease progression<sup>313</sup>, indicating a region-specific and stimulus dependent adaption of specific histone post-translational modifications that differs in acute and chronic conditions. A sustained induction of repressive histone marks has been identified in models of acute and chronic stress, where it has been shown that transcriptional repression via H3K9me3 has a diverse and brain region specific role, as it is induced during acute stress and slightly diminished by chronic stress.<sup>314,315</sup> Moreover, the authors detected differential regulation of specific repressive and permissive histone modifications in their stress model, indicating a compensation of reduced transcriptional response during stress. Therefore, to investigate the regulation of H3K9me2 and additional histone marks in MS patients in different stages of the disease would help to decipher the epigenetic code based on histone modifying enzymes and provide information about meaningful timing of treatment and putative compensatory effects.

To test the efficacy of UNC0642 in human cells, the compound was tested in human iPSC derived neurons in response to ferroptosis induction via erastin (Fig. 3.19 C). Reassuringly, H3K9me2 level was also elevated in human neurons during erastin treatment, highlighting the translatability of this finding across species. Moreover, ferroptosis induction in human iPSC neurons upon UNC0642 treatment resulted in the induction of *GPX4*, *SLC7A11*, and *GCLC* (Fig. 3.19 D) manifesting its applicability and efficiency in human cells and thereby emphasizing its potential in human MS therapy. Furthermore, to approve neuronal ferroptosis as a causal factor of neurodegeneration in MS patients, *GPX4* expression was assessed within brains of MS patients in NAGM and cortical lesions using RNAscope. This approach revealed a diminished expression of *GPX4* in NAGM and MS lesions in comparison to controls (Fig. 3.19 B), reflecting the results in the animal model.

Besides the application of G9a inhibitors to treat diseases of the CNS, pharmacological modification of aberrant G9a activity has also been investigated in other disorders, especially in cancer therapy as it has been shown that G9a activity is enhanced in several malignancies<sup>245</sup>. There have been a wide range G9a inhibitors developed in recent years, but so far, no one have been used in clinical trials<sup>264</sup>. One reason might be that G9a inhibitors are still in the early stages of exploration and needs to be optimized to improve cell permeability and selectivity. However, there are other histone methyltransferase inhibitors that have already been tested in clinical trials, including EZH2 (H3K27) histone methyltransferase inhibitor Tazemetostat which is in phase II trials against relapsed or refractory non-Hodgkin lymphoma. Due to the emerging findings of G9a dysregulation in neurological disorders, G9a inhibitors are appealing candidates for the treatment of neurodegenerative diseases. As G9a has diverse functions in different cell types, one limitation of a long-term therapy using G9a inhibitors might be a low specificity accompanied by multi-targeted and multi-cellular side effects. Further studies are needed to investigate the selectivity of the drug, the timepoint of application, and the appropriate dosage. A big advantage of G9a inhibition is that it boosts the expression of several

neuroprotective genes without directly targeting them. Furthermore, as epigenetic modifications are stable, a single acute treatment might trigger a long-lasting effect, that circumvents the persisting induction of H3K9me2 during chronic disease and diminish neurodegeneration. An option to circumvent off-target effects of the epigenetic drug might be to directly target the ferroptosis pathway by applying ferroptosis inhibiting compounds and test their efficacy on neurodegeneration in mouse models. Ferroptosis-inhibitors have already been successfully applied in animal models of ischemic stroke<sup>193,194</sup>, HD<sup>196</sup>, and PD<sup>197</sup> but further investigations are needed to determine long-term effects of the compounds on different cell types, as ferroptosis inhibitors lack a cell type specificity. Moreover, persistent application of ferroptosis inhibitors in patients might be required, as they do not induce stable alterations.

Together, G9a activity was induced in brains of MS patients as shown by elevated H3K9me2 levels. Moreover, the induction of ferroptosis in MS patients have been confirmed by reduced *GPX4* expression. For the establishment of UNC0642 as a therapeutic agent, its efficacy in human neurons on the regulation of ferroptosis-relevant genes have been validated.

#### 4.7 Conclusion and outlook

This work offers a new perspective of epigenetically regulated pathways that trigger neurodegeneration in CNS inflammation. The transcriptional regulator G9a emerges as a valuable target to study neuron-intrinsic mechanisms that control neuronal resilience. Moreover, the iron-dependent cell death pathway ferroptosis turned out to be a major driver of inflammation-induced neurodegeneration. Targeting ferroptosis by G9a inhibition in clinical applications provides a promising tool to treat MS and other ferroptosis-dependent pathologies. Nevertheless, many aspects need to be investigated to determine the impact of G9a-regulated neuronal ferroptosis in CNS inflammation and study the consequences of pharmacological G9a inhibition in neurodegenerative diseases.

To definitely pinpoint neuronal G9a activity as a neurodegenerative driver *in vivo*, a genetic knockout system would be of high value. Therefore, the appropriate neuron-specific mouse model needs to be established. A variety of neuronal Cre mouse lines exists that can be tested for an efficient and specific deletion of G9a, preferably a system that allows the induction of Cre-protein in adult mice to circumvent a neurodevelopmental effect of G9a. One opportunity would be a tamoxifen-inducible Cre-driver line containing a neuron-specific promoter. Another way to evoke a neuron-specific Cre-mediated recombination in adult mice is the delivery of the Cre-protein via AAVs that can be injected intravenously. Moreover, clustered regularly interspaced palindromic repeats (CRISPR)/Cas-based systems enables the cell type specific repression of endogenous gene expression and can be used as a tool to validate G9a-dependent function in neurons during CNS inflammation. Having a suitable mouse model will enable to study neuron-specific effects of G9a during EAE, validate the specificity of the G9a

inhibitor UNC0642, quantify the immune cell activation and infiltration to exclude the involvement of the immune system on G9a-mediated phenotype, and verify the transcriptional regulation of ferroptosis-relevant genes in those mice.

Furthermore, to elucidate the mechanism of action of G9a-mediated transcriptional repression of ferroptosis genes, chromatin immunoprecipitation should be performed. Thereby the occupancy of H3K9me2 on target genes will be determined to examine if the observed transcriptional gene repression is due to the presence of H3K9me2 mark or if other mechanisms like interactions of G9a with chromatin modifying enzymes result in transcriptional changes.

Another important step will be to test the therapeutic effect of ferroptosis inhibiting compounds in the EAE model. Several classes of ferroptosis inhibitors have been identified that act on different molecules in the ferroptosis pathway<sup>316</sup>. To apply ferroptosis inhibitors in the MS mouse model will evaluate the significance of ferroptosis during inflammation-induced neurodegeneration and might reveal a modifiable pathway that can be targeted for future therapy.<sup>316</sup>

## 5 Summary

Neurodegeneration is a major contributor to neurological disability in MS. Current therapies focus on immune modulation but are only poorly effective in halting disease progression. Thus, the development of therapeutics that counteract neurodegeneration by enhancing neuronal resilience to inflammation is a major unmet clinical need in MS. A fundamental pathological feature in affected neurons is the transcriptional dysregulation that mediates a variety of pathways that result in the decay of neurons. Epigenetic modifiers control the transcriptional landscape in a broad fashion and thereby emerges as viable tool to rebalance the deregulated transcriptional response in injured neurons. A clear understanding of epigenetic processes within neurons of MS patients might deliver new strategies for the development of epigenetic therapies. Thus, the goal of this project was to investigate the epigenetic regulation in the mouse model of MS and identify pathways that can be targeted to modulate neuronal susceptibility during inflammation.

By *in vivo* translome profiling of inflamed neurons, the histone methyltransferase G9a was identified as a driver of inflammation-induced neuronal loss. G9a-dependent epigenetic repressive mark H3K9me2 has been found to be upregulated during glutamate excitotoxicity *in vitro* and in the MS mouse model *in vivo*. Pharmacological inhibition and genetic disruption of G9a improved neuronal viability and prevented toxic calcium accumulation during glutamate exposure and oxidative stress. Moreover, G9a inhibition resulted in an improved clinical outcome and reduced neuronal loss in the EAE model. By the investigation of the underlying molecular mechanisms that drive neuronal resilience upon G9a inactivation, the programmed cell death pathway ferroptosis was identified to be controlled by G9a activity in neurons. Thereby, glutamate excitotoxicity induced ferroptosis and led to the depletion of intracellular glutathione levels, both of which could be reversed by G9a inhibition. Additionally, induction of ferroptosis was selectively diminished by G9a interference. Of note, ferroptosis was identified as a pivotal mechanism in neuroinflammation that induces neuronal cell death by the initiation of lipid peroxidation in the acute and chronic phase of the MS mouse model. G9a controlled the initiation of ferroptosis by transcriptionally de-repressing anti-ferroptosis genes in the glutathione/GPX4 axis that resulted in ferroptosis inhibition as measured by lower 4-HNE levels during EAE. Furthermore, enhanced G9a activity was validated in brains of MS patients. Accordingly, GPX4 transcript levels were reduced, highlighting the implication of ferroptosis in neuronal cell death initiation of MS patients. The applicability of G9a inhibitor was explored in human iPSC derived neurons, where G9a inactivation prevented the induction of H3K9me2 during ferroptosis and initiated the expression of anti-ferroptosis genes. These findings indicate a role of G9a as inflammation-induced epigenetic modulator of ferroptosis genes in neurons and suggests pharmacological G9a inhibition as a promising therapeutic approach to counteract neurodegeneration.

## 6 Zusammenfassung

Die Neurodegeneration ist einer der Hauptgründe für neurologische Beeinträchtigung in der MS. Die derzeitigen Therapien konzentrieren sich auf die Modulation des Immunsystems, sind aber nur wenig wirksam, um das Fortschreiten der Krankheit aufzuhalten. Daher ist die Entwicklung von Therapeutika, die der Neurodegeneration entgegenwirken, indem sie die Widerstandsfähigkeit der Neuronen gegenüber Entzündungen stärken, ein wichtiger ungedeckter klinischer Bedarf bei MS. Ein grundlegendes pathologisches Merkmal der betroffenen Neuronen ist die Dysregulation der Transkription, die eine Vielzahl von Signalwegen beeinflusst, was zum Untergang der Neurone führen kann. Epigenetische Modulatoren kontrollieren die Transkription weitreichend und stellen somit ein Instrument dar, um die deregulierte Transkriptionsantwort in geschädigten Neuronen wieder ins Gleichgewicht zu bringen. Ein klares Verständnis der epigenetischen Prozesse in den Neuronen von MS Patienten könnte neue Strategien für die Entwicklung epigenetischer Therapien liefern. Ziel dieses Projekts war es daher, die epigenetische Regulierung im Mausmodell der MS zu untersuchen und Wege zu identifizieren, die gezielt zur Beeinflussung der neuronalen Anfälligkeit während der Entzündung eingesetzt werden können.

Durch *in vivo* Translatom Untersuchungen entzündeter Neuronen wurde die Histon-Methyltransferase G9a als eine treibende Kraft für den entzündungsbedingten neuronalen Verlust identifiziert. Es wurde festgestellt, dass die von G9a vermittelte, epigenetische Modifizierung H3K9me2 bei Glutamat Exzitotoxizität *in vitro* und im MS-Mausmodell *in vivo* hochreguliert wird. Die pharmakologische Hemmung und genetische Deletion von G9a verbesserte die neuronale Lebensfähigkeit und verhinderte die toxische Kalziumakkumulation bei Glutamat Exposition und oxidativem Stress. Darüber hinaus führte die Hemmung von G9a zu einem verbesserten klinischen Ergebnis und einem geringeren Neuronenverlust im EAE-Modell. Durch die Untersuchung der zugrundeliegenden molekularen Mechanismen, die die neuronale Resilienz bei G9a-Inaktivierung steuern, wurde festgestellt, dass der programmierte Zelltodweg Ferroptose durch die G9a-Aktivität in Neuronen kontrolliert wird. Dabei induzierte die Glutamat Exzitotoxizität die Ferroptose und führte zu einer Verminderung des intrazellulären Glutathionspiegels, was durch die Hemmung von G9a verhindert werden konnte. Darüber hinaus wurde die Induktion der Ferroptose durch G9a-Interferenz selektiv verhindert. Zudem wurde die Ferroptose als ein zentraler Mechanismus bei der Neuroinflammation identifiziert, der den neuronalen Zelltod durch die Auslösung der Lipidperoxidation in der akuten und chronischen Phase des MS Mausmodells auslöst. G9a verminderte die Einleitung der Ferroptose durch transkriptionelle Depressionen von Anti-Ferroptose Genen, die in der Glutathion/GPX4-Achse beteiligt sind. Die Hemmung der Ferroptose konnte durch eine geringere Freisetzung von 4-HNE während der EAE gemessen werden. Darüber hinaus wurde in Gehirnen von MS-Patienten eine erhöhte G9a-Aktivität nachgewiesen. Dementsprechend war das GPX4 Transkript

reduziert, was die Bedeutung der Ferroptose bei der Auslösung des neuronalen Zelltods bei MS-Patienten unterstreicht. Die Anwendbarkeit von G9a-Inhibitoren wurde an menschlichen iPSC-Neuronen untersucht, bei denen die Inaktivierung von G9a die Induktion von H3K9me2 während der Ferroptose verhinderte und die Expression von Anti-Ferroptose-Genen erhöhte. Diese Ergebnisse weisen auf eine Rolle von G9a als entzündungsgetriebener epigenetischer Modulator von Ferroptose-Genen in Neuronen hin und legen eine pharmakologische G9a-Inhibition als vielversprechenden therapeutischen Ansatz zur Bekämpfung der Neurodegeneration nahe.

## IV Bibliography

- 1 Lassmann, H., Bruck, W. & Lucchinetti, C. F. The immunopathology of multiple sclerosis: an overview. *Brain Pathol* **17**, 210-218, doi:10.1111/j.1750-3639.2007.00064.x (2007).
- 2 Feigin, V. L. *et al.* Global, regional, and national burden of neurological disorders during 1990–2015: a systematic analysis for the Global Burden of Disease Study 2015. *The Lancet Neurology* **16**, 877-897, doi:10.1016/s1474-4422(17)30299-5 (2017).
- 3 Loma, I. & Heyman, R. Multiple Sclerosis: Pathogenesis and Treatment. *Current Neuropharmacology* **9**, 409-416 (2011).
- 4 Thompson, A. J., Baranzini, S. E., Geurts, J., Hemmer, B. & Ciccarelli, O. Multiple sclerosis. *The Lancet* **391**, 1622-1636, doi:10.1016/s0140-6736(18)30481-1 (2018).
- 5 Leray, E. *et al.* Evidence for a two-stage disability progression in multiple sclerosis. *Brain* **133**, 1900-1913, doi:10.1093/brain/awq076 (2010).
- 6 Trapp, B., Peterson, J. R., R. M., Rudick, R., Mörk, S. & Bö, L. Axonal Transection in the Lesions of Multiple Sclerosis. *The New England Journal of Medicine* **338**, 278-285 (1998).
- 7 Klineova, S. & Lublin, F. D. Clinical Course of Multiple Sclerosis. *Cold Spring Harb Perspect Med* **8**, doi:10.1101/cshperspect.a028928 (2018).
- 8 Polman, C. H. *et al.* Diagnostic criteria for multiple sclerosis: 2010 revisions to the McDonald criteria. *Ann Neurol* **69**, 292-302, doi:10.1002/ana.22366 (2011).
- 9 Ziemssen, T., Akgun, K. & Bruck, W. Molecular biomarkers in multiple sclerosis. *J Neuroinflammation* **16**, 272, doi:10.1186/s12974-019-1674-2 (2019).
- 10 Dean, G. & Kurtzke, J. F. On the Risk of Multiple Sclerosis According to Age at Immigration to South Africa. *British Medical Journal* **3**, 725-729 (1971).
- 11 Hawkes, C. Smoking is a risk factor for multiple sclerosis: a metanalysis. *Mult Scler* **13**, 610-615 (2007).
- 12 Sundqvist, E. *et al.* Epstein-Barr virus and multiple sclerosis: interaction with HLA. *Genes Immun* **13**, 14-20, doi:10.1038/gene.2011.42 (2012).
- 13 Munger, K. L. *et al.* Childhood body mass index and multiple sclerosis risk: a long-term cohort study. *Mult Scler* **19**, 1323-1329, doi:10.1177/1352458513483889 (2013).
- 14 Hedstrom, A. K., Akerstedt, T., Hillert, J., Olsson, T. & Alfredsson, L. Shift work at young age is associated with increased risk for multiple sclerosis. *Ann Neurol* **70**, 733-741, doi:10.1002/ana.22597 (2011).
- 15 Orton, S.-M. *et al.* Sex ratio of multiple sclerosis in Canada: a longitudinal study. *The Lancet Neurology* **5**, 932-936, doi:10.1016/s1474-4422(06)70581-6 (2006).
- 16 Westerlind, H. *et al.* New data identify an increasing sex ratio of multiple sclerosis in Sweden. *Mult Scler* **20**, 1578-1583, doi:10.1177/1352458514530021 (2014).

- 17 Kampman, M. T., Wilsgaard, T. & Mellgren, S. I. Outdoor activities and diet in childhood and adolescence relate to MS risk above the Arctic Circle. *J Neurol* **254**, 471-477, doi:10.1007/s00415-006-0395-5 (2007).
- 18 Baarnhielm, M. *et al.* Sunlight is associated with decreased multiple sclerosis risk: no interaction with human leukocyte antigen-DRB1\*15. *Eur J Neurol* **19**, 955-962, doi:10.1111/j.1468-1331.2011.03650.x (2012).
- 19 Berer, K. *et al.* Commensal microbiota and myelin autoantigen cooperate to trigger autoimmune demyelination. *Nature* **479**, 538-541, doi:10.1038/nature10554 (2011).
- 20 Correale, J. & Farez, M. F. The impact of environmental infections (parasites) on MS activity. *Mult Scler* **17**, 1162-1169, doi:10.1177/1352458511418027 (2011).
- 21 Westerlind, H. *et al.* Modest familial risks for multiple sclerosis: a registry-based study of the population of Sweden. *Brain* **137**, 770-778, doi:10.1093/brain/awt356 (2014).
- 22 Compston, A. & Coles, A. Multiple sclerosis. *The Lancet* **359**, 1221-1231, doi:10.1016/s0140-6736(02)08220-x (2002).
- 23 Patsopoulos, N. A. *et al.* Fine-mapping the genetic association of the major histocompatibility complex in multiple sclerosis: HLA and non-HLA effects. *PLoS Genet* **9**, e1003926, doi:10.1371/journal.pgen.1003926 (2013).
- 24 International Multiple Sclerosis Genetics, C. *et al.* Genetic risk and a primary role for cell-mediated immune mechanisms in multiple sclerosis. *Nature* **476**, 214-219, doi:10.1038/nature10251 (2011).
- 25 International Multiple Sclerosis Genetics, C. *et al.* Analysis of immune-related loci identifies 48 new susceptibility variants for multiple sclerosis. *Nat Genet* **45**, 1353-1360, doi:10.1038/ng.2770 (2013).
- 26 Gregory, S. G. *et al.* Interleukin 7 receptor alpha chain (IL7R) shows allelic and functional association with multiple sclerosis. *Nat Genet* **39**, 1083-1091, doi:10.1038/ng2103 (2007).
- 27 Hafler, D. *et al.* Risk Alleles for Multiple Sclerosis Identified by a Genomewide Study. *The New England Journal of Medicine* **357**, 851-862 (2007).
- 28 Huynh, J. L. *et al.* Epigenome-wide differences in pathology-free regions of multiple sclerosis-affected brains. *Nat Neurosci* **17**, 121-130, doi:10.1038/nn.3588 (2014).
- 29 Kaliszewska, A. & De Jager, P. L. Exploring the role of the epigenome in multiple sclerosis: a window onto cell-specific transcriptional potential. *J Neuroimmunol* **248**, 2-9, doi:10.1016/j.jneuroim.2011.12.012 (2012).
- 30 Dendrou, C. A., Fugger, L. & Friese, M. A. Immunopathology of multiple sclerosis. *Nat Rev Immunol* **15**, 545-558, doi:10.1038/nri3871 (2015).

- 31 Minagar, A. & Alexander, J. S. Blood-brain barrier disruption in multiple sclerosis. *Mult Scler* **9**, 540-549 (2003).
- 32 Barnett, M. H. & Prineas, J. W. Relapsing and remitting multiple sclerosis: pathology of the newly forming lesion. *Ann Neurol* **55**, 458-468, doi:10.1002/ana.20016 (2004).
- 33 Gaitan, M. I. *et al.* Evolution of the blood-brain barrier in newly forming multiple sclerosis lesions. *Ann Neurol* **70**, 22-29, doi:10.1002/ana.22472 (2011).
- 34 Faissner, S., Plemel, J. R., Gold, R. & Yong, V. W. Progressive multiple sclerosis: from pathophysiology to therapeutic strategies. *Nat Rev Drug Discov* **18**, 905-922, doi:10.1038/s41573-019-0035-2 (2019).
- 35 Hellings, N. *et al.* T-Cell Reactivity to Multiple Myelin Antigens in Multiple Sclerosis Patients and Healthy Controls. *Journal of Neuroscience Research* **63**, 290-302 (2001).
- 36 Ousman, S. S. *et al.* Protective and therapeutic role for alphaB-crystallin in autoimmune demyelination. *Nature* **448**, 474-479, doi:10.1038/nature05935 (2007).
- 37 Schoenborn, J. R. & Wilson, C. B. *Advances in Immunology* 41-101 (2007).
- 38 Zhu, J. & Paul, W. E. CD4 T cells: fates, functions, and faults. *Blood* **112**, 1557-1569, doi:10.1182/blood-2008-05-078154 (2008).
- 39 Ouyang, W., Kolls, J. K. & Zheng, Y. The biological functions of T helper 17 cell effector cytokines in inflammation. *Immunity* **28**, 454-467, doi:10.1016/j.immuni.2008.03.004 (2008).
- 40 Kondělková, K. *et al.* Regulatory T cells (Treg) and Their Roles in Immune System with Respect to Immunopathological Disorders. *Acta Medica* **53**, 73-77 (2010).
- 41 Venken, K. *et al.* Compromised CD4<sup>+</sup> CD25(high) regulatory T-cell function in patients with relapsing-remitting multiple sclerosis is correlated with a reduced frequency of FOXP3-positive cells and reduced FOXP3 expression at the single-cell level. *Immunology* **123**, 79-89, doi:10.1111/j.1365-2567.2007.02690.x (2008).
- 42 Feger, U. *et al.* Increased frequency of CD4<sup>+</sup> CD25<sup>+</sup> regulatory T cells in the cerebrospinal fluid but not in the blood of multiple sclerosis patients. *Clin Exp Immunol* **147**, 412-418, doi:10.1111/j.1365-2249.2006.03271.x (2007).
- 43 Johnson, A. J., Suidan, G. L., McDole, J. & Pirko, I. in *The Neurobiology of Multiple Sclerosis International Review of Neurobiology* 73-97 (2007).
- 44 Medana, I. *et al.* Fas ligand (CD95L) protects neurons against perforin-mediated T lymphocyte cytotoxicity. *J Immunol* **167**, 674-681, doi:10.4049/jimmunol.167.2.674 (2001).
- 45 Jurewicz, A., Biddison, W. E. & Antel, J. P. MHC Class I-Restricted Lysis of Human Oligodendrocytes by Myelin Basic Protein Peptide-Specific CD8 T Lymphocytes. *J Immunol* **160** (1998).

- 46 Rensing-Ehl, A., Malipiero, U., Irmeler, M., Tschopp, J. & Constam, D. F., A. . Neurons induced to express major histocompatibility complex class I antigen are killed via the perforin and not the Fas (APO-1/CD95) pathway. *Eur J Immunol* **26** (1996).
- 47 Link, H. & Huang, Y. M. Oligoclonal bands in multiple sclerosis cerebrospinal fluid: an update on methodology and clinical usefulness. *J Neuroimmunol* **180**, 17-28, doi:10.1016/j.jneuroim.2006.07.006 (2006).
- 48 Duddy, M. *et al.* Distinct effector cytokine profiles of memory and naive human B cell subsets and implication in multiple sclerosis. *J Immunol* **178**, 6092-6099, doi:10.4049/jimmunol.178.10.6092 (2007).
- 49 Hemmer, B., Kerschensteiner, M. & Korn, T. Role of the innate and adaptive immune responses in the course of multiple sclerosis. *The Lancet Neurology* **14**, 406-419, doi:10.1016/s1474-4422(14)70305-9 (2015).
- 50 Dhaiban, S. *et al.* Role of Peripheral Immune Cells in Multiple Sclerosis and Experimental Autoimmune Encephalomyelitis. *Sci* **3**, doi:10.3390/sci3010012 (2021).
- 51 Thompson, A. & Ciccarelli, O. Towards treating progressive multiple sclerosis. *Nat Rev Neurol* **16**, 589-590, doi:10.1038/s41582-020-00421-4 (2020).
- 52 Rivers, T. M., Sprunt, D. H. & Berry, G. P. OBSERVATIONS ON ATTEMPTS TO PRODUCE ACUTE DISSEMINATED ENCEPHALOMYELITIS IN MONKEYS. *Journal of Experimental Medicine* **58** (1933).
- 53 Tsunoda, I. & Fujinami, R. S. Neuropathogenesis of Theiler's murine encephalomyelitis virus infection, an animal model for multiple sclerosis. *J Neuroimmune Pharmacol* **5**, 355-369, doi:10.1007/s11481-009-9179-x (2010).
- 54 Matsushima, G. K. & Morell, P. The neurotoxicant, cuprizone, as a model to study demyelination and remyelination in the central nervous system. *Brain Pathol* **11** (2001).
- 55 Freund, J. & McDermott, K. Sensitization to Horse Serum by Means of Adjuvants. *Experimental Biology and Medicine* **49**, 548-553, doi:10.3181/00379727-49-13625 (1942).
- 56 Constantinescu, C. S., Farooqi, N., O'Brien, K. & Gran, B. Experimental autoimmune encephalomyelitis (EAE) as a model for multiple sclerosis (MS). *Br J Pharmacol* **164**, 1079-1106, doi:10.1111/j.1476-5381.2011.01302.x (2011).
- 57 Munoz, J. J., Bernard, C. C. & Mackay, I. R. Elicitation of experimental allergic encephalomyelitis (EAE) in mice with the aid of pertussigen. *Cellular Immunology* **83** (1984).
- 58 Linthicum, D., Munoz, JJ, Blaskett, A. Acute experimental autoimmune encephalomyelitis in mice. I. Adjuvant action of Bordetella pertussis is due to vasoactive amine sensitization and increased vascular permeability of the central nervous system. *Cellular Immunology* **73** (1982).

- 59 Miller, S. D. & Karpus, W. J. The immunopathogenesis and regulation of T-cell-mediated demyelinating diseases. *Immunology Today* **18** (1994).
- 60 Freund, J. & Stern, E. R. P., T. M. . Isoallergic Encephalomyelitis and Radiculitis in Guinea Pigs After One Injection of Brain and Mycobacteria in Water-in-Oil Emulsion. *Journal of Immunology* **53** (1947).
- 61 Olitsky, P. K. Y., R. H. EXPERIMENTAL DISSEMINATED ENCEPHALOMYELITIS IN WHITE MICE. *Journal of Experimental Medicine* **90** (1949).
- 62 Lipton, M. M. & Freund, J. Encephalomyelitis in the Rat Following Intracutaneous Injection of Central Nervous System Tissue with Adjuvant. *Experimental Biology and Medicine* **81**, 260-261 (1952).
- 63 McCarthy, D. P., Richards, M. H. & Miller, S. D. Mouse models of multiple sclerosis: experimental autoimmune encephalomyelitis and Theiler's virus-induced demyelinating disease. *Methods Mol Biol* **900**, 381-401, doi:10.1007/978-1-60761-720-4\_19 (2012).
- 64 Tuohy, V. K., Lu, Z., Sobel, R. A. & Laursen, R. A. L. M. B. Identification of an encephalitogenic determinant of myelin proteolipid protein for SJL mice. *The Journal of Immunology* **142** (1989).
- 65 Tompkins, S. M. *et al.* De novo central nervous system processing of myelin antigen is required for the initiation of experimental autoimmune encephalomyelitis. *J Immunol* **168**, 4173-4183, doi:10.4049/jimmunol.168.8.4173 (2002).
- 66 Yednock, T. A., Cannon, C., Fritz, L. C. S.-M., F. & Steinman, L. K., N. Prevention of experimental autoimmune encephalomyelitis by antibodies against  $\alpha 4\beta 1$  integrin. *Nature* **356** (1992).
- 67 Kawakami, N. *et al.* The activation status of neuroantigen-specific T cells in the target organ determines the clinical outcome of autoimmune encephalomyelitis. *J Exp Med* **199**, 185-197, doi:10.1084/jem.20031064 (2004).
- 68 Lees, J. R., Golumbek, P. T., Sim, J., Dorsey, D. & Russell, J. H. Regional CNS responses to IFN-gamma determine lesion localization patterns during EAE pathogenesis. *J Exp Med* **205**, 2633-2642, doi:10.1084/jem.20080155 (2008).
- 69 Kroenke, M. A., Carlson, T. J., Andjelkovic, A. V. & Segal, B. M. IL-12- and IL-23-modulated T cells induce distinct types of EAE based on histology, CNS chemokine profile, and response to cytokine inhibition. *J Exp Med* **205**, 1535-1541, doi:10.1084/jem.20080159 (2008).
- 70 Berard, J. L., Wolak, K., Fournier, S. & David, S. Characterization of relapsing-remitting and chronic forms of experimental autoimmune encephalomyelitis in C57BL/6 mice. *Glia* **58**, 434-445, doi:10.1002/glia.20935 (2010).
- 71 Traugott, U., Stone, S. H. & Raine, C. S. Chronic relapsing experimental allergic encephalomyelitis: Correlation of circulating lymphocyte fluctuations with disease activity in suppressed and unsuppressed animals. *Journal of Neurological Sciences* **41** (1979).

- 72 Boyle, E. A. & McGeer, P. L. Cellular immune response in multiple sclerosis plaques. *The American Journal of Pathology* **137** (1990).
- 73 Epstein, L. G. & Prineas, J. W. R., C. S. . Attachment of myelin to coated pits on macrophages in experimental allergic encephalomyelitis. *Journal of Neurological Sciences* **61** (1983).
- 74 Colover, J. Immunological and cytological studies of autoimmune demyelination and multiple sclerosis. *Brain, Behavior, and Immunity* **2** (1988).
- 75 Karcher, D., Lassmann, H., Lowenthal, A., Kitz, K. & Wisniewski, H. M. Antibodies-restricted heterogeneity in serum and cerebrospinal fluid of chronic relapsing experimental allergic encephalomyelitis. *Journal of Neuroimmunology* **2** (1982).
- 76 Mestas, J. & Hughes, C. C. Of mice and not men: differences between mouse and human immunology. *J Immunol* **172**, 2731-2738, doi:10.4049/jimmunol.172.5.2731 (2004).
- 77 Ransohoff, R. M. Animal models of multiple sclerosis: the good, the bad and the bottom line. *Nat Neurosci* **15**, 1074-1077, doi:10.1038/nn.3168 (2012).
- 78 Kuhlmann, T., Lingfeld, G., Bitsch, A., Schuchardt, J. & Brück, W. Acute axonal damage in multiple sclerosis is most extensive in early disease stages and decreases over time. **125** (2002).
- 79 Bø, L., Vedeler, C. A., Nyland, H., Trapp, B. D. & Mørk, S. J. Intracortical multiple sclerosis lesions are not associated with increased lymphocyte infiltration. *Mult Scler* **9** (2003).
- 80 Gilmore, C. P. *et al.* Regional variations in the extent and pattern of grey matter demyelination in multiple sclerosis: a comparison between the cerebral cortex, cerebellar cortex, deep grey matter nuclei and the spinal cord. *J Neurol Neurosurg Psychiatry* **80**, 182-187, doi:10.1136/jnnp.2008.148767 (2009).
- 81 Magliozzi, R. *et al.* A Gradient of neuronal loss and meningeal inflammation in multiple sclerosis. *Ann Neurol* **68**, 477-493, doi:10.1002/ana.22230 (2010).
- 82 Geurts, J. J. G. & Barkhof, F. Grey matter pathology in multiple sclerosis. *The Lancet Neurology* **7**, 841-851, doi:10.1016/s1474-4422(08)70191-1 (2008).
- 83 Kornek, B. *et al.* Multiple Sclerosis and Chronic Autoimmune Encephalomyelitis. *The American Journal of Pathology* **157**, 267-276, doi:10.1016/s0002-9440(10)64537-3 (2000).
- 84 Na, S. Y. *et al.* Naive CD8 T-cells initiate spontaneous autoimmunity to a sequestered model antigen of the central nervous system. *Brain* **131**, 2353-2365, doi:10.1093/brain/awn148 (2008).
- 85 Fischer, M. T. *et al.* NADPH oxidase expression in active multiple sclerosis lesions in relation to oxidative tissue damage and mitochondrial injury. *Brain* **135**, 886-899, doi:10.1093/brain/aws012 (2012).

- 86 Brosnan, C. F. & Raine, C. S. The astrocyte in multiple sclerosis revisited. *Glia* **61**, 453-465, doi:10.1002/glia.22443 (2013).
- 87 Sharma, R. *et al.* Inflammation induced by innate immunity in the central nervous system leads to primary astrocyte dysfunction followed by demyelination. *Acta Neuropathol* **120**, 223-236, doi:10.1007/s00401-010-0704-z (2010).
- 88 Parratt, J. D. & Prineas, J. W. Neuromyelitis optica: a demyelinating disease characterized by acute destruction and regeneration of perivascular astrocytes. *Mult Scler* **16**, 1156-1172, doi:10.1177/1352458510382324 (2010).
- 89 Smith, K. J., Kapoor, R. & Felts, P. A. Demyelination: the role of reactive oxygen and nitrogen species. *Brain Pathol* **9** (1999).
- 90 Werner, P., Pitt, D. & Raine, C. S. Multiple sclerosis: altered glutamate homeostasis in lesions correlates with oligodendrocyte and axonal damage. *Ann Neurol* **50** (2001).
- 91 Mahad, D., Ziabreva, I., Lassmann, H. & Turnbull, D. Mitochondrial defects in acute multiple sclerosis lesions. *Brain* **131**, 1722-1735, doi:10.1093/brain/awn105 (2008).
- 92 Waxman, S. G. Mechanisms of disease: sodium channels and neuroprotection in multiple sclerosis-current status. *Nat Clin Pract Neurol* **4**, 159-169, doi:10.1038/ncpneuro0735 (2008).
- 93 Connor, J. R. & Menzies, S. L. Cellular management of iron in the brain. *Journal of Neurological Sciences* **134** (1995).
- 94 Schattling, B. *et al.* Bassoon proteinopathy drives neurodegeneration in multiple sclerosis. *Nat Neurosci* **22**, 887-896, doi:10.1038/s41593-019-0385-4 (2019).
- 95 Cannella, B., Gaupp, S., Omari, K. M. & Raine, C. S. Multiple sclerosis: death receptor expression and oligodendrocyte apoptosis in established lesions. *J Neuroimmunol* **188**, 128-137, doi:10.1016/j.jneuroim.2007.05.018 (2007).
- 96 Friese, M. A., Schattling, B. & Fugger, L. Mechanisms of neurodegeneration and axonal dysfunction in multiple sclerosis. *Nat Rev Neurol* **10**, 225-238, doi:10.1038/nrneurol.2014.37 (2014).
- 97 Haider, L. *et al.* Oxidative damage in multiple sclerosis lesions. *Brain* **134**, 1914-1924, doi:10.1093/brain/awr128 (2011).
- 98 Murphy, M. P. How mitochondria produce reactive oxygen species. *Biochem J* **417**, 1-13, doi:10.1042/BJ20081386 (2009).
- 99 Mahad, D. H., Trapp, B. D. & Lassmann, H. Pathological mechanisms in progressive multiple sclerosis. *The Lancet Neurology* **14**, 183-193, doi:10.1016/s1474-4422(14)70256-x (2015).
- 100 Campbell, G. R. *et al.* Mitochondrial DNA deletions and neurodegeneration in multiple sclerosis. *Ann Neurol* **69**, 481-492, doi:10.1002/ana.22109 (2011).

- 101 Hametner, S. *et al.* Iron and neurodegeneration in the multiple sclerosis brain. *Ann Neurol* **74**, 848-861, doi:10.1002/ana.23974 (2013).
- 102 van Horssen, J. *et al.* Severe oxidative damage in multiple sclerosis lesions coincides with enhanced antioxidant enzyme expression. *Free Radic Biol Med* **45**, 1729-1737, doi:10.1016/j.freeradbiomed.2008.09.023 (2008).
- 103 Gray, E. *et al.* Increased microglial catalase activity in multiple sclerosis grey matter. *Brain Res* **1559**, 55-64, doi:10.1016/j.brainres.2014.02.042 (2014).
- 104 Carvalho, A. N., Lim, J. L., Nijland, P. G., Witte, M. E. & Van Horssen, J. Glutathione in multiple sclerosis: more than just an antioxidant? *Mult Scler* **20**, 1425-1431, doi:10.1177/1352458514533400 (2014).
- 105 van Horssen, J. *et al.* Nrf2 and DJ1 are consistently upregulated in inflammatory multiple sclerosis lesions. *Free Radic Biol Med* **49**, 1283-1289, doi:10.1016/j.freeradbiomed.2010.07.013 (2010).
- 106 Nijland, P. G. *et al.* Astroglial PGC-1alpha increases mitochondrial antioxidant capacity and suppresses inflammation: implications for multiple sclerosis. *Acta Neuropathol Commun* **10** (2014).
- 107 Fatokun, A. A., Stone, T. W. & Smith, R. A. Oxidative stress in neurodegeneration and available means of protection *Frontiers in Bioscience* **13** (2008).
- 108 Olney, J. W. Excitatory transmitter neurotoxicity. *Neurobiology Aging* **15** (1994).
- 109 Bano, D. *et al.* Cleavage of the plasma membrane Na<sup>+</sup>/Ca<sup>2+</sup> exchanger in excitotoxicity. *Cell* **120**, 275-285, doi:10.1016/j.cell.2004.11.049 (2005).
- 110 Belanger, M., Allaman, I. & Magistretti, P. J. Brain energy metabolism: focus on astrocyte-neuron metabolic cooperation. *Cell Metab* **14**, 724-738, doi:10.1016/j.cmet.2011.08.016 (2011).
- 111 Chaudhry, F. A. *et al.* Glutamate transporters in glial plasma membranes: highly differentiated localizations revealed by quantitative ultrastructural immunocytochemistry. *Neuron* **15** (1995).
- 112 Coulter, D. A. & Eid, T. Astrocytic regulation of glutamate homeostasis in epilepsy. *Glia* **60**, 1215-1226, doi:10.1002/glia.22341 (2012).
- 113 Arundine, M. & Tymianski, M. Molecular mechanisms of calcium-dependent neurodegeneration in excitotoxicity. *Cell Calcium* **34**, 325-337, doi:10.1016/s0143-4160(03)00141-6 (2003).
- 114 Mayer, M. L., Westbrook, G. L. & Guthrie, P. B. Voltage-dependent block by Mg<sup>2+</sup> of NMDA responses in spinal cord neurones. *Nature* **309** (1984).

- 115 Zhou, Y. & Danbolt, N. C. Glutamate as a neurotransmitter in the healthy brain. *J Neural Transm (Vienna)* **121**, 799-817, doi:10.1007/s00702-014-1180-8 (2014).
- 116 Kaufman, A. M. *et al.* Opposing roles of synaptic and extrasynaptic NMDA receptor signaling in cocultured striatal and cortical neurons. *J Neurosci* **32**, 3992-4003, doi:10.1523/JNEUROSCI.4129-11.2012 (2012).
- 117 Hardingham, G., Arnold, F. & Bading, H. Nuclear calcium signaling controls CREB-mediated gene expression triggered by synaptic activity. *Nature Neuroscience* **4**, 261–267 (2001).
- 118 Hardingham, G. & Bading, H. Coupling of extrasynaptic NMDA receptors to a CREB shut-off pathway is developmentally regulated. *Biochimica et Biophysica Acta (BBA) - Proteins and Proteomics* **1600**, 148-153 (2002).
- 119 Hardingham, G. E. & Bading, H. Synaptic versus extrasynaptic NMDA receptor signalling: implications for neurodegenerative disorders. *Nat Rev Neurosci* **11**, 682-696, doi:10.1038/nrn2911 (2010).
- 120 Mehta, A., Prabhakar, M., Kumar, P., Deshmukh, R. & Sharma, P. L. Excitotoxicity: bridge to various triggers in neurodegenerative disorders. *Eur J Pharmacol* **698**, 6-18, doi:10.1016/j.ejphar.2012.10.032 (2013).
- 121 Pitt, D., Werner, P. & Raine, C. Glutamate excitotoxicity in a model of multiple sclerosis. *Nature Medicine* **6**, 67–70 (2000).
- 122 McDonald, J. W., Althomsons, S. P., Hyrc, K. L., Choi, D. W. & Goldberg, M. P. Oligodendrocytes from forebrain are highly vulnerable to AMPA/kainate receptor-mediated excitotoxicity. *Nature Medicine* **4** (1998).
- 123 Wallström, E. D., P., Ljungdahl, A., Khademi, M., Nilsson, C. & Olsson, T. Memantine abrogates neurological deficits, but not CNS inflammation, in Lewis rat experimental autoimmune encephalomyelitis. *Journal of Neurological Sciences* **137** (1995).
- 124 Smith, T., Groom, A., Zhu, B. & Turski, L. Autoimmune encephalomyelitis ameliorated by AMPA antagonists. *Nature Medicine* **6**, 62-66 (2000).
- 125 Woo, M. S. *et al.* Neuronal metabotropic glutamate receptor 8 protects against neurodegeneration in CNS inflammation. *J Exp Med* **218**, doi:10.1084/jem.20201290 (2021).
- 126 Stover, J. F., Pleines, U. E. M.-K., M. C., Kossmann, T. L., K. & Kempfski, O. S. Neurotransmitters in cerebrospinal fluid reflect pathological activity. *Eur J Clin Invest* **27** (1997).
- 127 Srinivasan, R., Sailasuta, N., Hurd, R., Nelson, S. & Pelletier, D. Evidence of elevated glutamate in multiple sclerosis using magnetic resonance spectroscopy at 3 T. *Brain* **128**, 1016-1025, doi:10.1093/brain/awh467 (2005).

- 128 Pampliega, O. *et al.* Association of an EAAT2 polymorphism with higher glutamate concentration in relapsing multiple sclerosis. *J Neuroimmunol* **195**, 194-198, doi:10.1016/j.jneuroim.2008.01.011 (2008).
- 129 Newcombe, J. *et al.* Glutamate receptor expression in multiple sclerosis lesions. *Brain Pathol* **18**, 52-61, doi:10.1111/j.1750-3639.2007.00101.x (2008).
- 130 Pacheco, R. *et al.* Glutamate released by dendritic cells as a novel modulator of T cell activation. *J Immunol* **177**, 6695-6704, doi:10.4049/jimmunol.177.10.6695 (2006).
- 131 Evonuk, K. S. *et al.* Inhibition of System Xc(-) Transporter Attenuates Autoimmune Inflammatory Demyelination. *J Immunol* **195**, 450-463, doi:10.4049/jimmunol.1401108 (2015).
- 132 Pampliega, O. *et al.* Increased expression of cystine/glutamate antiporter in multiple sclerosis. *Journal of Neuroinflammation* **63** (2011).
- 133 Pitt, D. N., I. E., Wilson, H. C. & Raine, C. S. Glutamate uptake by oligodendrocytes: Implications for excitotoxicity in multiple sclerosis. *Neurology* **61** (2003).
- 134 Apostolakis, S. & Kypraiou, A. M. Iron in neurodegenerative disorders: being in the wrong place at the wrong time? *Rev Neurosci* **28**, 893-911, doi:10.1515/revneuro-2017-0020 (2017).
- 135 Trumpower, B. L. Function of the iron-sulfur protein of the cytochrome b-c1 segment in electron-transfer and energy-conserving reactions of the mitochondrial respiratory chain. *Biochimica et Biophysica Acta (BBA) - Reviews on Bioenergetics* **639** (1981).
- 136 Todorich, B., Pasquini, J. M., Garcia, C. I., Paez, P. M. & Connor, J. R. Oligodendrocytes and myelination: the role of iron. *Glia* **57**, 467-478, doi:10.1002/glia.20784 (2009).
- 137 Simpson, I. A. *et al.* A novel model for brain iron uptake: introducing the concept of regulation. *J Cereb Blood Flow Metab* **35**, 48-57, doi:10.1038/jcbfm.2014.168 (2015).
- 138 Wu, L. J. *et al.* Expression of the iron transporter ferroportin in synaptic vesicles and the blood-brain barrier. *Brain Res* **1001**, 108-117, doi:10.1016/j.brainres.2003.10.066 (2004).
- 139 Zecca, L., Youdim, M. B., Riederer, P., Connor, J. R. & Crichton, R. R. Iron, brain ageing and neurodegenerative disorders. *Nat Rev Neurosci* **5**, 863-873, doi:10.1038/nrn1537 (2004).
- 140 Hentze, M. W., Muckenthaler, M. U., Galy, B. & Camaschella, C. Two to tango: regulation of Mammalian iron metabolism. *Cell* **142**, 24-38, doi:10.1016/j.cell.2010.06.028 (2010).
- 141 Taylor, E. M. & Morgan, E. H. Developmental changes in transferrin and iron uptake by the brain in the rat. *Brain Res Dev Brain Res* **55** (1990).
- 142 Stankiewicz, J. M. & Brass, S. D. Role of iron in neurotoxicity: a cause for concern in the elderly? *Curr Opin Clin Nutr Metab Care* **12**, 22-29, doi:10.1097/MCO.0b013e32831ba07c (2009).
- 143 Lane, D. J. R., Ayton, S. & Bush, A. I. Iron and Alzheimer's Disease: An Update on Emerging Mechanisms. *J Alzheimers Dis* **64**, S379-S395, doi:10.3233/JAD-179944 (2018).

- 144 Wang, J. Y. *et al.* Meta-analysis of brain iron levels of Parkinson's disease patients determined by postmortem and MRI measurements. *Sci Rep* **6**, 36669, doi:10.1038/srep36669 (2016).
- 145 Moreau, C. *et al.* Could Conservative Iron Chelation Lead to Neuroprotection in Amyotrophic Lateral Sclerosis? *Antioxid Redox Signal* **29**, 742-748, doi:10.1089/ars.2017.7493 (2018).
- 146 Muller, M. & Leavitt, B. R. Iron dysregulation in Huntington's disease. *J Neurochem* **130**, 328-350, doi:10.1111/jnc.12739 (2014).
- 147 Lassmann, H. Mechanisms of neurodegeneration shared between multiple sclerosis and Alzheimer's disease. *J Neural Transm (Vienna)* **118**, 747-752, doi:10.1007/s00702-011-0607-8 (2011).
- 148 Hagemeyer, J., Geurts, J. & Zivadinov, R. Brain iron accumulation in aging and neurodegenerative disorders. *Expert Reviews of Neurotherapeutics* **12(12)**, 1467-1480 (2012).
- 149 Zarruk, J. G. *et al.* Expression of iron homeostasis proteins in the spinal cord in experimental autoimmune encephalomyelitis and their implications for iron accumulation. *Neurobiol Dis* **81**, 93-107, doi:10.1016/j.nbd.2015.02.001 (2015).
- 150 Huleta, S. W., Powers, S. & Connor, J. R. Distribution of transferrin and ferritin binding in normal and multiple sclerotic human brains. *Journal of the Neurological Sciences* **165** 48-55 (1998).
- 151 Bagnato, F. *et al.* Tracking iron in multiple sclerosis: a combined imaging and histopathological study at 7 Tesla. *Brain* **134**, 3602-3615, doi:10.1093/brain/awr278 (2011).
- 152 Pitt, D. *et al.* Imaging Cortical Lesions in Multiple Sclerosis With Ultra-High-Field Magnetic Resonance Imaging. *Arch Neurol* **67 (7)**, 812-818 (2010).
- 153 Piloni, N. E., Perazzo, J. C., Fernandez, V., Videla, L. A. & Puntarulo, S. Sub-chronic iron overload triggers oxidative stress development in rat brain: implications for cell protection. *Biometals* **29**, 119-130, doi:10.1007/s10534-015-9902-4 (2016).
- 154 Fricker, M., Tolkovsky, A. M., Borutaite, V., Coleman, M. & Brown, G. C. Neuronal Cell Death. *Physiol Rev* **98**, 813-880, doi:10.1152/physrev.00011.2017 (2018).
- 155 Kerr, J. F., Wyllie, A. H. & Currie, A. R. Apoptosis: a basic biological phenomenon with wide-ranging implications in tissue kinetics. *Br J Cancer* **26** (1972).
- 156 Fulda, S. & Debatin, K. M. Extrinsic versus intrinsic apoptosis pathways in anticancer chemotherapy. *Oncogene* **25**, 4798-4811, doi:10.1038/sj.onc.1209608 (2006).
- 157 Puthalakath, H. & Strasser, A. Keeping killers on a tight leash: transcriptional and post-translational control of the pro-apoptotic activity of BH3-only proteins. *Cell Death and Differentiation* **9**, 505-512, doi:10.1038/sj/cdd/4400998 (2002).
- 158 Huang, D. C. & Strasser, A. BH3-Only proteins-essential initiators of apoptotic cell death. *Cell* **103** (2000).

- 159 Wu, C. C. & Bratton, S. B. Regulation of the intrinsic apoptosis pathway by reactive oxygen species. *Antioxid Redox Signal* **19**, 546-558, doi:10.1089/ars.2012.4905 (2013).
- 160 Hebb, A. L. O. *et al.* Expression of the inhibitor of apoptosis protein family in multiple sclerosis reveals a potential immunomodulatory role during autoimmune mediated demyelination. *Multiple Sclerosis* **14** (5), 577-594 (2008).
- 161 Xiao, J., Liu, W., Chen, Y. & Deng, W. Recombinant human PDCD5 (rhPDCD5) protein is protective in a mouse model of multiple sclerosis. *J Neuroinflammation* **12**, 117, doi:10.1186/s12974-015-0338-0 (2015).
- 162 Meyer, R. *et al.* Acute Neuronal Apoptosis in a Rat Model of Multiple Sclerosis. *The Journal of Neuroscience* **21**(16), 6214–6220 (2001).
- 163 Peterson, J. W., Bo, L., Mork, S., Chang, A. & Trapp, B. D. Transected neurites, apoptotic neurons, and reduced inflammation in cortical multiple sclerosis lesions. *Ann Neurol* **50**, 389-400, doi:10.1002/ana.1123 (2001).
- 164 Lisak, R. P. *et al.* B cells from patients with multiple sclerosis induce cell death via apoptosis in neurons in vitro. *J Neuroimmunol* **309**, 88-99, doi:10.1016/j.jneuroim.2017.05.004 (2017).
- 165 Laurien, L. *et al.* Autophosphorylation at serine 166 regulates RIP kinase 1-mediated cell death and inflammation. *Nat Commun* **11**, 1747, doi:10.1038/s41467-020-15466-8 (2020).
- 166 Cho, Y. S. *et al.* Phosphorylation-driven assembly of the RIP1-RIP3 complex regulates programmed necrosis and virus-induced inflammation. *Cell* **137**, 1112-1123, doi:10.1016/j.cell.2009.05.037 (2009).
- 167 Sun, L. *et al.* Mixed lineage kinase domain-like protein mediates necrosis signaling downstream of RIP3 kinase. *Cell* **148**, 213-227, doi:10.1016/j.cell.2011.11.031 (2012).
- 168 Picon, C. *et al.* Neuron-specific activation of necroptosis signaling in multiple sclerosis cortical grey matter. *Acta Neuropathol* **141**, 585-604, doi:10.1007/s00401-021-02274-7 (2021).
- 169 Ofengeim, D. *et al.* Activation of necroptosis in multiple sclerosis. *Cell Rep* **10**, 1836-1849, doi:10.1016/j.celrep.2015.02.051 (2015).
- 170 Zhang, S. *et al.* RIP1 kinase inhibitor halts the progression of an immune-induced demyelination disease at the stage of monocyte elevation. *Proc Natl Acad Sci U S A* **116**, 5675-5680, doi:10.1073/pnas.1819917116 (2019).
- 171 Wang, Y. *et al.* Necrostatin-1 ameliorates the pathogenesis of experimental autoimmune encephalomyelitis by suppressing apoptosis and necroptosis of oligodendrocyte precursor cells. *Exp Ther Med* **18**, 4113-4119, doi:10.3892/etm.2019.8005 (2019).
- 172 Brennan, M. A. & Cookson, B. T. Salmonella induces macrophage death by caspase-1-dependent necrosis. *Mol Microbiol* **38** (2000).

- 173 Shi, J. *et al.* Cleavage of GSDMD by inflammatory caspases determines pyroptotic cell death. *Nature* **526**, 660-665, doi:10.1038/nature15514 (2015).
- 174 Ding, J. *et al.* Pore-forming activity and structural autoinhibition of the gasdermin family. *Nature* **535**, 111-116, doi:10.1038/nature18590 (2016).
- 175 Voet, S., Srinivasan, S., Lamkanfi, M. & van Loo, G. Inflammasomes in neuroinflammatory and neurodegenerative diseases. *EMBO Mol Med* **11**, doi:10.15252/emmm.201810248 (2019).
- 176 McKenzie, B. A. *et al.* Caspase-1 inhibition prevents glial inflammasome activation and pyroptosis in models of multiple sclerosis. *Proc Natl Acad Sci U S A* **115**, E6065-E6074, doi:10.1073/pnas.1722041115 (2018).
- 177 Li, S. *et al.* Gasdermin D in peripheral myeloid cells drives neuroinflammation in experimental autoimmune encephalomyelitis. *J Exp Med* **216**, 2562-2581, doi:10.1084/jem.20190377 (2019).
- 178 Humphries, F. *et al.* Succination inactivates gasdermin D and blocks pyroptosis. *Science* **369** (2020).
- 179 Dixon, S. J. *et al.* Ferroptosis: an iron-dependent form of nonapoptotic cell death. *Cell* **149**, 1060-1072, doi:10.1016/j.cell.2012.03.042 (2012).
- 180 Yagoda, N. *et al.* RAS-RAF-MEK-dependent oxidative cell death involving voltage-dependent anion channels. *Nature* **447**, 864-868, doi:10.1038/nature05859 (2007).
- 181 Doll, S. *et al.* ACSL4 dictates ferroptosis sensitivity by shaping cellular lipid composition. *Nature Chemical Biology* **13(1)**, 93-98 (2016).
- 182 Yang, W. S. *et al.* Regulation of ferroptotic cancer cell death by GPX4. *Cell* **156**, 317-331, doi:10.1016/j.cell.2013.12.010 (2014).
- 183 Stockwell, B. R. *et al.* Ferroptosis: A Regulated Cell Death Nexus Linking Metabolism, Redox Biology, and Disease. *Cell* **171**, 273-285, doi:10.1016/j.cell.2017.09.021 (2017).
- 184 Wu, G., Fang, Y., Yang, S., Lupton, J. R. & Turner, N. D. Glutathione Metabolism and Its Implications for Health. *The Journal of Nutrition* **134**, 489-492 (2004).
- 185 Zheng, J. & Conrad, M. The Metabolic Underpinnings of Ferroptosis. *Cell Metab* **32**, 920-937, doi:10.1016/j.cmet.2020.10.011 (2020).
- 186 Kuang, F., Liu, J., Xie, Y., Tang, D. & Kang, R. MGST1 is a redox-sensitive repressor of ferroptosis in pancreatic cancer cells. *Cell Chem Biol* **28**, 765-775 e765, doi:10.1016/j.chembiol.2021.01.006 (2021).
- 187 Doll, S. *et al.* FSP1 is a glutathione-independent ferroptosis suppressor. *Nature* **575**, 693-698, doi:10.1038/s41586-019-1707-0 (2019).
- 188 Jiang, X., Stockwell, B. R. & Conrad, M. Ferroptosis: mechanisms, biology and role in disease. *Nat Rev Mol Cell Biol*, doi:10.1038/s41580-020-00324-8 (2021).

- 189 Dixon, S. J. & Stockwell, B. R. The Hallmarks of Ferroptosis. *Annual Review of Cancer Biology* **3**, 35-54 (2019).
- 190 Angeli, J. P. F., Shah, R., Pratt, D. A. & Conrad, M. Ferroptosis Inhibition: Mechanisms and Opportunities. *Trends Pharmacol Sci* **38**, 489-498, doi:10.1016/j.tips.2017.02.005 (2017).
- 191 Stockwell, B. R. & Jiang, X. The Chemistry and Biology of Ferroptosis. *Cell Chem Biol* **27**, 365-375, doi:10.1016/j.chembiol.2020.03.013 (2020).
- 192 Reichert, C. O. *et al.* Ferroptosis Mechanisms Involved in Neurodegenerative Diseases. *Int J Mol Sci* **21**, doi:10.3390/ijms21228765 (2020).
- 193 DeGregorio-Rocasolano, N. *et al.* Iron-loaded transferrin (Tf) is detrimental whereas iron-free Tf confers protection against brain ischemia by modifying blood Tf saturation and subsequent neuronal damage. *Redox Biol* **15**, 143-158, doi:10.1016/j.redox.2017.11.026 (2018).
- 194 Tuo, Q. Z. *et al.* Tau-mediated iron export prevents ferroptotic damage after ischemic stroke. *Mol Psychiatry* **22**, 1520-1530, doi:10.1038/mp.2017.171 (2017).
- 195 Zhang, Y. & He, M. L. Deferoxamine enhances alternative activation of microglia and inhibits amyloid beta deposits in APP/PS1 mice. *Brain Res* **1677**, 86-92, doi:10.1016/j.brainres.2017.09.019 (2017).
- 196 Agrawal, S., Fox, J., Thyagarajan, B. & Fox, J. H. Brain mitochondrial iron accumulates in Huntington's disease, mediates mitochondrial dysfunction, and can be removed pharmacologically. *Free Radic Biol Med* **120**, 317-329, doi:10.1016/j.freeradbiomed.2018.04.002 (2018).
- 197 Devos, D. *et al.* Targeting chelatable iron as a therapeutic modality in Parkinson's disease. *Antioxid Redox Signal* **21**, 195-210, doi:10.1089/ars.2013.5593 (2014).
- 198 McLachlan, D. R. C. *et al.* Intramuscular desferrioxamine in patients with Alzheimer's disease. *The Lancet* **337** (1991).
- 199 Hu, C. L. *et al.* Reduced expression of the ferroptosis inhibitor glutathione peroxidase-4 in multiple sclerosis and experimental autoimmune encephalomyelitis. *J Neurochem* **148**, 426-439, doi:10.1111/jnc.14604 (2019).
- 200 Schirmer, L. *et al.* Neuronal vulnerability and multilineage diversity in multiple sclerosis. *Nature* **573**, 75-82, doi:10.1038/s41586-019-1404-z (2019).
- 201 Yan, C. & Higgins, P. J. Drugging the undruggable: transcription therapy for cancer. *Biochim Biophys Acta* **1835**, 76-85, doi:10.1016/j.bbcan.2012.11.002 (2013).
- 202 Vakhitov, V. A. *et al.* Epigenetic Mechanisms of the Pathogenesis of Multiple Sclerosis. *Human Physiology* **46**, 104-112, doi:10.1134/s0362119720010144 (2020).
- 203 Qureshi, I. A. & Mehler, M. F. Epigenetic mechanisms governing the process of neurodegeneration. *Mol Aspects Med* **34**, 875-882, doi:10.1016/j.mam.2012.06.011 (2013).

- 204 Xylaki, M., Atzler, B. & Outeiro, T. F. Epigenetics of the Synapse in Neurodegeneration. *Curr Neurol Neurosci Rep* **19**, 72, doi:10.1007/s11910-019-0995-y (2019).
- 205 Hermann, A., Goyal, R. & Jeltsch, A. The Dnmt1 DNA-(cytosine-C5)-methyltransferase methylates DNA processively with high preference for hemimethylated target sites. *J Biol Chem* **279**, 48350-48359, doi:10.1074/jbc.M403427200 (2004).
- 206 Jia, D., Jurkowska, R. Z., Zhang, X., Jeltsch, A. & Cheng, X. Structure of Dnmt3a bound to Dnmt3L suggests a model for de novo DNA methylation. *Nature* **449**, 248-251, doi:10.1038/nature06146 (2007).
- 207 He, Y.-F. *et al.* Tet-mediated formation of 5-carboxylcytosine and its excision by TDG in mammalian DNA. *Science* **333** (2011).
- 208 Kouzarides, T. Chromatin modifications and their function. *Cell* **128**, 693-705, doi:10.1016/j.cell.2007.02.005 (2007).
- 209 He, H., Hu, Z., Xiao, H., Zhou, F. & Yang, B. The tale of histone modifications and its role in multiple sclerosis. *Hum Genomics* **12**, 31, doi:10.1186/s40246-018-0163-5 (2018).
- 210 Huynh, J. L. & Casaccia, P. Epigenetic mechanisms in multiple sclerosis: implications for pathogenesis and treatment. *The Lancet Neurology* **12**, 195-206, doi:10.1016/s1474-4422(12)70309-5 (2013).
- 211 Lee, B. M. & Mahadevan, L. C. Stability of histone modifications across mammalian genomes: implications for 'epigenetic' marking. *J Cell Biochem* **108**, 22-34, doi:10.1002/jcb.22250 (2009).
- 212 Barrand, S., Andersen, I. S. & Collas, P. Promoter-exon relationship of H3 lysine 9, 27, 36 and 79 methylation on pluripotency-associated genes. *Biochem Biophys Res Commun* **401**, 611-617, doi:10.1016/j.bbrc.2010.09.116 (2010).
- 213 Chen, X. *et al.* G9a/GLP-dependent histone H3K9me2 patterning during human hematopoietic stem cell lineage commitment. *Genes Dev* **26**, 2499-2511, doi:10.1101/gad.200329.112 (2012).
- 214 Dillon, S. C., Zhang, X., Trievel, R. C. & Cheng, X. The SET-domain protein superfamily: protein lysine methyltransferases. *Genome Biol* **6**, 227, doi:10.1186/gb-2005-6-8-227 (2005).
- 215 Feng, Q. *et al.* Methylation of H3-lysine 79 is mediated by a new family of HMTases without a SET domain. *Current Biology* **12** (2002).
- 216 Bannister, A. J. & Kouzarides, T. Regulation of chromatin by histone modifications. *Cell Res* **21**, 381-395, doi:10.1038/cr.2011.22 (2011).
- 217 Roidl, D. & Hacker, C. Histone methylation during neural development. *Cell Tissue Res* **356**, 539-552, doi:10.1007/s00441-014-1842-8 (2014).
- 218 Maze, I., Noh, K. M., Soshnev, A. A. & Allis, C. D. Every amino acid matters: essential contributions of histone variants to mammalian development and disease. *Nat Rev Genet* **15**, 259-271, doi:10.1038/nrg3673 (2014).

- 219 Lai, W. K. M. & Pugh, B. F. Understanding nucleosome dynamics and their links to gene expression and DNA replication. *Nat Rev Mol Cell Biol* **18**, 548-562, doi:10.1038/nrm.2017.47 (2017).
- 220 Huntzinger, E. & Izaurralde, E. Gene silencing by microRNAs: contributions of translational repression and mRNA decay. *Nat Rev Genet* **12**, 99-110, doi:10.1038/nrg2936 (2011).
- 221 Sati, S., Ghosh, S., Jain, V., Scaria, V. & Sengupta, S. Genome-wide analysis reveals distinct patterns of epigenetic features in long non-coding RNA loci. *Nucleic Acids Res* **40**, 10018-10031, doi:10.1093/nar/gks776 (2012).
- 222 Berson, A., Nativio, R., Berger, S. L. & Bonini, N. M. Epigenetic Regulation in Neurodegenerative Diseases. *Trends Neurosci* **41**, 587-598, doi:10.1016/j.tins.2018.05.005 (2018).
- 223 Zhang, Z. & Zhang, R. Epigenetics in autoimmune diseases: Pathogenesis and prospects for therapy. *Autoimmun Rev* **14**, 854-863, doi:10.1016/j.autrev.2015.05.008 (2015).
- 224 Hwang, J. Y., Aromolaran, K. A. & Zukin, R. S. The emerging field of epigenetics in neurodegeneration and neuroprotection. *Nat Rev Neurosci* **18**, 347-361, doi:10.1038/nrn.2017.46 (2017).
- 225 Handel, A. E., Giovannoni, G., Ebers, G. C. & Ramagopalan, S. V. Environmental factors and their timing in adult-onset multiple sclerosis. *Nat Rev Neurol* **6**, 156-166, doi:10.1038/nrneurol.2010.1 (2010).
- 226 Graves, M. C. *et al.* Methylation differences at the HLA-DRB1 locus in CD4+ T-Cells are associated with multiple sclerosis. *Mult Scler* **20**, 1033-1041, doi:10.1177/1352458513516529 (2014).
- 227 Kular, L. *et al.* DNA methylation as a mediator of HLA-DRB1\*15:01 and a protective variant in multiple sclerosis. *Nat Commun* **9**, 2397, doi:10.1038/s41467-018-04732-5 (2018).
- 228 Maltby, V. E. *et al.* Genome-wide DNA methylation profiling of CD8+ T cells shows a distinct epigenetic signature to CD4+ T cells in multiple sclerosis patients. *Clin Epigenetics* **7**, 118, doi:10.1186/s13148-015-0152-7 (2015).
- 229 Kulakova, O. G. *et al.* Whole-Genome DNA Methylation Analysis of Peripheral Blood Mononuclear Cells in Multiple Sclerosis Patients with Different Disease Courses. *Acta Naturea* **8**, 103-110 (2016).
- 230 Ayuso, T. *et al.* Vitamin D receptor gene is epigenetically altered and transcriptionally up-regulated in multiple sclerosis. *PLoS One* **12**, e0174726, doi:10.1371/journal.pone.0174726 (2017).
- 231 Field, J. *et al.* Interleukin-2 receptor-alpha proximal promoter hypomethylation is associated with multiple sclerosis. *Genes Immun* **18**, 59-66, doi:10.1038/gene.2016.50 (2017).

- 232 Chomyk, A. M. *et al.* DNA methylation in demyelinated multiple sclerosis hippocampus. *Sci Rep* **7**, 8696, doi:10.1038/s41598-017-08623-5 (2017).
- 233 Kular, L. *et al.* Neuronal methylome reveals CREB-associated neuro-axonal impairment in multiple sclerosis. *Clin Epigenetics* **11**, 86, doi:10.1186/s13148-019-0678-1 (2019).
- 234 Pedre, X. *et al.* Changed histone acetylation patterns in normal-appearing white matter and early multiple sclerosis lesions. *J Neurosci* **31**, 3435-3445, doi:10.1523/JNEUROSCI.4507-10.2011 (2011).
- 235 Shen, S. *et al.* Age-dependent epigenetic control of differentiation inhibitors is critical for remyelination efficiency. *Nat Neurosci* **11**, 1024-1034, doi:10.1038/nn.2172 (2008).
- 236 Singhal, N. K. *et al.* Changes in Methionine Metabolism and Histone H3 Trimethylation Are Linked to Mitochondrial Defects in Multiple Sclerosis. *J Neurosci* **35**, 15170-15186, doi:10.1523/JNEUROSCI.4349-14.2015 (2015).
- 237 Junker, A. *et al.* MicroRNA profiling of multiple sclerosis lesions identifies modulators of the regulatory protein CD47. *Brain* **132**, 3342-3352, doi:10.1093/brain/awp300 (2009).
- 238 Prozorovski, T. *et al.* Regulation of sirtuin expression in autoimmune neuroinflammation: Induction of SIRT1 in oligodendrocyte progenitor cells. *Neurosci Lett* **704**, 116-125, doi:10.1016/j.neulet.2019.04.007 (2019).
- 239 Lim, H. W. *et al.* SIRT1 deacetylates ROR $\gamma$  and enhances Th17 cell generation. *J Exp Med* **212**, 607-617, doi:10.1084/jem.20132378 (2015).
- 240 Liu, Z. *et al.* The histone H3 lysine-27 demethylase Jmjd3 plays a critical role in specific regulation of Th17 cell differentiation. *J Mol Cell Biol* **7**, 505-516, doi:10.1093/jmcb/mjv022 (2015).
- 241 Subramanian, S., Bates, S. E., Wright, J. J., Espinoza-Delgado, I. & Piekarz, R. L. Clinical Toxicities of Histone Deacetylase Inhibitors. *Pharmaceuticals (Basel)* **3**, 2751-2767, doi:10.3390/ph3092751 (2010).
- 242 Giri, A. K. & Aittokallio, T. DNMT Inhibitors Increase Methylation in the Cancer Genome. *Front Pharmacol* **10**, 385, doi:10.3389/fphar.2019.00385 (2019).
- 243 Chateauvieux, S., Morceau, F., Dicato, M. & Diederich, M. Molecular and therapeutic potential and toxicity of valproic acid. *J Biomed Biotechnol* **2010**, doi:10.1155/2010/479364 (2010).
- 244 Bhat, K. P., Umit Kaniskan, H., Jin, J. & Gozani, O. Epigenetics and beyond: targeting writers of protein lysine methylation to treat disease. *Nat Rev Drug Discov*, doi:10.1038/s41573-020-00108-x (2021).
- 245 Cao, H. *et al.* Recent progress in histone methyltransferase (G9a) inhibitors as anticancer agents. *Eur J Med Chem* **179**, 537-546, doi:10.1016/j.ejmech.2019.06.072 (2019).

- 246 Benevento, M., van de Molengraft, M., van Westen, R., van Bokhoven, H. & Kasri, N. N. The role of chromatin repressive marks in cognition and disease: A focus on the repressive complex GLP/G9a. *Neurobiol Learn Mem* **124**, 88-96, doi:10.1016/j.nlm.2015.06.013 (2015).
- 247 Tachibana, M. *et al.* G9a histone methyltransferase plays a dominant role in euchromatic histone H3 lysine 9 methylation and is essential for early embryogenesis. *Genes Dev* **16**, 1779-1791, doi:10.1101/gad.989402 (2002).
- 248 Milner, C. M. C., R. D. The G9a gene in the human major histocompatibility complex encodes a novel protein containing ankyrin-like repeats. *Biochem J.* **15**, 811-818 (1993).
- 249 Mauger, O. *et al.* Alternative splicing regulates the expression of G9A and SUV39H2 methyltransferases, and dramatically changes SUV39H2 functions. *Nucleic Acids Res* **43**, 1869-1882, doi:10.1093/nar/gkv013 (2015).
- 250 Shankar, S. R. *et al.* G9a, a multipotent regulator of gene expression. *Epigenetics* **8**, 16-22, doi:10.4161/epi.23331 (2013).
- 251 Trievel, R. C., Beach, B. M., Dirk, L. M. A., Houtz, R. L. & Hurley, J. H. Structure and Catalytic Mechanism of a SET Domain Protein Methyltransferase. *Cell* **111**, 91-103 (2002).
- 252 Collins, R. E. *et al.* The ankyrin repeats of G9a and GLP histone methyltransferases are mono- and dimethyllysine binding modules. *Nat Struct Mol Biol* **15**, 245-250, doi:10.1038/nsmb.1384 (2008).
- 253 Tachibana, M. *et al.* Histone methyltransferases G9a and GLP form heteromeric complexes and are both crucial for methylation of euchromatin at H3-K9. *Genes Dev* **19**, 815-826, doi:10.1101/gad.1284005 (2005).
- 254 Shinkai, Y. & Tachibana, M. H3K9 methyltransferase G9a and the related molecule GLP. *Genes Dev* **25**, 781-788, doi:10.1101/gad.2027411 (2011).
- 255 Schaefer, A. *et al.* Control of cognition and adaptive behavior by the GLP/G9a epigenetic suppressor complex. *Neuron* **64**, 678-691, doi:10.1016/j.neuron.2009.11.019 (2009).
- 256 Maze, I. *et al.* G9a influences neuronal subtype specification in striatum. *Nat Neurosci* **17**, 533-539, doi:10.1038/nn.3670 (2014).
- 257 Ginjala, V. *et al.* Protein-lysine methyltransferases G9a and GLP1 promote responses to DNA damage. *Sci Rep* **7**, 16613, doi:10.1038/s41598-017-16480-5 (2017).
- 258 Sharma, S., Kelly, T. K. & Jones, P. A. Epigenetics in cancer. *Carcinogenesis* **31**, 27-36, doi:10.1093/carcin/bgp220 (2010).
- 259 Hua, K.-T. *et al.* The H3K9 methyltransferase G9a is a marker of aggressive ovarian cancer that promotes peritoneal metastasis. *Molecular Cancer* **13**, 189, doi:10.1186/1476-4598-13-189 (2014).

- 260 De Smedt, E. *et al.* G9a/GLP targeting in MM promotes autophagy-associated apoptosis and boosts proteasome inhibitor-mediated cell death. *Blood Adv* **5**, 2325-2338, doi:10.1182/bloodadvances.2020003217 (2021).
- 261 Cao, Y. P. *et al.* Inhibition of G9a by a small molecule inhibitor, UNC0642, induces apoptosis of human bladder cancer cells. *Acta Pharmacol Sin* **40**, 1076-1084, doi:10.1038/s41401-018-0205-5 (2019).
- 262 Ho, J. C. *et al.* Inhibition of the H3K9 methyltransferase G9A attenuates oncogenicity and activates the hypoxia signaling pathway. *PLoS One* **12**, e0188051, doi:10.1371/journal.pone.0188051 (2017).
- 263 Li, F. *et al.* G9a Inhibition Induces Autophagic Cell Death via AMPK/mTOR Pathway in Bladder Transitional Cell Carcinoma. *PLoS One* **10**, e0138390, doi:10.1371/journal.pone.0138390 (2015).
- 264 Jan, S. *et al.* Targeting EHMT2/ G9a for cancer therapy: Progress and perspective. *Eur J Pharmacol* **893**, 173827, doi:10.1016/j.ejphar.2020.173827 (2021).
- 265 Zheng, Y. *et al.* Inhibition of EHMT1/2 rescues synaptic and cognitive functions for Alzheimer's disease. *Brain* **142**, 787-807, doi:10.1093/brain/awy354 (2019).
- 266 Griñán-Ferré, C. *et al.* Pharmacological inhibition of G9a/GLP restores cognition and reduces oxidative stress, neuroinflammation and  $\beta$ -Amyloid plaques in an early-onset Alzheimer's disease mouse model. *Aging* **11**, 11591–11608 (2019).
- 267 Gupta, S. *et al.* Histone methylation regulates memory formation. *J Neurosci* **30**, 3589-3599, doi:10.1523/JNEUROSCI.3732-09.2010 (2010).
- 268 Wang, Z. J. *et al.* Amelioration of autism-like social deficits by targeting histone methyltransferases EHMT1/2 in Shank3-deficient mice. *Mol Psychiatry* **25**, 2517-2533, doi:10.1038/s41380-019-0351-2 (2020).
- 269 Maze, I. *et al.* Essential role of the histone methyltransferase G9a in cocaine-induced plasticity. *Sci* **327** (2010).
- 270 Subbanna, S. *et al.* G9a-mediated histone methylation regulates ethanol-induced neurodegeneration in the neonatal mouse brain. *Neurobiol Dis* **54**, 475-485, doi:10.1016/j.nbd.2013.01.022 (2013).
- 271 Laumet, G. *et al.* G9a is essential for epigenetic silencing of K(+) channel genes in acute-to-chronic pain transition. *Nat Neurosci* **18**, 1746-1755, doi:10.1038/nn.4165 (2015).
- 272 Malekzadeh, A. *et al.* Plasma proteome in multiple sclerosis disease progression. *Ann Clin Transl Neurol* **6**, 1582-1594, doi:10.1002/acn3.771 (2019).
- 273 Stromnes, I. M. & Goverman, J. M. Active induction of experimental allergic encephalomyelitis. *Nat Protoc* **1**, 1810-1819, doi:10.1038/nprot.2006.285 (2006).

- 274 Schattling, B. *et al.* Bassoon proteinopathy drives neurodegeneration in multiple sclerosis. *Nat Neurosci* **22**, 887-896, doi:10.1038/s41593-019-0385-4 (2019).
- 275 Tandon, R. *et al.* Generation of two human isogenic iPSC lines from fetal dermal fibroblasts. *Stem Cell Res* **33**, 120-124, doi:10.1016/j.scr.2018.10.004 (2018).
- 276 Brennand, K. J. *et al.* Modelling schizophrenia using human induced pluripotent stem cells. *Nature* **473**, 221-225, doi:10.1038/nature09915 (2011).
- 277 Djuric, U. *et al.* MECP2e1 isoform mutation affects the form and function of neurons derived from Rett syndrome patient iPS cells. *Neurobiol Dis* **76**, 37-45, doi:10.1016/j.nbd.2015.01.001 (2015).
- 278 Birkner, K. *et al.* beta1-Integrin- and KV1.3 channel-dependent signaling stimulates glutamate release from Th17 cells. *J Clin Invest* **130**, 715-732, doi:10.1172/JCI126381 (2020).
- 279 Liu, F. *et al.* Discovery of an in vivo chemical probe of the lysine methyltransferases G9a and GLP. *J Med Chem* **56**, 8931-8942, doi:10.1021/jm401480r (2013).
- 280 Vergun, O. *et al.* Exploration of the role of reactive oxygen species in glutamate neurotoxicity in rat hippocampal neurones in culture. *Journal of Physiology* **531**, 147-163 (2001).
- 281 Bell, K. F., Fowler, J. H., Al-Mubarak, B., Horsburgh, K. & Hardingham, G. E. Activation of Nrf2-regulated glutathione pathway genes by ischemic preconditioning. *Oxid Med Cell Longev* **2011**, 689524, doi:10.1155/2011/689524 (2011).
- 282 Harvey, C. J. *et al.* Nrf2-regulated glutathione recycling independent of biosynthesis is critical for cell survival during oxidative stress. *Free Radic Biol Med* **46**, 443-453, doi:10.1016/j.freeradbiomed.2008.10.040 (2009).
- 283 Tonelli, C., Chio, I. I. C. & Tuveson, D. A. Transcriptional Regulation by Nrf2. *Antioxid Redox Signal* **29**, 1727-1745, doi:10.1089/ars.2017.7342 (2018).
- 284 Abdalkader, M., Lampinen, R., Kanninen, K. M., Malm, T. M. & Liddell, J. R. Targeting Nrf2 to Suppress Ferroptosis and Mitochondrial Dysfunction in Neurodegeneration. *Front Neurosci* **12**, 466, doi:10.3389/fnins.2018.00466 (2018).
- 285 Taylor, B. C. & Young, N. L. Combinations of histone post-translational modifications. *Biochem J* **478**, 511-532, doi:10.1042/BCJ20200170 (2021).
- 286 Gupta, R., Saha, P., Sen, T. & Sen, N. An augmentation in histone dimethylation at lysine nine residues elicits vision impairment following traumatic brain injury. *Free Radic Biol Med* **134**, 630-643, doi:10.1016/j.freeradbiomed.2019.02.015 (2019).
- 287 Caravagna, C. *et al.* Diversity of innate immune cell subsets across spatial and temporal scales in an EAE mouse model. *Sci Rep* **8**, 5146, doi:10.1038/s41598-018-22872-y (2018).

- 288 Macrez, R., Stys, P. K., Vivien, D., Lipton, S. A. & Docagne, F. Mechanisms of glutamate toxicity in multiple sclerosis: biomarker and therapeutic opportunities. *The Lancet Neurology* **15**, 1089-1102, doi:10.1016/s1474-4422(16)30165-x (2016).
- 289 Chinopoulos, C. & Adam-Vizi, V. Calcium, mitochondria and oxidative stress in neuronal pathology. Novel aspects of an enduring theme. *FEBS J* **273**, 433-450, doi:10.1111/j.1742-4658.2005.05103.x (2006).
- 290 Ramalingam, M. & Kim, S. J. Reactive oxygen/nitrogen species and their functional correlations in neurodegenerative diseases. *J Neural Transm (Vienna)* **119**, 891-910, doi:10.1007/s00702-011-0758-7 (2012).
- 291 Wohler, J. E., Smith, S. S., Zinn, K. R., Bullard, D. C. & Barnum, S. R. Gammadelta T cells in EAE: early trafficking events and cytokine requirements. *Eur J Immunol* **39**, 1516-1526, doi:10.1002/eji.200839176 (2009).
- 292 Ge, Z. *et al.* Vorinostat, a histone deacetylase inhibitor, suppresses dendritic cell function and ameliorates experimental autoimmune encephalomyelitis. *Exp Neurol* **241**, 56-66, doi:10.1016/j.expneurol.2012.12.006 (2013).
- 293 Camelo, S. *et al.* Transcriptional therapy with the histone deacetylase inhibitor trichostatin A ameliorates experimental autoimmune encephalomyelitis. *J Neuroimmunol* **164**, 10-21, doi:10.1016/j.jneuroim.2005.02.022 (2005).
- 294 Zhang, Z., Zhang, Z. Y., Wu, Y. & Schluesener, H. J. Valproic acid ameliorates inflammation in experimental autoimmune encephalomyelitis rats. *Neuroscience* **221**, 140-150, doi:10.1016/j.neuroscience.2012.07.013 (2012).
- 295 Castelo-Branco, G. *et al.* Acute treatment with valproic acid and l-thyroxine ameliorates clinical signs of experimental autoimmune encephalomyelitis and prevents brain pathology in DA rats. *Neurobiol Dis* **71**, 220-233, doi:10.1016/j.nbd.2014.08.019 (2014).
- 296 Mangano, K. *et al.* Hypomethylating agent 5-aza-2'-deoxycytidine (DAC) ameliorates multiple sclerosis in mouse models. *J Cell Physiol* **229**, 1918-1925, doi:10.1002/jcp.24641 (2014).
- 297 Chan, M. W. *et al.* Low-dose 5-aza-2'-deoxycytidine pretreatment inhibits experimental autoimmune encephalomyelitis by induction of regulatory T cells. *Mol Med* **20**, 248-256, doi:10.2119/molmed.2013.00159 (2014).
- 298 Deimling, S. J., Olsen, J. B. & Tropepe, V. The expanding role of the Ehmt2/G9a complex in neurodevelopment. *Neurogenesis (Austin)* **4**, e1316888, doi:10.1080/23262133.2017.1316888 (2017).
- 299 Ankarcrona, M. *et al.* Glutamate-induced neuronal death: a succession of necrosis or apoptosis depending on mitochondrial function. *Neuron* **15** (1995).

- 300 Lewerenz, J., Ates, G., Methner, A., Conrad, M. & Maher, P. Oxytosis/Ferroptosis-(Re-) Emerging Roles for Oxidative Stress-Dependent Non-apoptotic Cell Death in Diseases of the Central Nervous System. *Front Neurosci* **12**, 214, doi:10.3389/fnins.2018.00214 (2018).
- 301 Gao, M., Monian, P., Quadri, N., Ramasamy, R. & Jiang, X. Glutaminolysis and Transferrin Regulate Ferroptosis. *Mol Cell* **59**, 298-308, doi:10.1016/j.molcel.2015.06.011 (2015).
- 302 Alim, I. *et al.* Selenium Drives a Transcriptional Adaptive Program to Block Ferroptosis and Treat Stroke. *Cell* **177**, 1262-1279 e1225, doi:10.1016/j.cell.2019.03.032 (2019).
- 303 Bao, W. D. *et al.* Loss of ferroportin induces memory impairment by promoting ferroptosis in Alzheimer's disease. *Cell Death Differ*, doi:10.1038/s41418-020-00685-9 (2021).
- 304 Pedrera, L. *et al.* Ferroptotic pores induce Ca(2+) fluxes and ESCRT-III activation to modulate cell death kinetics. *Cell Death Differ* **28**, 1644-1657, doi:10.1038/s41418-020-00691-x (2021).
- 305 Maher, P. *et al.* The role of Ca(2+) in cell death caused by oxidative glutamate toxicity and ferroptosis. *Cell Calcium* **70**, 47-55, doi:10.1016/j.ceca.2017.05.007 (2018).
- 306 Cao, J. Y. & Dixon, S. J. Mechanisms of ferroptosis. *Cell Mol Life Sci* **73**, 2195-2209, doi:10.1007/s00018-016-2194-1 (2016).
- 307 Eagle, H. Nutrition Needs of Mammalian Cells in Tissue Culture. *Science* **122**, 501-504 (1955).
- 308 Conrad, M. *et al.* Regulation of lipid peroxidation and ferroptosis in diverse species. *Genes Dev* **32**, 602-619, doi:10.1101/gad.314674.118 (2018).
- 309 Eugene, M., Cranford, M. R. & Banerjee, R. The Quantitatively Important Relationship between Homocysteine Metabolism and Glutathione Synthesis by the Transsulfuration Pathway and Its Regulation by Redox Changes. *Biochemistry* **39**, 13005-13011 (2000).
- 310 Singhal, S. S. *et al.* Antioxidant role of glutathione S-transferases: 4-Hydroxynonenal, a key molecule in stress-mediated signaling. *Toxicol Appl Pharmacol* **289**, 361-370, doi:10.1016/j.taap.2015.10.006 (2015).
- 311 Knight, T. R., Choudhuri, S. & Klaassen, C. D. Constitutive mRNA expression of various glutathione S-transferase isoforms in different tissues of mice. *Toxicol Sci* **100**, 513-524, doi:10.1093/toxsci/kfm233 (2007).
- 312 Zhang, Y. *et al.* Histone methyltransferase G9a protects against acute liver injury through GSTP1. *Cell Death Differ* **27**, 1243-1258, doi:10.1038/s41418-019-0412-8 (2020).
- 313 Hernandez-Ortega, K., Garcia-Esparcia, P., Gil, L., Lucas, J. J. & Ferrer, I. Altered Machinery of Protein Synthesis in Alzheimer's: From the Nucleolus to the Ribosome. *Brain Pathol* **26**, 593-605, doi:10.1111/bpa.12335 (2016).
- 314 Hunter, R. G., McCarthy, K. J., Milne, T. A., Pfaff, D. W. & McEwen, B. S. Regulation of hippocampal H3 histone methylation by acute and chronic stress. *Proc Natl Acad Sci U S A* **106**, 20912-20917, doi:10.1073/pnas.0911143106 (2009).

- 315 Hunter, R. G. *et al.* Acute stress and hippocampal histone H3 lysine 9 trimethylation, a retrotransposon silencing response. *Proc Natl Acad Sci U S A* **109**, 17657-17662, doi:10.1073/pnas.1215810109 (2012).
- 316 Hadian, K. & Stockwell, B. R. A roadmap to creating ferroptosis-based medicines. *Nat Chem Biol* **17**, 1113-1116, doi:10.1038/s41589-021-00853-z (2021).

## V Publication list

Gromova KV, Muhia M, **Rothammer N**, Gee CE, Thies E, Schaefer I, Kress S, Kilimann MW, Shevchuk O, Oertner TG, Kneussel M. Neurobeachin and the Kinesin KIF21B Are Critical for Endocytic Recycling of NMDA Receptors and Regulate Social Behavior. *Cell Rep.* 2018 May 29;23(9):2705-2717.

Schattling B, Engler JB, Volkmann C, **Rothammer N**, Woo MS, Petersen M, Winkler I, Kaufmann M, Rosenkranz SC, Fejtova A, Thomas U, Bose A, Bauer S, Träger S, Miller KK, Brück W, Duncan KE, Salinas G, Soba P, Gundelfinger ED, Merkler D, Friese MA. Bassoon proteinopathy drives neurodegeneration in multiple sclerosis. *Nat Neurosci.* 2019 Jun;22(6):887-896.

Woo MS, Ufer F, **Rothammer N**, Di Liberto G, Binkle L, Haferkamp U, Sonner JK, Engler JB, Hornig S, Bauer S, Wagner I, Egervari K, Raber J, Duvoisin RM, Pless O, Merkler D, Friese MA. Neuronal metabotropic glutamate receptor 8 protects against neurodegeneration in CNS inflammation. *J Exp Med.* 2021 May 3;218(5):e20201290.

Manuscript submitted:

**Nicola Rothammer**, Marcel S. Woo, Simone Bauer, Lars Binkle-Ladisch, Giovanni Di Liberto, Ingrid Wagner, Undine Haferkamp, Ole Pless, Doron Merkler, Jan Broder Engler, Manuel A. Friese. G9a dictates neuronal vulnerability to inflammatory stress via transcriptional control of ferroptosis.

## VI Acknowledgements

First of all, I would like to thank Prof. Dr. Manuel A. Friese for the great supervision, the scientific discussions, and his constant encouragement for this project. I sincerely appreciate his patience and guidance during my PhD studies and I am very thankful for the opportunity to expand my scientific skills by visiting workshops and congresses.

I thank Prof. Dr. Christian Lohr for the evaluation of my thesis and together with Prof. Dr. Matthias Kneussel and Prof. Dr. Thomas Oertner for being members of my examination commission. I want to thank the members of my ZMNH thesis committee Prof. Dr. Christian Kubisch and Dr. Michael Kreutz for supporting the project with their scientific expertise and helpful ideas.

Many thanks to Dr. Dr. Jan Broder Engler for his excellent supervision of this project, his great ideas and immense knowledge, and for the inspiring discussions. I am grateful for the bioinformatic contributions to this work and the proof-reading of my thesis.

I would like to thank Prof. Dr. Doron Merkler, Dr. Giovanni Di Liberto, and Ingrid Wagner for the staining's and RNAscope experiments on human brain slices. Thanks to Dr. Undine Haferkamp and Dr. Ole Pless for generously providing human iPSC neurons and Kristin Hartmann for mouse histopathology.

Thanks to all members of the INIMS lab for their help, the good working atmosphere, and the scientific and non-scientific discussions. Special thanks to Simone Bauer for her invaluable support with experimental procedures and to Dr. Lars Binkle-Ladisch for his advice on experimental design and analysis.

In the end, I am very thankful for everybody who supported and motivated me in the last years. I am especially thankful to my friends and my family for the unconditional support.

## VII Affidavit

Hiermit erkläre ich an Eides statt, dass ich die vorliegende Dissertationsschrift selbst verfasst und keine anderen als die angegebenen Quellen und Hilfsmittel benutzt habe.

I hereby confirm that this dissertation is my own written work and that I have used no sources and aids other than indicated.

---

Nicola Rothammer

Place, Date